MSc Thesis Earth, Surface & Water

Utrecht University

Moraine derived debris supply and distribution on a Himalayan glacier

van Woerkom, T.A.A.

3998185

09-10-2017

Under supervision from:
dr. Walter Immerzeel
MSc Jakob Steiner
MSc Philip Kraaijenbrink

Abstract

Many glaciers throughout the Himalayas are debris covered, which substantially alters the melt processes. Though the extent of these glaciers is well studied, there is less information available of the debris thickness. This debris thickness is spatially variable, and partly caused by sediment transport processes from the slopes adjacent to the glacier.

To quantify and understand these processes field data was analyzed and based on these insights a simple erosion-transport model was developed.

Using UAV images and DEMs from April 2013 to May 2017, the amount of erosion and the causing processes could be distinguished. Erosion rates on the moraine are 0.25 m yr^{-1}, which almost completely happens during the wet season. Debris flows and sediment entrainment by water flow are the processes here. The lower loose part of the moraine moves downslope with a velocity of 0.5-1.5 m yr^{-1}. This may be caused by solifluction or large slumping processes. Furthermore, smaller slumps and small rockfalls also contribute to the sediment transport down the moraine.

The model calculates that the average debris extent outward from the moraine is approximately 30 m, covering in total 22% of the glacier surface with an average thickness of 2.2 m. This is in sharp contrast with the fact that the glacier is currently entirely covered in debris. Not all the debris is thus derived from the lateral moraines.

Table of Contents

Table of figures

Table of tables

1 Introduction and literature review

1.1 General region introduction

The Himalayas in Asia are the worlds' highest mountain range with many peaks over 8000 m. The mountain range hosts over 95.000 different glaciers, with a total area of 97.605 km^2 (Pfeffer et al., 2014). These glaciers feed large rivers that flow through South-Asia, such as the Ganges, Indus and Brahmaputra. The water from these rivers is used for irrigation and drinking water, but it is also a challenge as periodic flooding affects a lot of people. With predicted climate change in the coming century, the glacier area will decrease by 36 to 64% (Kraaijenbrink et al., 2017), altering the contribution of glacial melt to the runoff. As many as 1.4 billion people live near rivers that are partly fed by Himalayan glaciers, hence it is important to understand the physics of these glaciers, to be able to make predictions about their response to climate change (Immerzeel et al., 2009).

Currently, retreat rates are highly variable in the range of -80 to +40 m yr^{-1} (Scherler et al., 2011a) (Figure 1, A). In the Southern Central Himalaya, where the study area is located (Scherler et al., 2011a), the largest part of the glaciers is melting with a maximum retreat rate of 63 m yr^{-1}. In this region 35% of the glaciers are advancing or stable.

1.2 Behavior and importance of debris covered glaciers

Two types of glaciers are abundant in the Himalaya: Clean-ice glaciers and debris-covered glaciers. Approximately 11% of the glaciated area throughout all regions in the Himalayas has a debris cover, though the amount and extent of debris cover differs between the glaciers (Kraaijenbrink et al., 2017). If the amount of debris is large enough it can potentially alter the dynamics of the glacier. A debris cover causes lower melt rates in comparison to a clean-ice glacier as the debris cover thickness is larger than ca. 2 cm (Östrem, 1959). With a thinner debris cover, melt rates peak with a thickness of 0.5 cm, but decrease again with thinner debris covers. With a consistent debris thickness of 20 cm, the melt rates are approximately 4 times lower than on a clean-ice glacier.

As a result, many of the debris covered glaciers in the area seem to have lower melt rates then the clean glaciers. The lowering of melt rates is also observed in the Southern Central Himalaya, where the relatively high amount of stable glaciers corresponds to a relatively high fraction of largely debris covered glaciers (36%; Scherler et al., 2011a). This is supported by (Brun et al., 2017), who found that the glaciers in East-Nepal and Bhutan do not have a sharp increase in melt rates at lower elevations, probably due to the extensive debris cover on the lower reaches of these glaciers. With this they indicate to an important implication of debris covered glaciers. Although debris-covered glaciers are a minority, they are important as 30% of the ice mass below the equilibrium line altitude is covered with debris (Kraaijenbrink et al., 2017). In addition, Gibson et al. (2017) found that the debris cover is thickest in near the glacier terminus. Without debris cover most melt is expected here, but the debris cover might lower the melt rate. This results in errors in mass balance predictions and the contribution of glacial melt to river systems if the debris cover is not taken into account (Bolch et al., 2012).

Though a positive link between supraglacial debris and melt rate is observed, the debris cover also alters melt processes which are locally able to speed up the glacier. As a result, other studies suggest that the melt rates of debris-covered glaciers are not necessarily lower than those of clean ice glaciers (Ragettli et al., 2016; Buri et al., 2016). One of the main causes for the locally enlarged melt

rates on debris covered glaciers is the abundance of supraglacial ponds and cliffs (Figure 1, B). Melt rates at cliffs are much higher than on the covered parts of the glacier, and these melt rates are even enlarged, when a supraglacial pond is located at the bottom of the cliff. Furthermore, these ponds are an important factor in maintaining the cliff, as they increase the melt rate at the bottom. Ragettli et al. (2016) supported this theory with data, as they found higher melt rates on debris-covered glaciers that had more ice cliffs and ponds. As the occurrence of these ponds is seasonal, with their peak during the monsoon season (Miles et al., 2016), melt rates will probably also be higher during these periods. These processes may counteract the slowing effect of the debris cover, so the overall melt rate is not lower than that of clean-ice glaciers (Buri et al., 2016).

Nonetheless, there are conflicting results regarding the melt processes on debris-covered glaciers, and further research is needed on this subject. This is important as the glacier melt processes are included in hydrological models of the area, and the current lack of understanding of the subject raises the possibility for large errors in these models.

1.3 Origin and processes of supraglacial debris supply

The amount of debris on a glacier is controlled by many factors (Figure 1), but a prerequisite is often the abundance of steep slopes near the glacier (Benn & Owen, 2002). From these steep slopes, mass movements deliver rocks to the glacier surface, either from the headwalls or from already existing glacial sediments (moraines). Local factors contributing to the amount of supraglacial debris are the amount and intensity of the precipitation, the glacier size, and the erodibility of the adjacent rocks and sediments (Benn & Owen, 2002). In addition to these, the transport mechanism has a large influence on the supraglacial debris distribution (Reznichenko et al., 2011; Schomacker, 2008). The distribution processes of debris on the glacier can have an important role in changing melt processes and melt rates on the glacier (Ragettli et al., 2016).

Many processes can transport debris to a glacier surface, but potentially the three most important are distinguished here. Previous research focused mostly on bedrock erosion and debris surfacing towards the terminus of the glacier as a result of ablation (Scherler et al., 2011b) and deposition of debris on glaciers from the headwalls (Dunning et al., 2015). A third option is erosion from steep lateral moraines bordering the glacier.

Basal debris seems to be only of minor importance on debris covered glaciers in the Himalaya (Benn & Owen, 2002). Though basal debris is likely to come to the glacier surface in the ablation zone, the amount is typically much lower than the supraglacially derived sediment. However, the subglacial sediment might be locally important for the sediment load on glaciers, as the subglacial sediment is typically assembling in discontinuous longitudinal ridges, mostly elevated along medial flowlines of the glaciers (Figure 1, C) (Benn & Owen, 2002; Gibson et al., 2017).

Thus most of the debris cover must have an origin off the surface area of the glacier. Rock avalanches, originating on mountain slopes, are known to supply substantial amounts of debris (Figure 1, D). From many events it is known that they were triggered by seismic events, but this is not necessary. Extreme rainfall events also seem to play a minor role in triggering rock avalanches (Soldati et al., 2004). Recent work suggest that a loss of ice is decreasing pressure on the rocks and that this might influence the increase in rockfall and rock avalanches observed (Fischer et al., 2006; McColl et al, 2010). After a rock avalanche is triggered, the material slides and rolls downhill,

dispersing on its way. As the rock avalanche hits the glacier, it continues to scatter until it stops. The deposited result of a rock avalanche on a glacier is usually thinner than non-supraglacial rock avalanches, as the ice surface lowers the basal friction, which results in a wider distributing of the rock volume. This results in a very large proportion of the glacier being covered by debris of one to several meters thick (Reznichenko et al., 2011; Dunning et al., 2015). Furthermore, Hewitt (2009) argues that the importance of rock avalanches and landslides on glacial development is often underestimated. First of all, many of the rock avalanches likely remain unobserved, as they happen in inaccessible terrain. This is because deposits in accumulation zones are easily buried by snow, and in ablation zones the ice movement is likely to disperse the sediment and its distinctive depositional pattern (McSaveney, 2002). Research in the Karakoram showed that large landslides and rock avalanches originated in a period with early summer melting and intense monsoonal storms (Hewitt, 2009). Some 20 years later, reworking of the sediment resulted in that the original outline of the deposit could hardly be recognized, and without prior knowledge it was not different from the debris cover on other locations. Individual rockfall also contributes to the supraglacial debris, but as there volume is relatively small, their contribution to the supraglacial debris cover is probably smaller.

However, sometimes the headwall is not connected anymore to the glacier, and thus these glaciers do not receive debris from the higher slopes. For these glaciers, material originating from the lateral moraines can be the largest source of sediment (Figure 1, E). The studied glacier in this research, Lirung glacier (Nepal), also has decoupled moraine walls along most of its length. Lukas et al. (2012) studied the lateral moraines bordering the similar Findelenglacier in Switzerland. They indicate some of the basic characteristics of the lateral moraine; a proximal slope angle between 41^{o}-64^{o}, and at certain locations multiple ridges below each other, which are not attached to each other. As these lateral moraines border the glacier over long distances, erosion from the moraines provides sediment along the entire length of the glacier. As many of the glaciers are entirely covered by debris, which is less likely if it happens from single large scale events (Dunning et al., 2015), it is possible that large amounts of the debris on these glaciers originate from the lateral moraines. Especially if the moraines were recently glaciated and are still influenced by glacial processes (paraglacial system, Ballantyne (2002)), supply rates can be substantial.

1.4 Processes of lateral moraine erosion

The upper part of the lateral moraine is often intensely gullied, which indicates that erosion takes place at these locations. Curry et al. (2005) found similar features, with debris flows being the most important transport phenomena. For many sediment-mantled slopes in recently glaciated terrain, this is the case (Ballantyne, 2002). If the moraine is ice cored, the ice can play an important role in releasing mass movements, as melting of the underlying ice reduces the strength of the overlying material. However, the majority of failures are still caused by rainfall (83%), where only 14% is possibly caused by buried ice melt (Ballantyne, 2002). The probability of lateral moraine susceptibility to debris flow erosion is not only dependent on the climate. Curry et al. (2000) suggests that steep moraine gradients of over 30^{o} are necessary to create a heavily gullied moraine where extensive erosion can happen. After reworking the exposed moraines, often the terrain ends up with a steep gullied upper part, where the original slope is completely lost, and a lower zone that consists of mainly reworked debris. This lower part mostly consists of coalescing cones, which sometimes merge into one large talus slope (Ballantyne, 2002).

The very steep (up to 64°) proximal slope of the moraine (Lukas et al., 2012) may be susceptible to rock fallout from the glacially oversteepened moraine, which develops talus accumulations below. However, the amount of talus at the bottom is not in line with the current frequency of rockfall. It is argued that the amount of rockfall was much larger directly after deglaciation (Marion et al., 1995). This theory is supported with observations in regions with recent glacial melt, such as Mexico (Palacios, 1998) and Svalbard (André, 1997). Augustinus (1995) furthermore found that cycles of downwasting and glacial growth rework the rocks deposit, which in combination with a debutressing of the slopes causes a rise in rockfall frequency. This may result in a larger amount of rockfall deposits than expected, if only the last retreat phase is considered.

Not all of the material from the processes described above is directly deposited on the glacier. Much material remains on the adjacent slopes as talus debris, and is reworked by secondary processes. Examples of these are wet flows, avalanches and solifluction processes. As the loose valley slope sediment consists of course boulders and rocks, but also of finer grained material, small slumps may change into debris flows that, because of the course material, can entrain bed material and grow in size substantially (de Haas & van Woerkom, 2016). Snow avalanches are also capable of transporting this loose material further downstream (Figure 1, F). Wet snow avalanches have often not enough shear strength to erode the bedrock, but are an important process in distributing the sediment from these temporary storage sites. Moore et al. (2013) found sedimentation rates in Switzerland of approximately 4 mm/yr. Sediment deposition rates in the Hindu Kush are estimated between 0.74 and 0.21 mm/yr (Bell et al., 1990).

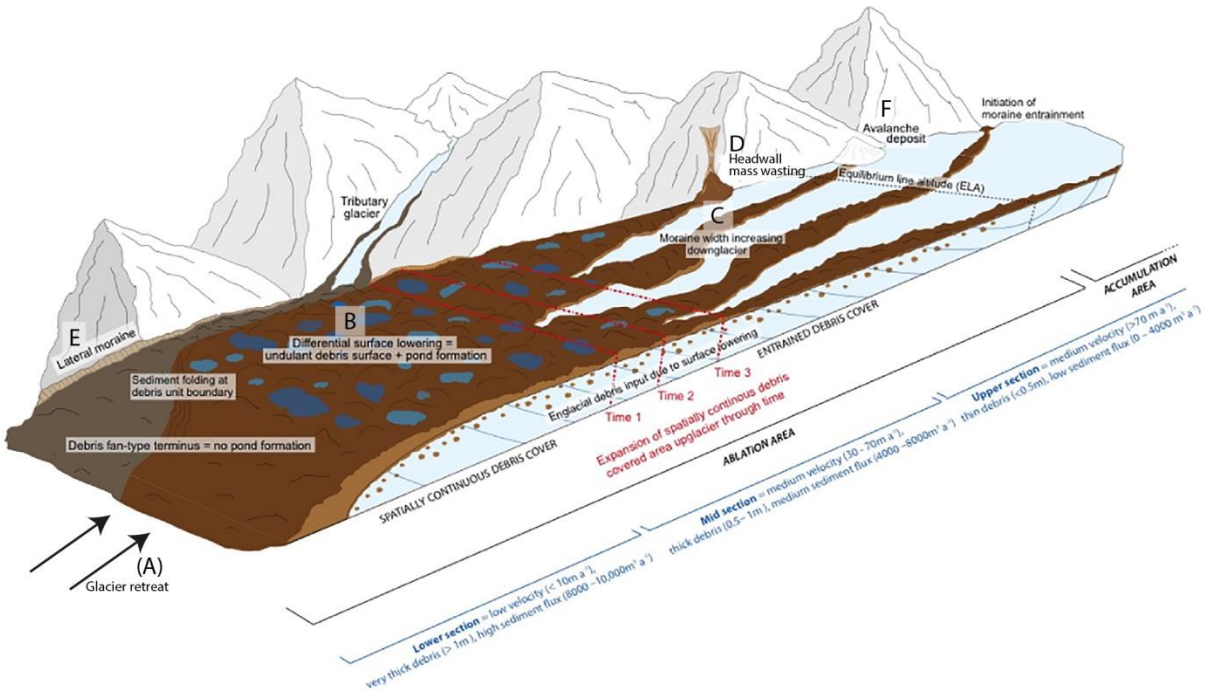

Figure 1; General overview of most processes influencing the supraglacial debris. Modified from Gibson et al. (2017).

A third process that is known to transport loose material on paraglacial moraines, mostly on more gentle slopes, is solifluction (Ballantyne, 2002). Solifluction is the name of a range of freeze-thaw action induced processes, which displaces material downslope (Matsuoka, 2001). Movements due to solifluction are largest near the edge of downwasting glaciers, and remain so for 30 years after glaciation. Afterwards values slowly decline, due to a decrease in moisture content as the ice margin moves away. The high moisture content near the glacier edge promotes the formation of ice lenses, increasing the probability of creep and gelifluction processes (Ballantyne & Matthews, 1982). Furthermore, it is known that solifluction alters moraine slopes, resulting in smooth and stable slopes with an average angle between 25-30^{o}. The importance of solifluction processes is also indicated by Nagai et al. (2013), who found that south-west facing slopes became more often mobilized, as a result of permafrost melt due to higher incoming solar radiation.

1.5 Objectives and research questions

As said before, at glaciers where the headwall is not anymore connected to the glacier, lateral moraines can provide substantial sediment to the glacier. There already are estimations of debris erosion rates. On the Findelenglacier in Switzerland, average erosion rates on the entire lateral moraine range between 4-48 mm yr^{-1}, while sedimentation rates on the deposition cones are between 16-361 mm yr^{-1}. However, single gullies erode approximately 100 mm yr^{-1} on several lateral moraines in Switzerland (Curry et al. 2005). This fast erosion rate is only applicable within relatively short periods after deglaciation, as they assume the sediment availability diminishes exponentially. Erosion rates across the globe vary substantially, but mostly have the same order of magnitude as the values found by Curry et al. (2005). Dependent on the local climatic conditions, the range is between 1 and 170 mm yr^{-1} (Ballantyne, 2002). Sedimentation values can reach higher values, as multiple erosion features can merge and reach a single deposition location. Measurements in the Langtang area, considering the area that was deglaciated 550 years ago, show denudation rates between 0.4 – 8 mm yr^{-1} (Wanatabe et al., 1998). Erosion from gullied moraine walls consisting of glacial till is generally lower than could be expected in other regions, as the moraines have a very high stability. However all of these are long term averages, and do not capture the spatial and temporal variability. In this research, remote sensed data from an UAV is used with a resolution of 0.1 and 0.2 m, at which the high variability of the glacier and moraine surface can easily be observed. By doing this at several moments in time, the temporal variability is also captured. The aim of this research is therefore to quantify elevation changes on a lateral moraine, including detailed spatial and temporal data.

Furthermore, there already is much knowledge about transporting processes on these moraines (Section 1.4). However, a general overview of the relation and relative importance of these processes is currently lacking, and is provided in this research.

The combination of these transporting processes also partly determines the pattern and thickness of moraine derived debris on the glacier. Debris thickness is an important variable in glacier flow models (Rowan et al., 2015; Anderson & Anderson, 2016) and energy balance models (Reid & Brock, 2010; Carenzo et al., 2016), but determination of this debris pattern of a glacier is often not possible because of the inaccessibility of the area, and consequently other methods are needed to find the thickness of the debris. One method to assess the thickness of the debris cover is using remote sensing. The first step is to distinguish between clean and debris covered glaciers (Bhardwaj et al., 2014). Foster et al. (2012) developed a method to map the debris cover of glaciers using thermal

remote sensing, with highest accuracies in the range between 0 and 0.5 m debris cover thickness. Schauwecker et al. (2015) also used thermal remote sensing bands to map the debris cover, but found that correlation between measured and thermal energy model values were difficult, as the remote sensing values were derived from 90 by 90 m pixels. Besides that, the surface temperature is highly variable through time. As these studies often investigated only few moments in time, they do not represent the natural variation that occurs, questioning the suitability of these methods to defining the debris cover on a glacier. Moreover, only the distribution of the total debris can be studied this way, where this research specifically focusses on moraine derived debris. Therefore, the distribution of debris over the glacier surface is modelled.

Gibson et al. (2015) used the surface velocity and debris thickness of the Baltoro glacier in the Karakoram to calculate the debris flux, but they used measured debris thicknesses instead of modelled ones. Kellerer-Pirklbauer (2008) also calculated supraglacial sediment distribution based on measured surface velocities. Moore (in press) focused on another part of debris distribution, namely debris instability on glacier slopes. He successfully indicated possible zones of debris movement, but did not include parameters to quantify the sediment flux. Thus, a combined model including a dynamic input and multiple debris distribution factors is currently nonexistent. Such a model can probably contribute substantially to understanding the dynamics of supraglacial debris, and can indicate the importance of moraine derived supraglacial debris in this case.

These objectives have been translated to the following research question:

Which processes displace sediment from the moraine onto the glacier and how do these processes affect the distribution of sediment over the glacier?

Several sub questions will also be answered:

- *What is the amount of sediment supply from the lateral moraines, and how is this variable through space and time?*
- *Which debris transport processes are most important on lateral moraines?*
- *How does the process of lateral moraine erosion affect the spatial distribution of sediment on the glacier?*
- *How does the moraine derived debris cover thickness and pattern change on the glacier?*

Hereafter, first the study area will be described, and the investigation that is carried out at this location. Secondly, the setup of the supraglacial debris distribution model will be explained. The results section will start with a visual interpretation of the collected data, followed by a more statistical analysis. After these are coupled to erosional mechanisms, the results from the model will be explained. After comparing these results to comparable studies, conclusions will be drawn about the processes that cause lateral moraine erosion. More important, the importance of these processes for a supraglacial debris cover formation, and thus for the glacial melt, will be discussed.

2 Data and methods

2.1 Study area

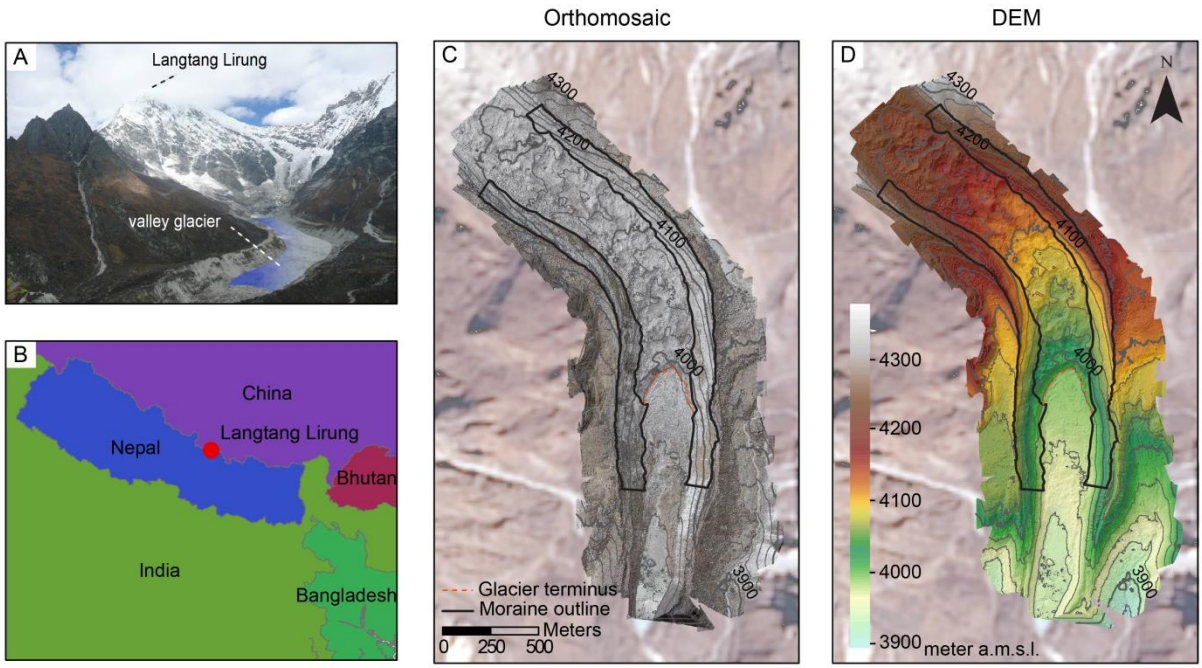

Figure 2; Study area introduction. (A) Photograph of the setting of the valley glacier and the moraines to the side. (B) Location of the study area. (C) Orthophoto of the study area, with the studied section of the moraine outlined. (D) same as C, but with elevation data.

The study area for this research is the Lirung glacier (28.234268 N, 85.561691 E), which is located in the Langtang valley in the Nepalese Himalayas north of Kathmandu. The glacier originates at the Langtang Lirung mountain, with its peak at 7227 m, and the Tsangbu Ri mountain, with an elevation of 6781 m. Flowing South, the glacier has steep headwalls near the mountain crest and an almost flat terminus. The lower part of the glacier is located in a valley and is covered entirely in debris. The study area is approximately located between 3900 and 4400 m above mean sea level (a.m.s.l.). In this section the moraine (Figure 2, black lines) is nowhere connected to the upper slopes, thus it can safely be assumed that the largest part of the material deposited on this section of the glacier is coming from the lateral moraines. From these lateral moraines, it can also be assumed that the glacier has melted over recent decades, and recent data shows that it is still melting (Immerzeel et al., 2014b). The climate in the region is dominated by the monsoon, with a wet season between June and September in which 70% of the annual precipitation falls (Figure 3). During the dry season between November and May, much less precipitation reaches the area, which mostly falls as snow (Immerzeel et al., 2014a).

Along the lower reach of Lirung glacier the moraines are approximately 4000 m in length, but for this investigation we use a fraction of the moraine, resulting in moraine lengths of 1945 and 2343 on the Western and Eastern side of the glacier respectively. This part of the moraine is used because of practical (most overlapping images) and investigative (not connected to upper slopes) reasons. The eastern moraine is slightly longer, as it is located in the outer bend of the glacier (Figure 2).

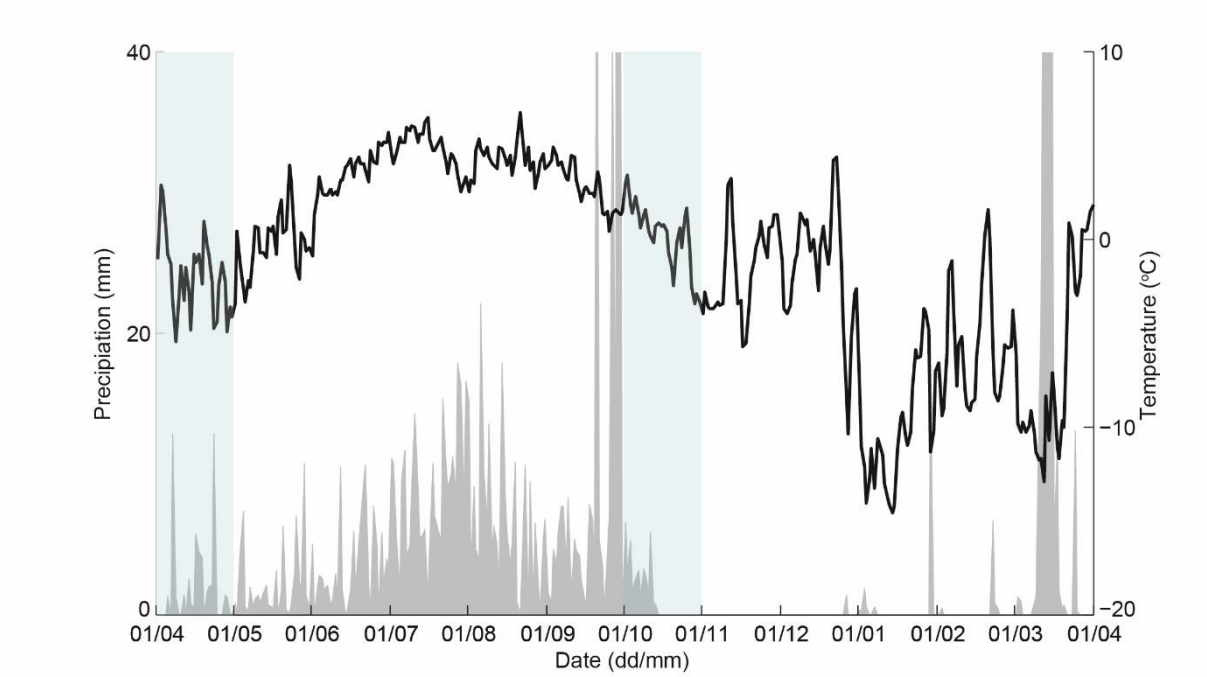

Figure 3; Example of weather data at Morimoto glacier. The period shown is from April 2016 to April 2017. Light blue areas indicate time of data caption.

2.2 Data acquisition and processing

The data of the moraine bordering Lirung glacier (Nepal) is assembled between 2013 and 2017, each time in the intermediate season between the dry winter and wet summer (Figure 3). The data was collected using an unmanned aerial vehicle (UAV). Different fixed-wing UAV's were used, that were flown both manually and using autopilot, with which it followed a predefined path. The UAV is equipped with a GPS, altimeter, wind meter and a Canon IXUS 125 HS digital camera. The 16 megapixel camera is automatically triggered by the autopilot at positions determined by the GPS device. Photographs with large distortions or a strong motion blur were removed. The sharp photographs collected by the UAV were processed into ortho-photos and digital elevation models (DEMs) of the glacier and its surroundings. This was done using a Structure from Motion workflow (Lucieer et al., 2014). For this glacier, the data was processed by Immerzeel et al. (2014b). Within the workflow used, first images with a large overlap from different positions are selected and image feature recognition is used to detect identical features on the different images. Camera orientation and per-image depth maps are derived from this information. Second, this information is used to derive dense xyz-point clouds (Furukawa & Ponce, 2009). Using collected ground control points along the lateral moraines and the camera GPS locations, the dense point clouds were georeferenced. After removing outlying points, the point cloud was exported to a grid based DEM and ortho-photo mosaic, with a resolution of 0.2 m and 0.1 m respectively. These steps were performed using the Agisoft PhotoScan Professional software (Agisoft, 2013).

Dataset	Mapped area (km^2)
May 2013	2.042
October 2013	3.246
October 2015	2.612
May 2016	1.970
October 2016	2.704
April 2017	1.428

Table 1; Date of acquisition and area of the different datasets

The workflow explained above was followed for 7 datasets, obtained between April 2013 and May 2017. Every dataset, existing of a DEM and an orthophoto, was created using many pictures, taken over several flights. Due to different objectives and flight conditions, the mapped area is not the same for every dataset (Table 1). As the composite images do not entirely overlap, the total area of investigation is approximately as large as the smallest of these mapped areas (1.5 km^2).

2.3 Delineation of lateral moraines

However, not the entire 1.5 km^2 is used for this investigation, which focusses on the lateral moraines. Therefore, the outline of these moraines should be extracted from the DEM and the orthophoto. As an automatic delineation algorithm did not succeed, this was done manually based on four parameters (Figure 4). The parameters used differed for the lower moraine boundary (bordering the glacier) and the upper boundary at the top of the moraine. The most important parameter that indicates the lower moraine boundary are a change in roughness, as can be seen from the hillshade (Lukas et al., 2012) and often also from the orthophoto (Figure4, A). Besides the hillshade, a change in slope (Figure 4, B) also indicated the edge of the moraine, as the slope steepness suddenly decreases from the moraine to the glacier. For the upper moraine boundary the orthophoto is an important indicator, as the start of the erosion scar is often clearly visible (Figure 4, C). If such a scar is not visible, the moraine boundary is set to the crest of the moraine, using the DEM (Figure 4, D). The upper boundary of the lateral moraine can at most locations be outlined very precisely, but the lower boundary is more difficult, as it is often hard to see the difference between the debris on the moraine and the debris covered glacier. Using the change in slope offers a solution, but still the location of the lower boundary could be less well established compared to the upper moraine boundary. The moraine extend, which is indicated by the previously explained characteristics, is used to extract the moraine from the DEM and the orthophoto.

2.4 DEM differencing

The high resolution DEMs of the lateral moraines bordering the glacier are used to calculate elevation differences between different time steps. To do this, and to get a first grip on the processes that cause erosion, the created moraine DEMs are subtracted from each other. The resulting difference in elevation between two time steps is assumed to be equal to the amount of sedimentation or erosion (Figure 5, A). In combination with a visual interpretation of the orthophotos, this information gives useful insights in the rate of erosion and the causing processes. By investigating the characteristics of sediment deposits on the lower moraine or at the edge of the glacier, different processes can be distinguished. Nonetheless difficulties may arise, as older deposits are likely to become indistinguishable within a couple of months (Dunning et al., 2015). Before examining the elevation differences is possible, the data has to be corrected for the abundant vegetation and for possible offsets in the data.

2.4.1 Vegetation correction

The moraine is partly covered by vegetation. The height and covered area of the grass and shrubs on the moraine differs per season and throughout the studied period. These differences distort the elevation change signal, as the vegetation has an additional elevation on top of the actual moraine surface. For each of the composite orthophotos, a supervised classification was performed using the maximum likelihood algorithm. The cells with vegetation were masked out of the different DEMs.

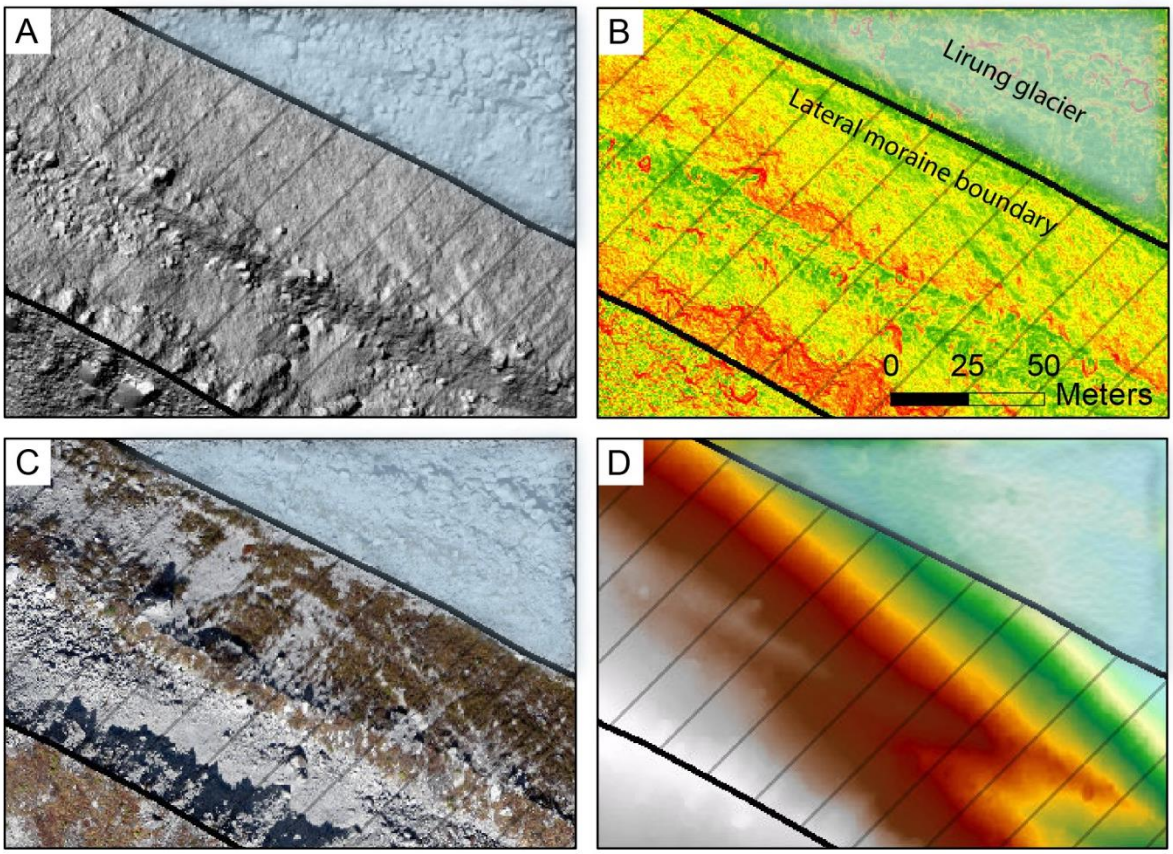

Figure 4; Method of moraine delineation, where the hillshade (A) and slope (B) are mostly used to determine the lower boundary. The orthophotos (C) and elevation model (D) are mostly used to detect the upper boundary.

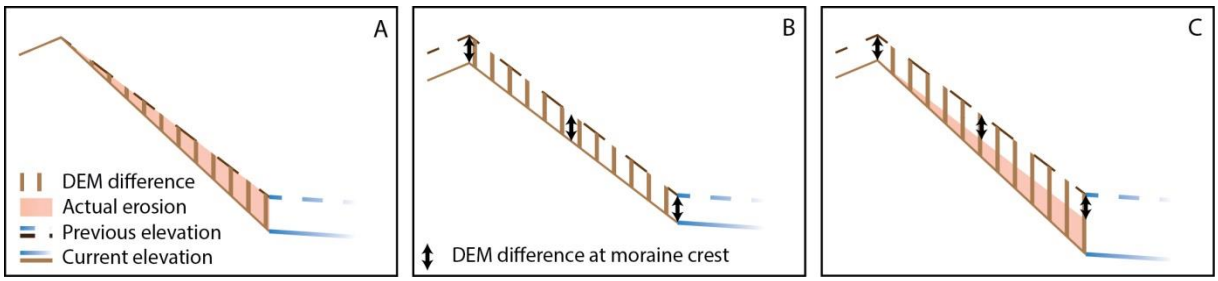

Figure 5; Method of DEM-differencing and offset correction. First, the UAV derived DEMs are subtracted to find the elevation difference (A). As the crest is stable, this value is equal to the amount of erosion/sedimentation. However, as the decrease in the buffer zone is as large as the difference on the moraine, no erosion/sedimentation took place, though an elevation difference is observed (B). Therefore, the DEM differencing values on the moraine are corrected for the DEM differences at the moraine crest, to find the actual rates erosion/sedimentation (C).

2.4.2 Offset correction

Besides the offset caused by vegetation, a less obvious, but equally important other factor also causes offset in the elevation difference data. This offset is caused by a raising or lowering of the entire moraine or small errors during georeferencing of the images. One of the causes of entire moraine lowering is the meltout of dead ice from in or underneath the moraine (Lukas et al., 2012). If the entire moraine elevation including the moraine crest decreases , the elevation difference between two time steps does not represent the amount of erosion anymore, but is likely to be dominated by a total rise or lowering of the area (Figure 5, B). A correction is made for the areas where this occurs.

At the upper boundary of the lateral moraine a buffer is created with a width of 5 m. This buffer, and the moraine below it, is divided in 10 zones on each side of the glacier. For each of these zones on top of the moraine crest is the mean elevation change calculated. This change is than subtracted from the calculated elevation change on the entire moraine. The result is the actual elevation change caused by erosion and/or sedimentation (Figure 5, C)

2.5 Relating elevation difference to causing factors

After correction for the factors described above, the results of the DEM-differencing are assessed with different methods, in order to understand the causes of the patterns seen. First, the elevation difference maps were examined visually together with the orthophotos, to spatially indicate patterns of moraine erosion and sedimentation (section 4.2.1). These results are explained by relating erosion values with parameters that could influence the amount of erosion or sedimentation. This was done by comparing elevation change values and process parameters on a 2 x 2 m window. The entire non vegetated area was examined in this way, but special attention was paid to the across-moraine assessment. By drawing 25 transects across the moraine at locations where no vegetation was present, differences between the upper and lower part of the moraine could more easily be studied. Non-vegetated areas were chosen as at these locations the elevation difference cannot be distorted by offsets caused by vegetation, but also because most of the lateral moraines worldwide are not vegetated (Figure 28). As the non-vegetated areas are not equally distributed over the Lirung glacier moraine, the across-moraine transects aren't either (Figure 9). However, as this research is working towards a general understanding of lateral moraine erosion in the area and not only specific for this glacier, this is not a large disadvantage.

First of all, the elevation difference between the different in surface types is discussed. Then, obvious parameters as slope, aspect, elevation were compared. As these factors are not substantially different between different time steps, the October 2015 DEM is used to derive this information. This DEM is chosen because it is in the center of the covered timespan and has a relatively large area covered (2.612 km^2). The amount of elevation difference will also be related to less obvious factors, such as moraine surface velocity and surface roughness. As the method corresponding to these last two factors is less straightforward, it will be explained more thoroughly hereafter.

2.5.1 Moraine movement velocity

Ballantyne & Matthews (1982) already noticed that solifluction can be an important factor in eroding and smoothening paraglacial slopes. A quick comparison of orthophotos from different moments in time seems to indicate that patches of moraine are shifting down the moraine. Cross-correlation feature tracking was used to calculate the displacement of debris on the lateral moraines. COSI-Corr

(Co-registration of Optically Sensed Images and Correlation) software is developed to calculate surface displacement by comparing two images and performing sub-pixel automated image correlation. This software package has been successfully applied on both coarse (Leprince et al., 2008) and high-resolution data (Kraaijenbrink et al., 2016) to determine glacier velocities. It is thus very likely to also be suitable to successfully calculate moraine displacements. The frequency correlator of the software is used, as the data is relatively noise-free. Kraaijenbrink et al. (2016), who partly used the same datasets, found that the correlator performs best when using the orthophoto and a multi-scale window decreasing from 265 to 64 pixels. These settings are also used in this approach. As the exact process is of less important for this research, further information about the usage of the software in general (Ayoub et al., 2017) or on high-resolution datasets (Kraaijenbrink et al., 2016) can be found in these papers, but will not be discussed in detail here. Afterwards surface velocities are computed by comparing the surface displacement and the timespan between the two correlated images.

The accuracy of the COSI-Corr algorithm for determining lateral moraine displacement is assessed by comparing the computed surface velocities with a set of 100 manually measured point velocities, all located on not vegetated areas of the lateral moraines.

2.5.2 Surface roughness

The surface roughness, when computed over a DEM, is measure of the differences in elevation. The surface roughness is often used within the context of turbulence (Munro, 1989) and is in this case also defined as the height above the ground at which a vertical wind velocity profile reaches zero (Smith, 2014). However, surface roughness also plays an important role in soil erosion by water flow (Bernard, 1997). In this context, a higher roughness causes water to become more concentrated, resulting in higher flow velocities and more erosion (Römkens et al., 2002). It is thus argued that, though the roughness is calculated in the context of turbulence, this same roughness is also suitable as a roughness value in the context erosion.

This is supported by Miles et al. (2017), who found that a small surface roughness (Smith, 2014) coincides with small differences in grain sizes. Nevertheless, the relation between roughness and erosivity is not uniform. On the one hand more rough surfaces are likely to indicate areas where erosion took/takes place (Römkens et al., 2002), as there is an alternation between patches that are not equally resistant to erosion. On the other hand, areas with a higher roughness can also indicate larger particles, which are less susceptible to erosion. In smooth areas it is the other way around: Though depositional surfaces are relatively smooth (Figure 15), the small particles in the deposition can afterwards easily be transported further downslope (Van Rijn, 1984).

To calculate the surface roughness, a DEM area of 5 x 5 m is detrended by creating the best fitted plane through the surface patch and subtracting this plane from the elevation values. Afterwards, the standard deviation from the detrended DEM is calculated.

The roughness length z_0 (m) is), according to Nield et al. (2013), computed as:

$$ln(z_0) = 0.65 + 1.37 * ln(\sigma_z) \quad (1)$$

where σ_z is the standard deviation of the detrended DEM (m). Though the size of the detrended patch is greatly influencing the calculated roughness, a surface area of 25 m^2 is found suitable for this approach. With a similar patch size suitable values were found on Lirung glacier (Miles et al., 2017).

To compare the roughness maps to the local grain size and the erosivity of that area, 100 grains and boulders were delineated, each by the eye corresponding to the average grain size in its vicinity.

3. Lateral moraine characteristics and transport processes

This section describes the characteristics of the lateral moraine bordering Lirung glacier, followed by the elevation change values. Furthermore a correlation is made between the elevation change and the causing processes.

3.1 Moraine characteristics

The first general characteristics of the lateral moraine are described in section 2.1, but an in depth description can be found here. First a visual interpretation is made, afterwards some not directly visible characteristics reported.

A clear division can visually be made between two different parts of the moraine (Figure 6). The upper part of the moraine consists of more firm material (till), from which larger boulders are sticking out. This is mainly the case in the lower firm part, where extensive gullies cut through the material at many locations, creating a high relief (Figure 6, A). The lowest part of the moraine consists of loose debris, with a size varying from large boulders (> 1 m) to small grains (approximately 1 mm). Though the division in a firm and loose part is generally relatively uniform, a second firm zone is observed on the North-Eastern moraine. In between the firm and loose zones, a washout zone can often be seen, with generally fine material that is likely washed out of the gullies above during rain events (Figure 6, A). However, this zone is not officially classified, as it is hard to distinguish it from the slightly coarser loose part of the moraine. A second important observation is that both the firm and loose section of the moraines are partly vegetated, indicating that these parts are less active. The least vegetated parts are the gullied part of the firm zone and the washout zone just below. Much less pronounced are different steps in the terrain that can be seen along large parts of the moraine (Figure 6, B-C). The ridges are especially visible at the western moraine along the upper part of the glacier, with a second ridge present between 30 m and 35 m below the crest of the moraine. These ridges can be linked to glacial growth and colder stages through time and are most likely remnants of already eroded lateral moraines. Another explanation is that these are the result of rock creep processes, which are correlated to a frozen or ice cored moraine. This explanation is less probable, as the moraine is fairly smooth over most of its surface, while intramoraine ice is usually accompanied by a hummocky surface (Lukas et al., 2012).

There are also characteristics that cannot be seen from the orthophotos of the moraine. These include the height and the slope of the moraine. The moraine height is on average 78 m and is largest at approximately 80% from the upper study area boundary (Figure 7, A). This is not surprising, as at that location the glacier terminus is located, and the moraine walls no longer stop at the ice mass, but end at the bottom of the valley. However, the increase in moraine height is not accompanied by a steeper moraine. Even further down the valley, the moraine height decreases again as the absolute height of the moraine wall also decreases. The lower slopes indicate less debris transport, which is supported by the extensive vegetation cover. However, the lowest slopes cannot be found at the lower and of the valley, but between 20% and 30% from the upper boundary. At this location, the moraine height is smallest (65 - 70 m). Further towards the upper boundary of the study area, the moraine elevation increases again, which is accompanied by a change to much steeper slopes as in the neighboring areas. These steeper slopes are an indication of a much more active moraine, without much vegetation, and are also less detached from the bedrock of the bordering mountains.

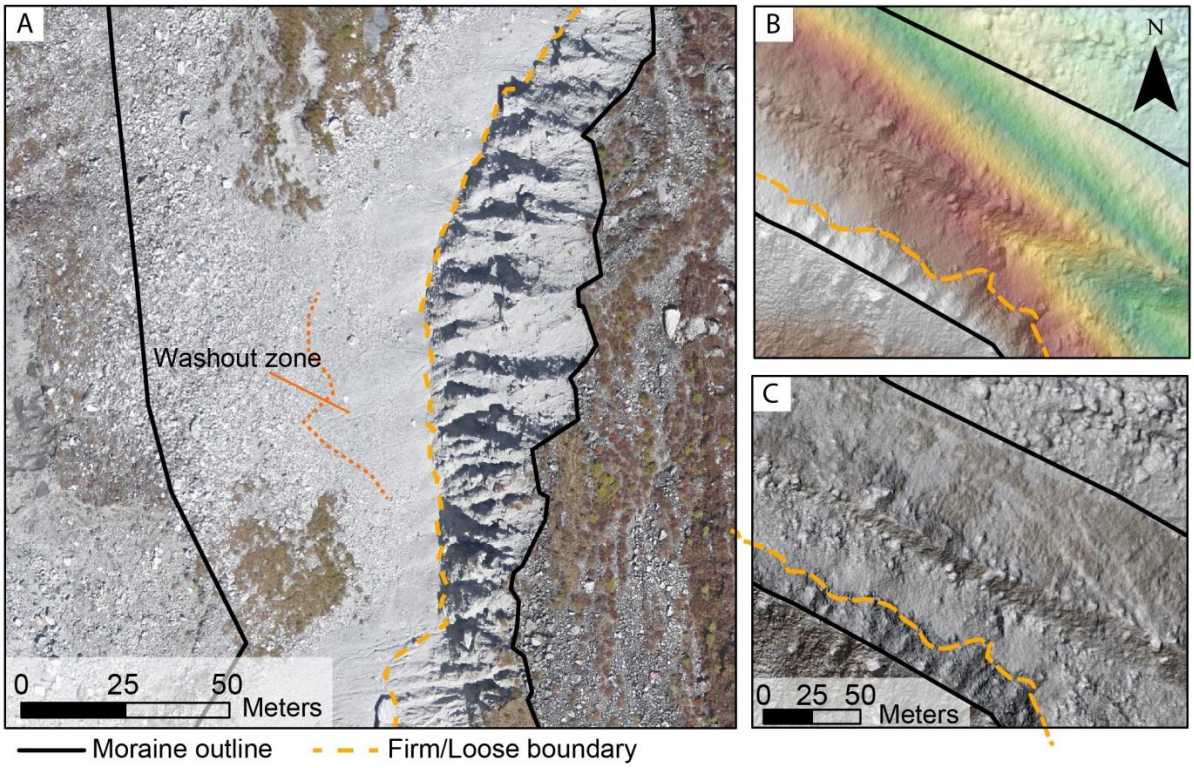

Figure 6; Visual moraine characteristics. The black lines (A) has been determined using the method in Figure 4, the difference between the firm (upper) part and loose (lower) part of the moraine is clearly visible. Secondary crests (B-C) are distinguished along some parts of the moraine, inhibiting direct flow to the bottom of the moraine.

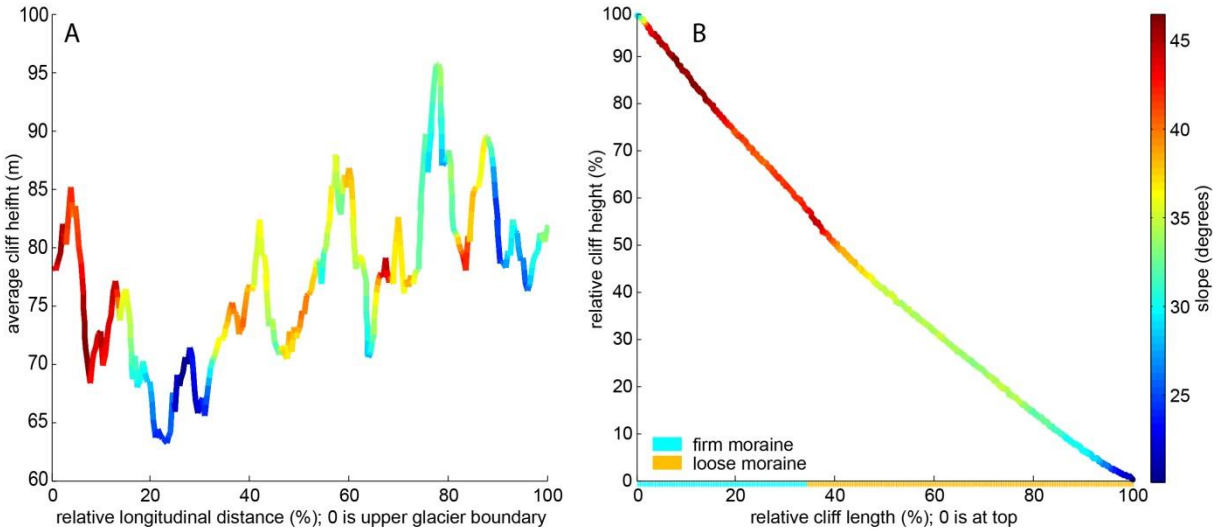

Figure 7; Differences in slope along the moraine walls. (A) shows the changes in moraine height and steepness along the glacier, and (B) shows the average changes in slope at all transects from the glacier up the moraine. On the y-axis the relative cliff height is shown, and changes in colors indicate changes in slope. The average cliff height is 78 m.

3.2 Moraine elevation changes

The moraine characteristics will later be important in describing differences in elevation change values and transport mechanisms of moraine areas with different characteristics, but first an overview of elevation change values across the entire moraine is presented. The total downwasting of the non-vegetated moraine over the entire period between May 2013 and April 2017 is -1.0 m, which corresponds to a volume of $2.5545*10^5$ m^3, and thus to an average value of $6.3861*10^4$ m^3 yr^{-1}, or -0.25 m yr^{-1}. Nonetheless, the pattern observed is very variable through space and time.

The average slope of the moraine is 35.3°, but the slope is not uniform over the moraine. Both in longitudinal as across-moraine direction the slope of the moraine changes, but changes are most striking (and important) in the across-moraine direction. In this direction, the steepness generally decreases from the top to the bottom of the moraine (Figure 7, B). The firm section thus has steeper slopes than the loose part of the moraine. Slopes up to 65° degrees are found in the firm part of the moraine, with a mean slope of around 45°. The steepness of the loose part of the moraine is lower, and tends to decrease even more towards the bottom. Nearly flat surfaces can be found near the bottom of the moraine, but for the entire loose moraine the mean slope is 32°.

3.2.1 Spatial and temporal differences

Almost all erosion happens during the wet season, which has a distinct pattern (Figure 8). The most common pattern can be seen in Figure 8 (B). On the firm part of the moraine, the pattern is consistent over the entire moraine, but has a large local variability. This variability is caused by gullied topography on the upper part, where erosion happens in the gullies, but the ridges in between remain almost stable. In the wet season, however, the elevation change of the firm zone is +0.016 m yr^{-1}. Besides a decrease in elevation inside single gullies, there are also large parts where these gullies are not abundant. These sections are much less susceptible to erosion or are even depositional areas (Figure 8, D). On the loose part during the wet season, the large scale variability is much more abundant, but the local variability is smaller. The elevation change on this section is also more negative than on the firm part of the moraine, with an average elevation change of -0.5 m yr^{-1} in the wet season.

In the dry season fewer patterns are observed, as there is on average no erosion. The elevation change is +0.034 m yr^{-1} on the firm part of the moraine and -0.020 m yr^{-1} on the loose part. This does not mean that there is no erosion found on the moraine, as there are still patches that are eroding. However, there are as many areas that show only sedimentation, thus they average out (Figure 8, C, E). In the dry season, erosion on the firm part is no longer concentrated to the gullied section on the moraine, but small randomly spaced areas show negative elevation change values. The alternation of negative and large positive elevation change values (Figure 8, E) is likely caused by small or larger slumps, solifluction, or by differences in the effectiveness of water erosion (Figure 10, B-C). Furthermore, in both A and D, large erosion values can be seen (< -3.2 m yr^{-1}) followed downslope by high (but generally lower) sedimentation values (> 0.8 m yr^{-1}). These larger slumps (Figure 10) are more observed during the wet season, but are also observed during the dry season, mostly initiating on the firm part of the moraine.

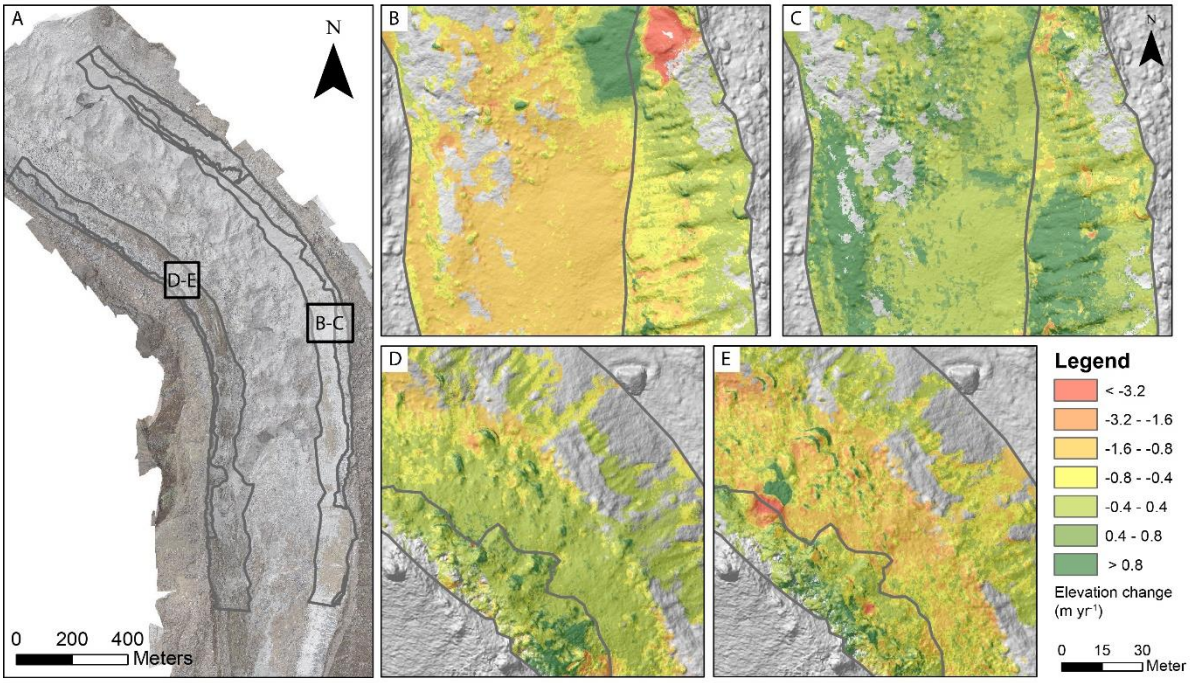

Figure 8; Elevation change pattern, both in the wet (B, D) and dry (C,E) season. (A) shows the locations along the glacier of the patches. Though on average the elevation change in the dry season is close to zero, individual patches do show erosion and sedimentation (D,E).

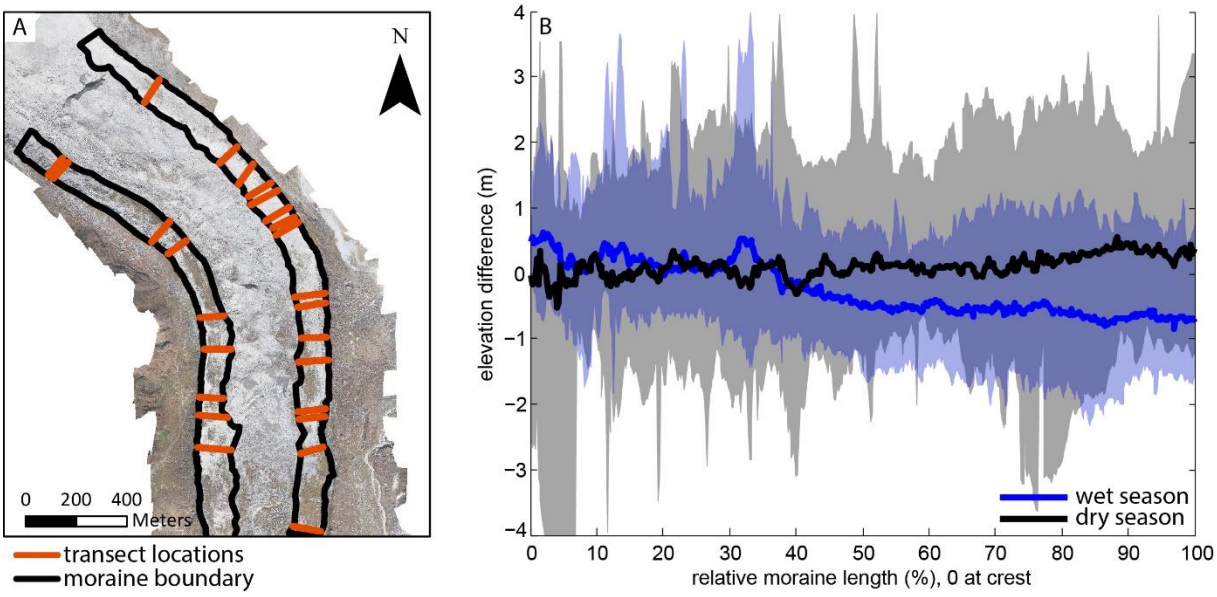

Figure 9; Erosion values along across-moraine transects, of which the locations are shown in (A). (B) shows the average elevation difference along these transects. Especially on the loose part (higher %, approximately from 40% onwards) erosion is occurring. The bands show the minimum and maximum value across all transects and indicates the variability of the elevation change values. This variability is in the dry season generally much larger than during the wet season.

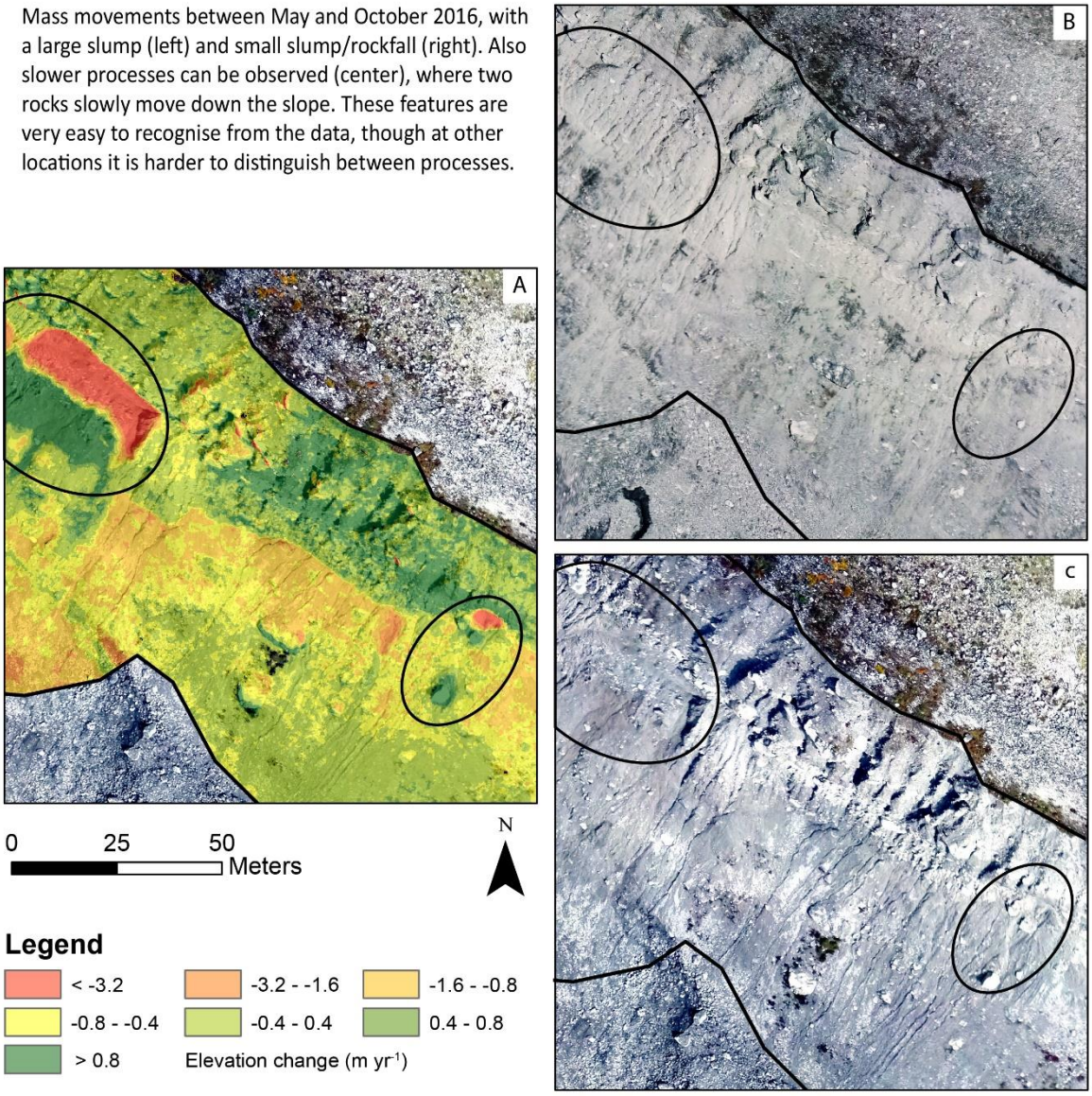

Figure 10; Mass movement processes on the moraine. The elevation difference between May and October 2016 (A) clearly shows two different erosional patches, followed by sedimentation below. If the orthophoto between May (B) and October (C) are compared, these two are immediately visible. In the upper left, a large block of moraine has slumped and is deposited below. On the right, (C) shows a rock that has moved between May and October 2016. Upslope of the deposited rock a clear transport path can be seen. Just below the moraine, as second rock deposit can be found.

3.2.2 Moraine transects

To better understand the sequence of processes playing a role from the crest of the moraine to the glacier boundary 25 transects were created across the moraine. These were drawn at locations where no vegetation was present along the entire transect length (Figure 9, A), so vegetation cannot affect the processes and the downslope effect of upslope processes should directly be seen in the data.

From the 25 transects elevation change values and trends are extracted. The general pattern is the same as derived from the 2 by 2 m windows (Section 3.2.1). A fairly stable, or even increasing moraine during the dry season is observed. In the wet season erosion occurs mainly in the loose part of the moraine (-0.54 m yr^{-1}). From the transects it can be seen that the upper part of the moraine has in the wet season even a higher elevation gain than the same area during the dry season (+0.3 and +0.16 m yr^{-1} respectively). The spatial variability of the data across the glacier is very large (Figure 9, B). In the dry season the standard deviation is 1.02 m, which is much higher than during the wet season (0.76 m). This seems to indicate that a larger range of processes alter the moraine slope in the dry season. During the wet season erosion is dominated by flow processes, but in the dry season these are less important. Therefore a wider range of processes as solifluction, larger mass movements and rock fallout are the major transport mechanisms, resulting in a larger range of elevation change values.

3.3 Erosion correlation

The elevation change values are compared to driving factors to indicate the processes that are causing the patterns explained above. First, it is compared to the slope, aspect and elevation of the moraine. After that, it is compared to the displacement of the moraine and to the local roughness, a measure of grain size variability.

3.3.1 Slope, aspect and elevation

Each of these three factors is known to play a role in erosion mechanisms (Renard, 1997); Cerda, 1998; Kääb & Vollmer, 2000). However, none of these seems to have a strong relation with the amount of erosion (Figure 11). Especially the firm part of the moraine is not influenced by any of these factors, as this section also hardly shows erosion. However, though not easily visible, these factors might play a minor role in the erosion process of the loose part of the moraine. Three of the plots show a trend, which are:

- A weak positive relation between moraine elevation and moraine elevation difference on the loose part of the moraine during the wet season.
- A weak negative relation between moraine elevation and moraine elevation difference on the loose part of the moraine during the dry season.
- A weak positive relation between moraine slope and moraine elevation difference on the loose part of the moraine during the wet season.

Though they are significant (p-values < 0.01), the applicability of those remains questionable, given the very low R^2.

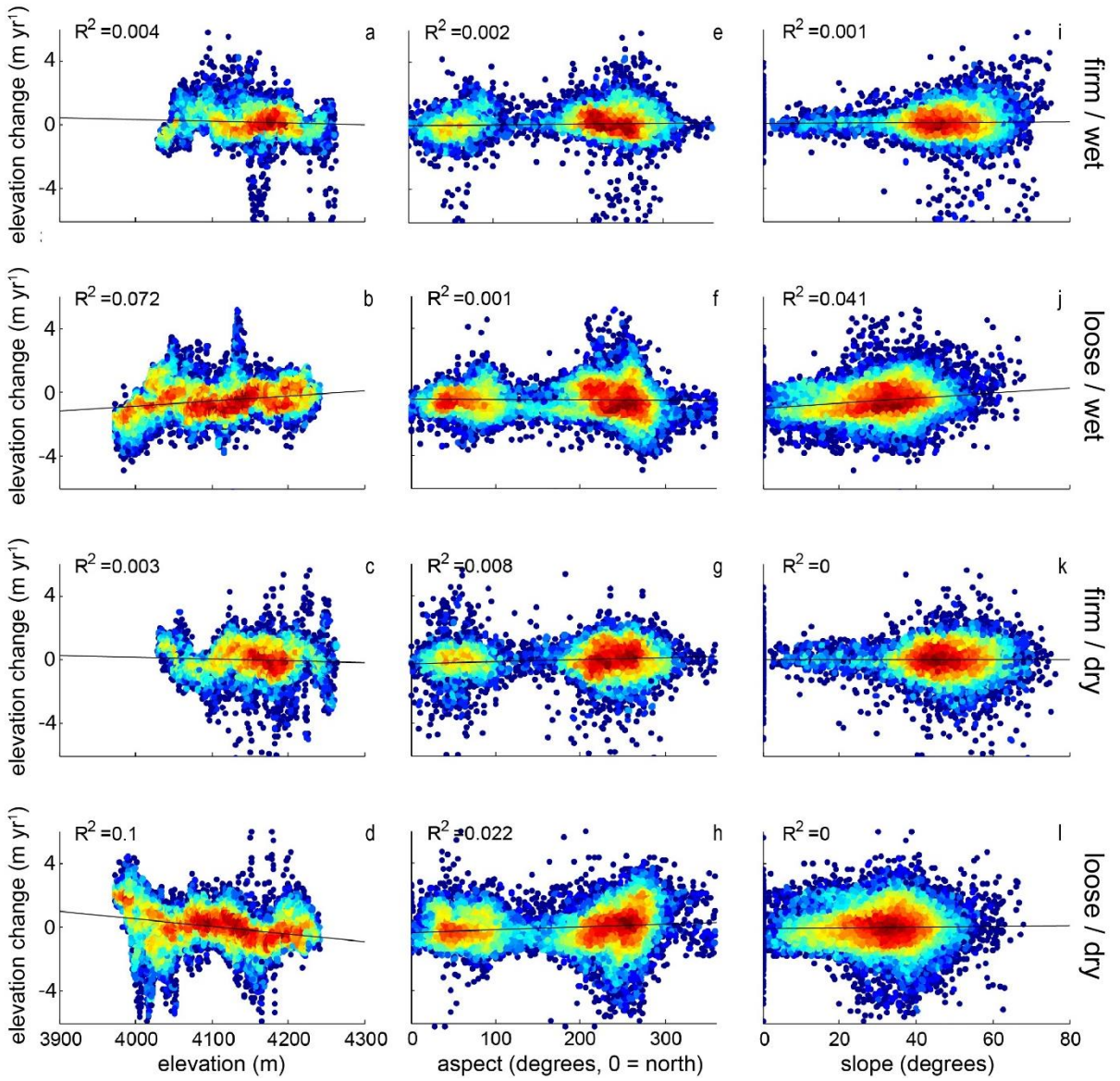

Figure 11; Correlation between elevation change and elevation (a-d), aspect (e-h) and slope (i-l), divided per season and surface type. None of them show a clear relation. From blue to red, the color indicates the data density.

3.3.2 Moraine velocity

The velocity of the moraine is determined using the COSI-Corr software (Ayoub et al., 2017) package as well as manually. It was found that the debris on the entire moraine slowly moves downslope as a block. First, the performance of the COSI-Corr software is assessed for this application, followed by the patterns observed. Finally these patterns will be compared with the elevation differences at these locations.

3.3.2.1 Applicability of COSI-Corr

The performance of the COSI-Corr software in computing moraine velocities is assessed by comparing the computed velocities to 100 manually measured point velocities (Figure 12). Over all ranges of displacements, the unfiltered COSI-Corr output has weak predicting capabilities, with an R^2 of 0.59 and a RMSE of 1.82 m yr^{-1}. The firm part of the moraine is not included in the sample points, but as the velocities on this section are generally low, the RMSE is likely to decrease if this section also is incorporated. The median error between the measured and calculated velocities is 27%. Of course, 50% of the values fall within this error margin. For the loose part of the moraine, 21% of the displacements are overpredicted by the COSI-Corr software, with a maximum error of 10.6 m yr^{-1}. At even more locations (29%), COSI-Corr underpredicts the actual displacements. This underpredicting is most likely caused by the fact that the software only works on blocks of cells, and does not trace individual features. On larger slow moving areas such as a glacier surface, this does not pose any problem. However, on more mobile areas, where besides a slow moving block also individual features are mobile, it seems less suitable.

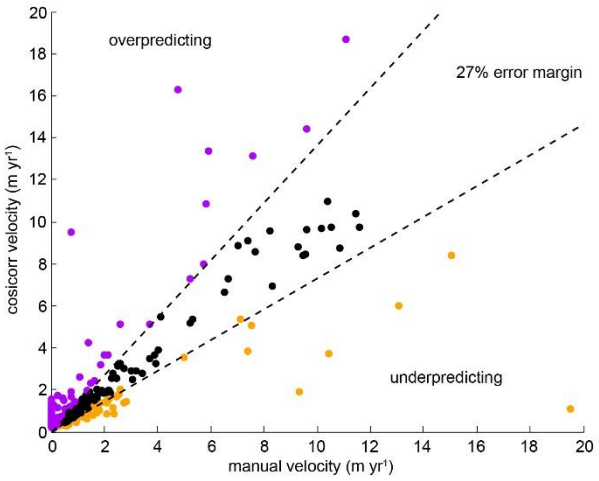

Figure 12; COSI-Corr correctness, with 27% error margin. Note the large amount of vales that are not predicted correctly. Each point represents one of the sample points that is tracked over the entire period.

The absolute error is often not as large as the RMSE calculated here, which is dominated by large errors at higher velocities. Seasonal velocities on the moraine are mostly below 2 m yr^{-1}. To see if the temporal and spatial pattern shows a better (visual) correlation, those will be compared now.

3.3.2.2 Spatial and temporal pattern

As already indicated from the sample points (Figure 12), there are large differences in velocity. These differences are observed both in the temporal and spatial dimension. First of all, there is a large difference in velocity between the wet and dry season. The median velocity in the dry season is 0.72 m yr^{-1}, compared to 0.76 m yr^{-1} measured manually. In the wet season the displacement is much larger, namely 1.06 m yr^{-1} according to the images, which also corresponds to the 1.16 m yr^{-1} from the samples. This increase in velocity is mostly caused by an increase on the loose part of the moraine, as the firm part only shows a minor difference in displacement between the wet and dry season (Table 2). The temporal difference between the loose and firm part of the moraine is also clearly visible in the spatial overview of the central part of the glacier, where the upper (firm) part of the moraine has smaller displacements throughout the year. Within the loose zone, there are also

large spatial differences (Figure 13). The patterns observed in the COSI-Corr images thus match with the patterns from the manual sample. Therefore it is assumed that this method is suitable to give first indications about the relation between the moraine sliding velocity (displacement) and the elevation differences at those locations.

Surface type / **Season**	*Loose*	*Firm*	*Mean*
Wet	1.24	0.44	1.06
Dry	0.80	0.38	0.72

Table 2; Average values of season velocities (m yr^{-1}), dependent on the season and surface type. The values are derived from the COSI-Corr software.

3.3.2.3 Correlation with elevation difference

On the firm part of the moraine, there is little difference between the displacements in different seasons, as is there little change in elevation difference between the seasons. Thus, as expected, no trend can be seen when comparing the variables velocity and elevation change for the firm part of the moraine. In the dry season, there also does not seem to be a relation between the between the velocity and elevation change on the loose part. During the wet season, with both high moraine velocities and erosion rates, a strong decreasing trend on the loose part can be observed considering displacements of less than 2 m yr^{-1} (Figure 14, B). On average, sedimentation seems to take place if velocities are smaller than 0.4 m yr^{-1}. If velocities get larger the amount of erosion increases until velocities approximately reach 2 m yr^{-1} (Figure 14). Between displacements of 0.4 m yr^{-1} and 2 m yr^{-1}, the average elevation change is -0.74 m yr^{-1} in the wet season. With higher velocities, the trend disappears and the average erosion rate is also smaller, with a mean of -0.3 m^{-1} per wet season.

By far the largest proportion of measured displacements (75%) is smaller than 2 m yr^{-1} in the wet season. Using a smaller range of velocities is susceptible to errors, but most of higher velocities are accompanied by a relatively low SNR (Signal to Noise Ratio). The high SNR might be caused by the fact that these higher velocities are related to tumbling rocks, which might cause erosion, but have a too large displacement to be correlated with erosion values. Thus at locations with a high velocity (>1.6 m yr^{-1}) it make less sense to compare these velocities with elevation change.

3.3.3 Surface roughness

In this investigation, the surface roughness is used as a measure for the average grain size of an area, as a larger roughness indicates larges differences in elevation, related to larger rocks and boulders. First, the characteristics of the roughness will be discussed, followed by a comparison with the local grain size and its relation to the active moraine.

3.3.3.1 Characteristics of surface roughness and grain size

Spatially, the roughness maps don't vary much in time, with minimum values of $z_o = 0$ and maximum values of z_0 ranging between 2.2 and 3.5. In general, the mean moraine roughness is slightly (5%) higher after the dry season (0.231) than after the wet season (0.220). This is probably caused by more widespread depositional zones, which generally have a lower roughness. For the remainder of this section, the roughness derived from the May 2016 DEM will be used, as this covers the entire study area and is a DEM from after the dry season, and thus has fewer disturbances from vegetation.

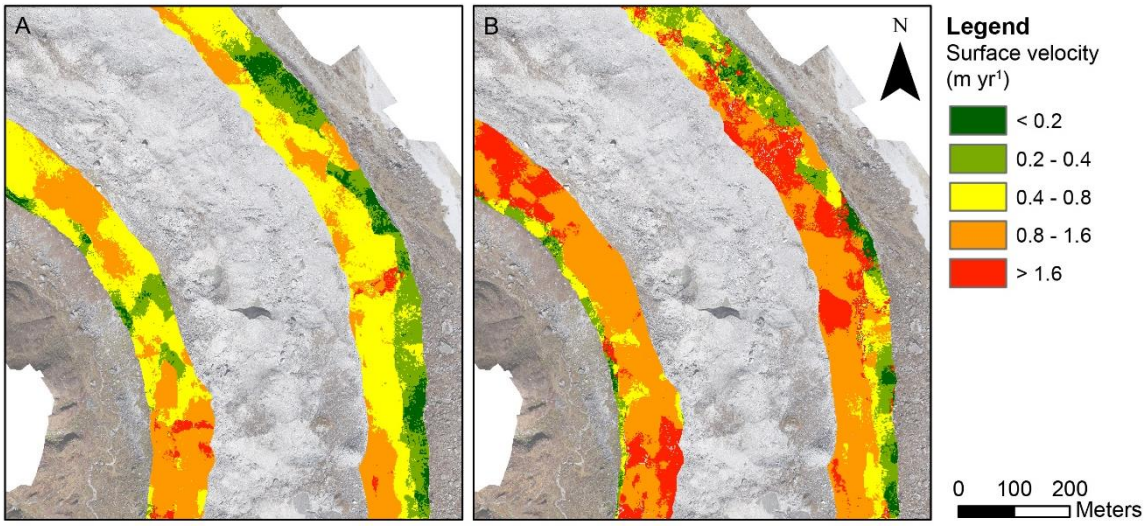

Figure 13; Surface velocity per season. Dry season values (A) are generally lower than wet season (B) values. In both seasons the firm part of the moraine is far less mobile than the loose part.

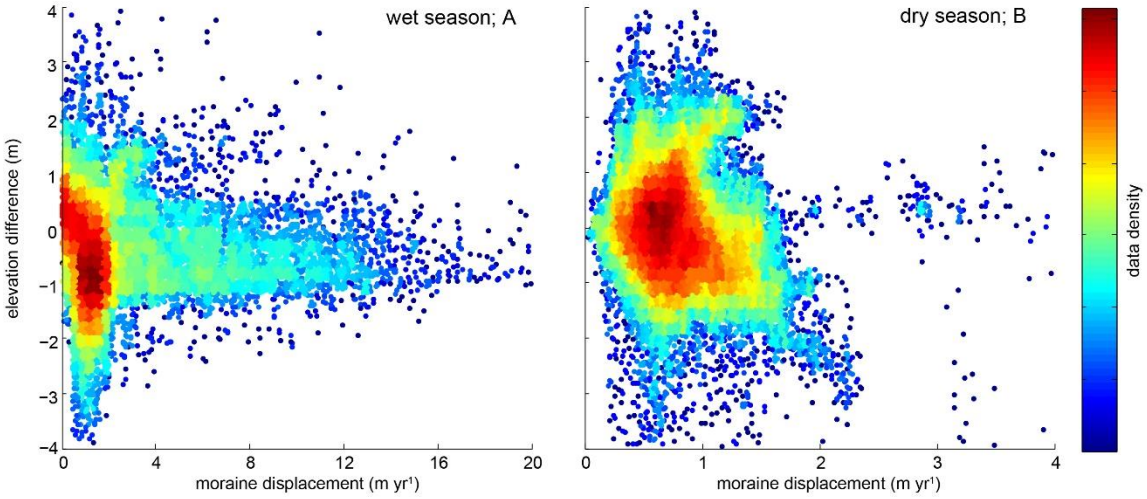

Figure 14; Relation between velocity and erosion on the loose part of the moraine. The relation is absent during the dry season (B), but a trend is observed regarding lower velocities (< 2 m.) in the wet season (A).

Despite that the vegetation cover after the dry season is smaller than after the wet season, it still affects the pattern. This causes the generally much higher roughness on the western moraine (Figure 15, A). The eastern moraine has less vegetation cover and the distinct pattern is clearly visible here. This pattern consists of high roughness values in the firm part of the moraine, caused by the gullied topography and many large boulders sticking out of the moraine wall. At many locations the smallest roughness can be found just below this firm zone (washout zone, Figure 6; Figure 15, B-C). In this washout zone fine material eroded from the gully systems in the firm part of the moraine is deposited, which causes these low roughness values. Towards the bottom of the moraine, grain sizes increase again.

When the roughness is compared to the manually delineated grain diameter, it is clear that there is a correlation between these two. Though the relation seems weak (R^2 = 0. 42), it is assumed that the surface roughness derived from the DEM (Nield et al., 2013) gives a good indication of the grain size, given the initial DEM resolution of 0.2 m (Figure 15, A). Highest grainsizes are found on the firm part of the moraine, with a maximum median grain size of 27 cm.

3.3.3.2 Relation to elevation difference

The roughness can be seen as a measure of erosivity of the debris, as large roughness lengths indicate larger grains which are more difficult to transport. No relation between the elevation difference and the roughness/grain size could be distinguished on the firm part of the moraine. This is probably caused by the fact that hardly any erosion happens on the firm part of the moraine. Second, roughness on the firm part is dominated by elevation differences between gullies and ridges, which are not directly related to the current erosivity of the material. Therefore the firm part of the moraine is excluded from the following section. On the loose part, the hypothetic nonuniform relation between roughness and erosion/sedimentation is true. Figure 16 shows a low surface roughness in the washout zone, where fine material from the firm part on the moraine is deposited.

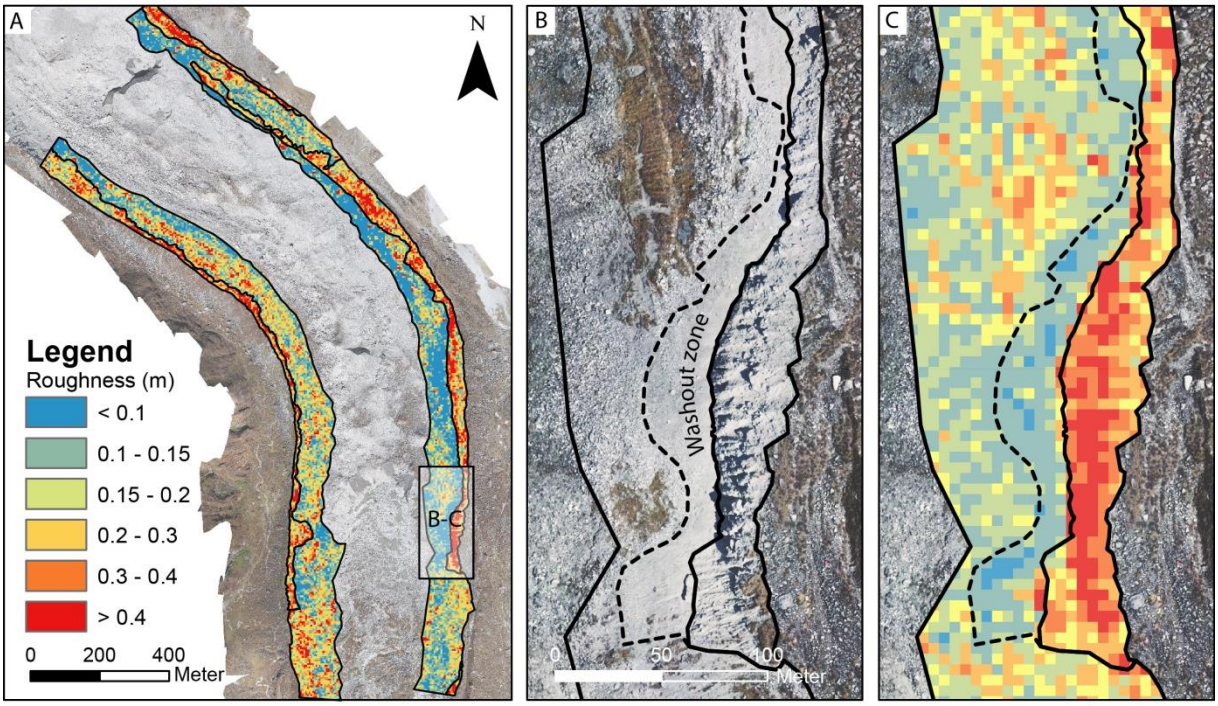

Figure 15; Roughness of the moraine in May 2016. The most rough patches are found on the firm part of the moraine (A), and most smooth patches are often observed just below that firm part in the 'washout zone' (B-C).

On the other hand, this area is often the location where most erosion happens, especially in the wet season (Figure 8-9). These figures also show that towards the bottom of the erosion decreases, in combination with an increase in roughness (Figure 16). The latter process seems to be more important, as there is a positive relation between grain diameter/roughness and elevation difference (Figure 16, B-C). Areas with a lower roughness are thus assumed to currently have a higher erosivity. However, this can only be seen with small grains, with a diameter up to 10 centimeters. This indicates a process where water flow is an important factor, as larger grains have a higher entrainment threshold (Van Rijn, 1984) and are thus not transported.

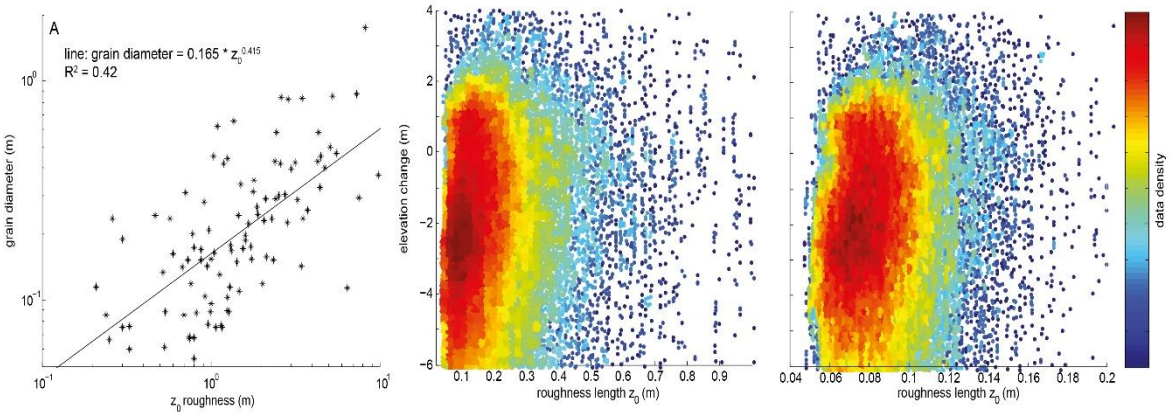

Figure 16; Correlation between roughness and erosion. A) Relation between DEM-derived roughness and 100 manually selected grains. B) Relation between roughness length and elevation difference from the loose part of the moraine C) Relation between elevation difference and grain diameter, not the larger spread as result from the relation between roughness and grain size.

3.4 Lateral moraine erosion processes

Correlating elevation change values to causing factors does give a first insight in the importance of different processes for debris transport on a lateral moraine, but do not provide a general overview of the relation between these processes. The data above is combined here to create a conceptual model of moraine erosion and sediment transport.

In terms of erosion processes, three processes could be distinguished from the data. These are erosion due to running water (entrainment and debris flows), larger mass movements (slumps or rockfall) and solifluction of the loose part of the moraine. Of these, erosion due to water is probably the most important. This can also be seen in the upper part of the orthophotos images (Figure 17, A-B), which is intensely gullied. From there debris flows and sediment loaded streams run down over the lower part of the moraine, and sometimes onto the glacier. These are most likely in the wet season, when rainfall intensity and duration is more favorable for triggering debris flows than during the dry season. Due to the high roughness of the terrain (Figure 17, F) and due to the local gullied topography, water concentrates quickly on the firm part of the moraine. The high slope (Figure 17, E) causes these flows to reach a high velocity, and thus increase in erosive power. Figure 17 (C) demonstrates this, as erosion values suddenly increase just beneath the firm part of the moraine. The sharp increase at this boundary is even exaggerated by a decrease in slope at this point (Figure 17, E), where the water accumulated above seems to plunge into the lower loose material. Towards the bottom of the moraine, erosion values decrease or sedimentation takes place, as the flow velocity decreases. Lowering of flow velocities and the accompanied sedimentation is enhanced by the higher roughness towards the bottom of the moraine (Figure 17, F). The increased roughness

is obstructing flow and furthermore the space in between grains increases, where water can flow through, leaving the previously entrained sediment immobile.

The second process, larger slumps or single rock slide, is observed multiple times over the entire period, but always initiates on the firm part of the moraine (Figure 8, 10). An example of small mass movements can also be seen along the upper edge of the moraine (Figure 17, C). These processes result in large negative elevation change values, and these are supported by the orthophoto where the slump scarf is observed. Furthermore the eroded area is often less rough, and multiple rocks that could be found here before, can be traced downslope. These mass wasting processes, especially larger ones, also have a great influence on the processes downslope. The material that slumps down, is deposited downslope and disturbs the general erosion pattern (Figure 17, C). At locations beneath a slump, the erosion increases in the years after, as the loose deposit is susceptible for erosion. Besides these slumps, there are also known cases of individual rocks tumbling down the moraine. This probably happens as a result of oversteepening of the slope below due to the processes mentioned above. The rocks included in the glacial till, which are generally much larger than the surrounding matrix, become unstable and roll or slide down (Figure 10). This process is still ongoing, as many of the currently stable rocks on the firm part of the moraine are already sticking out, instead of still being completely incorporated in the moraine (Figure 17, E).

With the third process, material slowly slides downslope as a whole, without altering the arrangement of the rocky surface. This process is most abundant on the loose part of the moraine, while the firm part is much more stable (Figure 17, D). It is most visible on those sections that are not so much affected by water flow, such as the lower part of Figure 17 (A-B). However, as the velocities on the entire loose part of the moraine are higher than those on the firm part, it is not unlikely that this process also happens on locations of which the surface is altered by water flow, though it is not always visible there. In the case of solifluction, this is even very likely, as the abundance of water flow favors the formation of ice lenses. Though this process is less severe than water flow erosion, and is probably responsible for less erosion of the total moraine, it is a process that continues all year, also in the dry season. The process also might have a large influence on the distribution of debris over the glacier, as the slowly moving material can push away the material that is currently at the edge of the glacier.

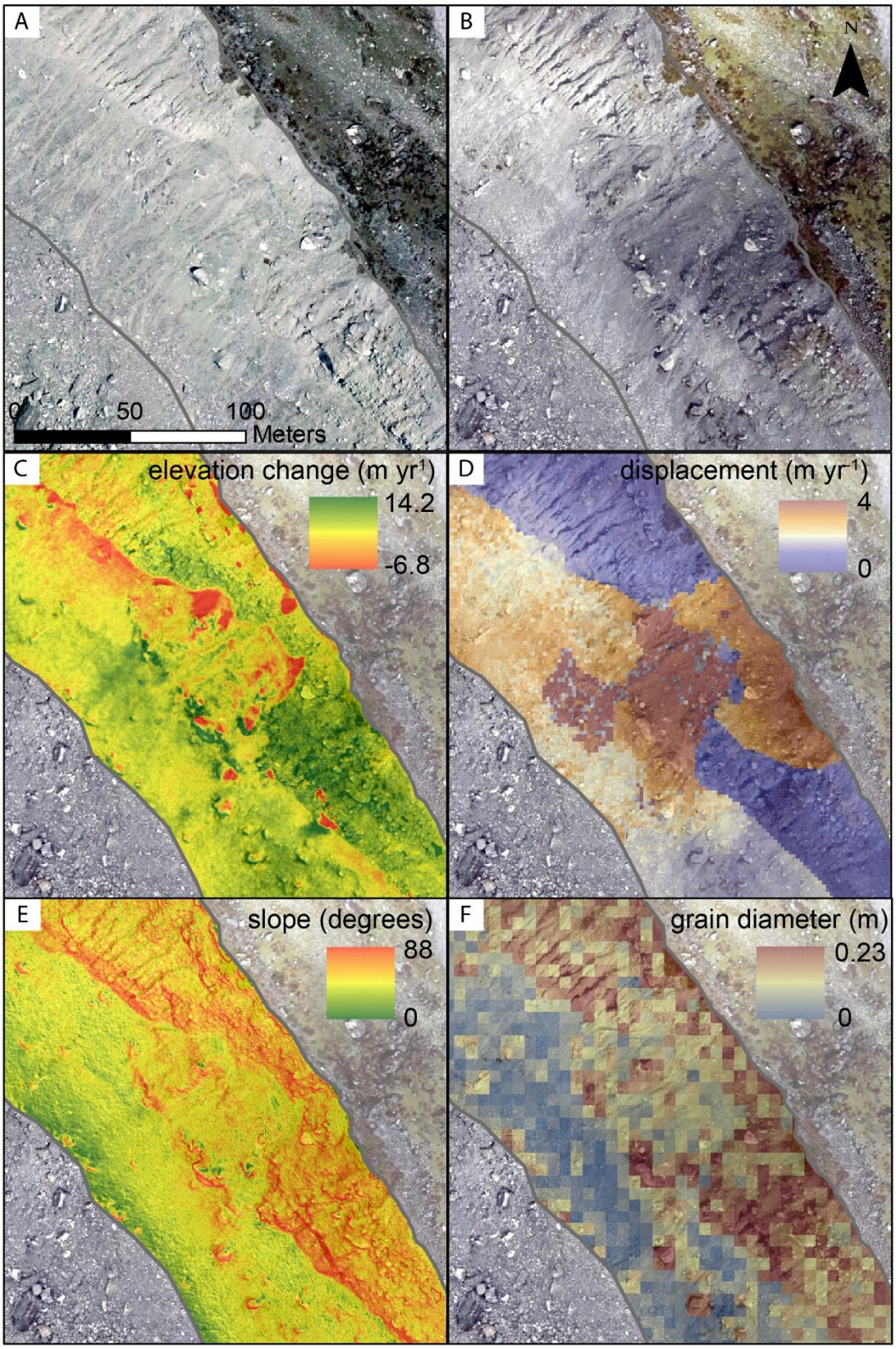

Figure 17; Erosion processes on the moraine. Observed features from May (A) and October (B) 2016, are compared with possible erosion triggers (C-F) to find the processes that occur on the lateral moraine and are responsible for the large amount of moraine downwasting observed.

4. General model setup

After focusing on the transport processes on the moraine in the previous part, the second part of the research works towards a model that simulates the transport processes on the glacier. The goal of the model is to calculate the distribution of moraine derived sediment over the glacier. The model consists of two different parts. The first part focusses on the moraines and the amount of material that is delivered to the glacier, which runs with a cell size of 0.2 m. The second part focusses on the glacier and the redistribution of the debris across the glacier, after it is deposited at the margins of the moraine, which runs at a cell size of 2 m. The general layout of the model is show in Figure 18, below which references can be found to more detailed explanations of the processes.

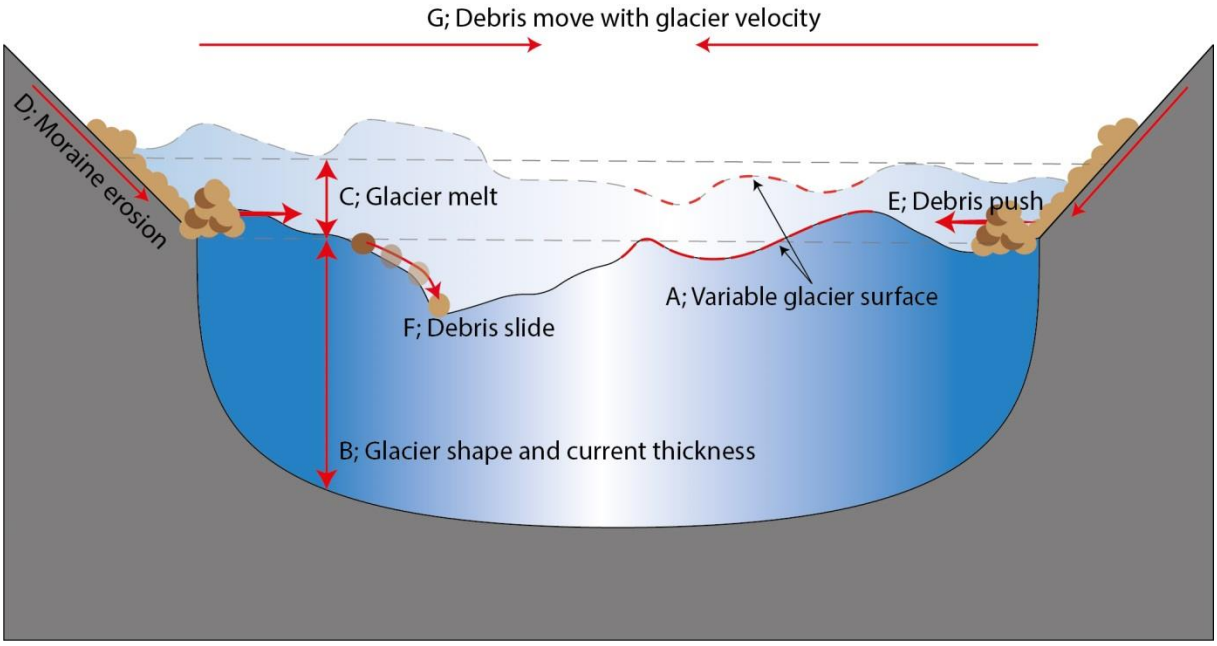

Figure 18; 1D visualization of the model processes. Additional information about the included process can be found in 4.1.1 (A), 4.1.2 (B), 4.1.3 (C), 4.2 (D), 4.3.2 (E), 4.3.3 (F) and 4.3.4 (G).

4.1 Modelling glacier characteristics

Two characteristics of the glacier, the surface variability and the glacier thickness, are included in the model. The method of creating these is first explained.

4.1.1 Glacier surface characteristics

The glacier surface elevation has lot of local variation (Figure 18, 19). These are initiated by differences in debris cover, and the accompanied differences in melt processes (Ragettli et al., 2016). Furthermore, in addition to a spatially variable surface elevation, it also varies through time, though no exact values are known for the rate of change. The current Lirung glacier also has a large local variation in ice thickness, as each patch of 100 x 100 m has on average a standard deviation of 10.7 m and an average difference between the highest and lowest variation of 70 m. This surface variation is also added to the smooth glacier surface in the model. The created variation for the model has approximately the same characteristics, with a standard variation of 11.4 m and a mean difference between the highest and lowest point of 63 m. It is assumed that over a period of 30 years, the surface variability changes completely, in such a way that the current surface variability is not influenced anymore by that of 30 years ago.

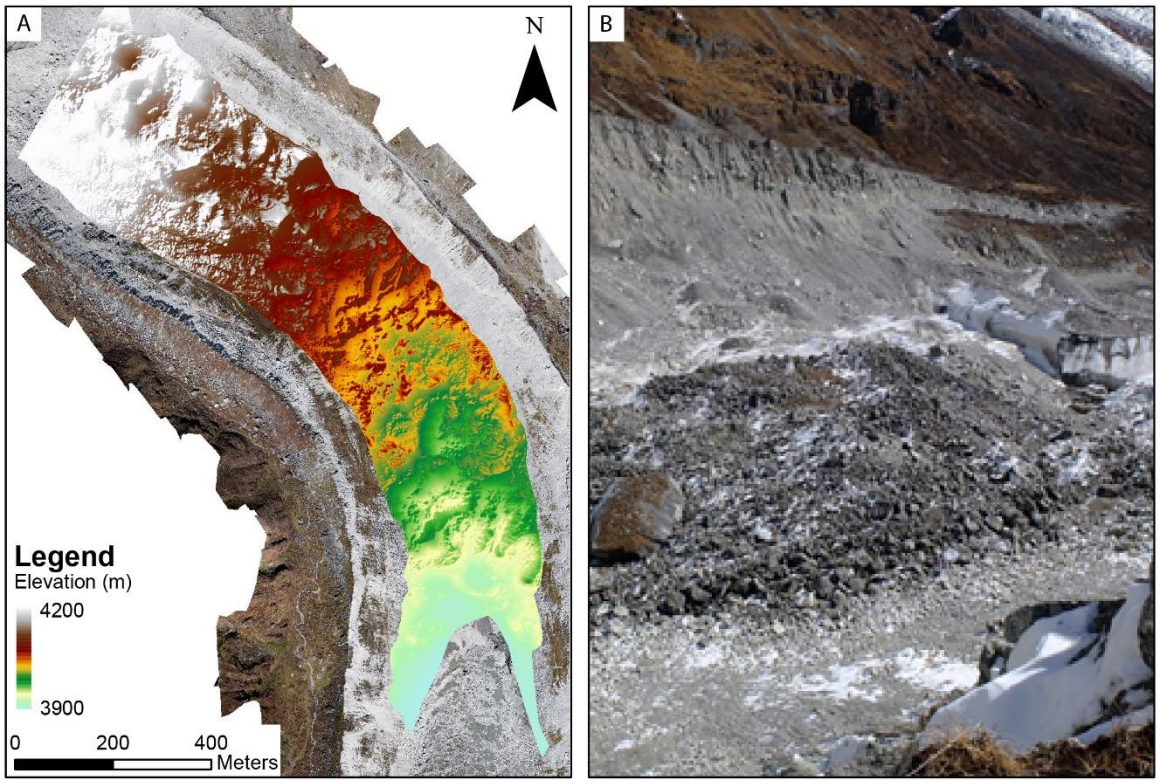

Figure 19; Surface variability on Lirung. The variability is visible in both the DEM (A) and on photographs taken from the lateral moraine of the glacier (B).

4.1.2 Current glacier thickness

On top of local variability on the glacier surface that changes the thickness of the glacier, the glacier thickness is also variable over its width (Figure 18). The glacier thickness is an important parameter in the model, as it alters the glacier velocity (Section 4.3.4), and as due to glacier melt it exposes moraine to erosional processes (Section 4.2).

First the current glacier thickness is determined using a method based on Haeberli & Hoelze (1995). They calculate the mean ice thickness (h_f) in km. along the central flow line of the glacier as:

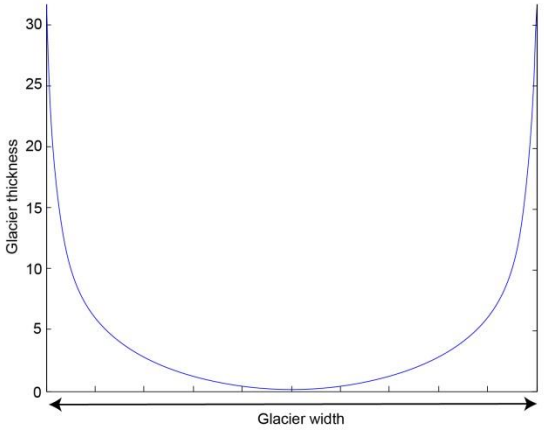

Figure 20; Cross section showing the shape of the modelled glacier. Glacier thickness values are derived from the terminus.

$$h_f = \frac{\tau}{f \rho g \sin \alpha} \quad (2)$$

With the constants f, the ratio between the driving stress and basal stress of the glacier, with a value of 0.8 (Haeberli & Hoelzle, 1995), ρ, the density of the glacier (900 kg/m^3) and g, the gravitational constant (9.81 ms^{-2}).

τ, the average basal shear stress (Pa) is calculated as a function of the elevation difference between the start and terminus of the glacier (ΔH) in km.

$$\tau = 0.5 + 159.8\,\Delta H - 43.8(\Delta H)^2 \quad (3)$$

The slope α is the mean slope over a reach of 200 m, to filter out any local variation and deriving the actual glacier slope.

After the glacier thickness along the central flowline is determined, the glacier thickness towards the side of the glacier is extrapolated using a logarithmic function, resulting in the shape of Figure 20.

4.1.3 Glacier downwasting

Besides the current glacier thickness, the debris thickness through time also is modelled (Figure 18). During the little ice age (LIA) the glaciers in the region advanced for the last time, resulting in the buildup of large lateral moraines. The glacier surface at that time was approximately at the elevation of the current moraine crest, and the glacier downwasted after this. For the Lirung glacier, the moraines corresponding to the last glacial advance in the LIA are dated to 1633 CE. The end of the LIA and start of the glacier melt is harder to determine, but many glaciers probably remained close to their LIA maximum until the end of the 20th century (Rowan, 2016). Therefore, we assume that substantial glacier melt started approximately 150 years ago.

The glacier downwasted by -0.78 m yr^{-1} between 1974 and 2000 and for -1.99 m yr^{-1} between 2000 and 2010 (Nuimura et al, 2017). These values correspond with the downwasting rate found over the wet summer season of 2013 by Immerzeel et al., (2014b), who reported a downwasting of -1.09 m over only the summer season. An average downwasting rate of -1.99 m yr^{-1} is assumed suitable for the 2000 – 2017 period. The maximum moraine height bordering the current glacier is approximately 85 m, and the glacier has thus downwasted this amount since the end of the LIA. From 1974 to 2017, a period of 43 years, the glacier thinned by approximately 54 m. In the years before the glacier has thus thinned 88 - 54 = 34 m. Assuming a total melt period of 150 years, the average downwasting rate between 1867 and 1974 was 0.32 m yr^{-1}.

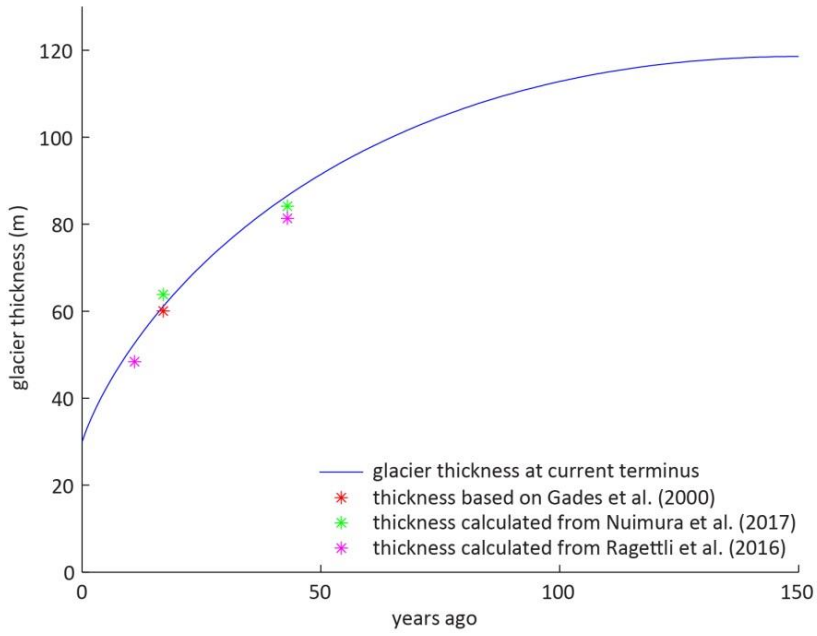

Figure 21; Glacier thickness at the current terminus. In total a decrease of 87 m over 150 years, an average downwasting rate of 0.58 m/yr. The modelled glacier thickness matches the values derived from other studies at Lirung glacier. The calculated thickness is in line with values found in literature.

As the melt rate probably changed gradually, a logarithmic function is used to describe the dynamic downwasting rate D_r (m yr^{-1}) of the glacier:

$$D_r = -0.6\log(time + 1) + 0.6\log(151) \quad (4)$$

where $time$ is the amount of years before present. This function was found having the best fit with the melt rates (Nuimura et al, 2017; Immerzeel et al., 2014b) and results in a total downwasting of 87 m (Figure 21).

Assuming a mean glacier thickness of 30 m at the glacier terminus, the glacier thickness through time at that location was approximately 115-120 m at the end of the LIA (Figure 21).

While the glacier melts, more and more moraine is exposed. The moraine is expected to have existed in its current state below the glacier, as no exact information is abundant about the evolution of the moraine walls after glacier melt. The part of the moraine that is above the glacier surface, is susceptible to erosion (as calculated in 4.2).

4.2 Modelling moraine erosion

As soon as the moraine elevation is larger than the glacier elevation, erosion starts to occur. The moraine model, focusing on this erosion, uses slope as a proxy for the amount of erosion. The moraines are divided into a firm and loose zone, of which the mean erosion is determined per season. In the dry season, the elevation change values are close to zero, and are set to 0 in the model (Section 4.2.1). In the wet season, the mean erosion for the loose part is set -0.5 m yr^{-1} and the mean erosion for the firm zone equals -0.1 m yr^{-1}. For the firm zone, this value is higher than the seasonal data found on the moraine (Section 3.2.1). However, the over the total observed area there is a decrease on the firm part of the moraine of -0.1 m yr^{-1}. The fact that the firm part also is eroding is confirmed by the many erosional features seen on the firm pat. The moraines on both sides of the glacier are divided in 10 zones with equal width at the same side of the glacier, resulting in a total of 20 input zones.

Though a weak change is observed between the slope steepness and the amount of erosion (Figure 11), a much stronger relation can be found between the slope and the area of erosion. To show this some preliminary results will be discussed, followed by the actual model input.

Per season the amount of cells that is eroding is calculated for any slope angle (Figure 22, A). This shows a normal distribution around the most occurring slope value, which is at slopes between 34 and 35 degrees (Figure 22, A). During the wet season, a maximum 1628 cells between 34° and 35° are eroding, while during the dry season only 675 cells are eroding at these slopes. Besides the fact that a larger area is eroding during the wet season, this on average also happens on steeper slopes than during the dry season (Figure 22, B). As the data is normalized against their maximum value a ratio can be calculated:

$$Ratio = \frac{dry\ season_{cells}}{wet\ season_{cells}} \quad (5)$$

As this ratio is larger than 1, relative more erosion occurs in the dry season. This is the case on lower slope angles, indicating that during the dry season lower slopes (probably on the loose moraine) are relatively more susceptible to erosion than during the wet season. At high slope angles, the fraction of erosion that happens in the wet season inreases, as these slopes are less abundant in the loose

part of the moraine. However, note that this does not imply that the total erosion volume is also larger, as the total eroding area (Figure 22, A) remains higher in the wet season.

As a final step, the moraine is further divided in a firm and loose part. Also, amount of eroding cells is divided by the total amount of cells in that zone, resulting in the fraction of cells that shows erosion. The fraction is calculated per slope and zone (Figure 22, C). It shows that more cells are eroding during the wet season. Furthermore, the eroding area on the firm part of the glacier seems to be independent from the slope angle, while on the loose part there is a negative relation between slope and eroding area. Through the irregular data, linear trendlines are fitted using the least-squares method.

$$Loose_{wet} = -8.2 * 10^{-3} * M_{\alpha} + 0.965$$

$$Firm_{wet} = -1.2 * 10^{-3} * M_{\alpha} + 0.4385$$

$$Loose_{dry} = -4.3 * 10^{-3} * M_{\alpha} + 0.390$$

$$Firm_{dry} = 0.0443$$

where M_{α} is the moraine slope (degrees). Though the $Firm_{dry}$ is also influenced by the slope steepness, its influence is so small that it is neglected for this purpose.

The negative relationship between slope and erosion area is counterintuitive, but is probably caused by deprivation of sediment on the steeper parts. Many authors (Wanatabe et al., 1998; Ballantyne & Benn, 1994) suggest that the highest erosion rates occur directly after deglaciation, and that the most erosive parts of the moraine get quickly stripped of its debris. This indicates an unstable and very active system, in which steep slopes are eroded and talus slopes are deposited below. This is supported by the fact that the current firm section is hardly eroding, and that almost the entire loose section is around its angle of repose (35^{o}). Combining these two facts, it is very well possible that steeper parts (generally steeper than the repose angle) are currently already deprived from most of its loose debris cover, inhibiting erosion. Assuming erosion occurs with slope processes as water flow erosion, it can be argued that these transport more material from the lower slopes, as the amount of transportable debris is simply higher.

The fraction of cells that are eroding can also be seen as the probability of a cell for erosion. If for example the trend line results in a value of 0.6, that location has 60% chance that it is eroding. The modelled amount of erosion is calculated by comparing these values with a random value between 0 and 1 (Figure 22, B1). As the random value is smaller than the trend line value, the mean erosion value for its zone (0.25 and 0.05 for the loose and dry part, during the wet season) is assigned (Figure 22, B2). Within each of the 20 lateral zones, the total amount of erosion is calculated by adding up the erosion values of all the cells (Figure 22, D1). The erosion input to the glacier is then calculated by dividing the total amount of erosion by the amount of cells from that zone which are bordering the glacier surface.

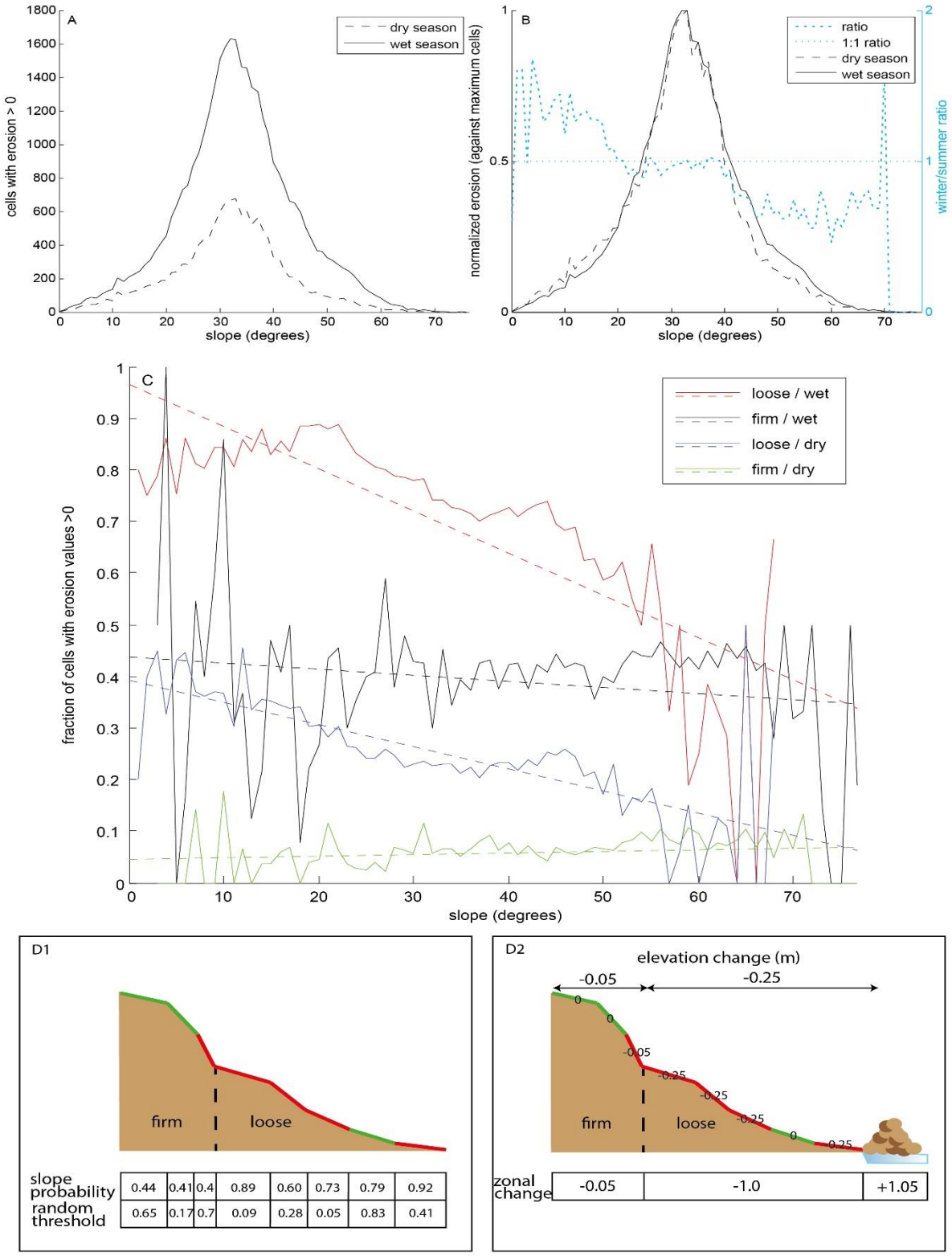

Figure 22; Method of moraine erosion calculation in the debris distribution model. (A) shows the absolute amount of cells that are eroding, in (B) these values are normalized against the maximum amount of eroding cells, showing the offset between the two seasons. The final plot (C) shows the fraction of cells that are eroding, and the least squares fitted lines through that data. (D) shows the method of final erosion calculation in 1D, which is in the model done for 2D zones instead of 1D transects. The slope probability values are those derived from the trend lines. If the random threshold is smaller than the trend line, erosion occurs (red surface). If no erosion occurs (green surface), 0 is assigned (D1). At all the eroding cells, the mean elevation change is assigned. To find the total erosion, all of these values are added up.

4.3 Modelling debris distribution

The second part of the model focusses on the debris displacement on the glacier, distributing the debris outward from the moraine. The debris that is eroded from the moraine walls, ends up at the boundary of the glacier and is from there further distributed over the glacier surface. The model uses three different processes to simulate this. First, material is pushed away from the boundary by the new debris, second, the material slides down on glacier slopes, and third the material moves along with the movement of the ice (Figure 18, 23).

4.3.1 Debris input

Along the boundary of the glacier, the eroded material is deposited according to the previously established lateral zones. The debris height at the boundary is obtained by dividing the total amount of erosion (m) by the amount of cells at the border between the glacier and the moraine.

4.3.2 Debris push

The first transport process is the debris push. As the new material slides or rolls down the moraines bordering the glacier, it pushes or knocks the existing debris away from the edge. The material is pushed away perpendicular to the moraine boundary, assuming mean aspect of the moraine at that location is approximately the same as the aspect of the lower boundary of the moraine. The push distance is set to the maximum runout distance of mass movements on the moraine.

A measure for this *'push distance'* is the reach angle of the movements on the moraine. The reach angle (R_α) is the maximum runout angle, between the start of a mass movement and its final depositing position, or

$$R_\alpha = \arctan(H/L) \tag{6}$$

Where H elevation difference (m) and L the horizontal length between the starting point and deposition location of the mass movement (m). The lateral moraines seem to be dominated by a combination of rockfall and debris flows. The minimum reach angle for rockfall ranges between 28° and 34° (Lied, 1997; Evans and Hungr, 1993). For debris flows the values are typically around 26° (de Haas et al., 2015), but have a large range between 3° and 45°. As the reach angle on the lateral moraines is generally steeper than this 26°, a minimum reach angle of 34° is chosen suitable for the moraine.

With this method, the maximum runout length dependent on the reach angle (R_L) increases with an increasing elevation difference between the base and crest of the moraine, which is calculated as

$$R_L = \frac{H}{\tan(R_\alpha)} \tag{7}$$

Thus, the runout length increases as the glacier melts. If R_L is larger than the length of the moraine, the push length is determined as the part of R_L that is larger than the length of the moraine. If the runout length is larger than the length of the moraine, the material will already deposit before it reaches the end of the moraine, and thus at these locations the push length is set to zero (Figure 23, C).

At the glacier boundary, all material is pushed as a result of the new material input. At the maximum distance of the push length, none of the material is pushed away anymore. In between, a logarithmic

function calculates the decrease in push fraction, given the distance away from the moraine boundary (Figure 23, B2).

4.3.3 Debris slide

The second process that moves material over the glacier velocity is the debris slide. The glacier surface is not a smooth surface, but contains many ridges and lower areas (Figure 19). Therefore, debris material moves over the glacier surface by sliding down these slopes. Moore (in press) modelled debris instability on a glacier and found that most instability is a result of slope over steepening. For the sake of simplicity, only this process is included in the model.

Sliding can only occur if the slope is steeper than a slope threshold, set to 35°, which is a common angle of repose for stable talus slopes with the characteristics of debris located on the glacier (Goudie, 2004). Also, the debris thickness has to be larger than a debris threshold, set to 0.2 m of debris. With a lower debris thickness, the debris probably only consists of one layer of boulders, which is assumed to be anchored in the ice, and thus not able to move.

The sliding distance of the debris is calculated using the reach angle of 34°. As the movement process is caused by the same processes as on the lateral moraine, namely slope oversteepening and water flow, a reach angle of 34° is also applicable for supraglacial debris movement (Figure 23, B1). However, as the terrain on the glacier is rough, many local pits exist, such as supraglacial lakes (Figure 23, A). Thus the sliding distance (S_L) per local catchment is calculated as

$$S_L = min\begin{cases} R_L \\ Pit_L \end{cases} \tag{8}$$

taking the minimum value of the runout length determined by the reach angle, and the maximum possible runout distance to the nearest pit on the glacier (Pit_L).

With these input parameters, the model calculates the effect of local debris sliding on the glacier surface. It is assumed that the material moves relatively fast, and is able to transfer the entire distance within one time step, being 3 months. To do this, first the surface elevation is computed, which is called combine (C, (m)).

$$C = DEM + D_{thick} + G_{var} \tag{9}$$

where DEM is the glacier elevation (m), D_{thick} is the debris thickness (m) and G_{var} is the glacier surface variation (m). Based on this elevation, material sliding down is based on the Moore neighborhood of a cell (8-connected pixels), which is expressed as $Variable_{i\pm1,j\pm1}$, and the center cell ($Variable_{i,j}$). First, the Moore neighborhood cells are checked to have a lower C than the center. To each of these cells debris will slide down, based on the difference in elevation to the neighboring cells. The steeper the gradient to the adjacent cell, the more material will slide towards that cell. The fraction F of the material that will slide to a lower boundary cell is:

$$F_{i\pm1,j\pm1} = \frac{C_{i\pm1,j\pm1} - C_{i,j}}{\sum (C_{i\pm1,j\pm1} - C_{i,j})} \tag{10}$$

which practically is the difference in elevation of a single cell divided by the sum of the differences in all surrounding cells.

The material that slides out of the center cell ($SO_{i,j}$, m) is calculated as

$$SO_{i,j} = \frac{min(C_{i\pm1,j\pm1} - C_{i,j})}{1 + F_{i\_min,j\_min}} \quad (11)$$

which divides the minimum elevation difference between the center cell ($C_{i,j}$) and one of the bordering cells ($C_{i\pm1,j\pm1}$) by the fraction (Equation 7) assigned to the cell with the minimum elevation difference F_{i_min,j_min} plus 1. This inhibits center cell values to become smaller than the surrounding lower cells. At last, the amount of material sliding out of the center cell ($SO_{i,j}$) cannot be larger than the amount of debris present in that cell ($D_{thick;i,j}$).

$$SO_{i,j} = min\begin{cases} SO_{i,j} \\ D_{thick;i,j} \end{cases} \quad (12)$$

The amount of material that slides in to the neighboring cells (SI, m) is then calculated by

$$SI_{i\pm1,j\pm1} = F_{i\pm1,j\pm1} * SO_{i,j} \quad (13)$$

Afterwards, the amount of material sliding in to a cell is added to the already existing debris cover at the same location. This process is repeated several times, so the maximum sliding distance calculated before can be reached. An algorithm roughly based on the same assumptions, though more complex and including more variables, is included in mass transport models such as RAMMS (Christen et al., 2010) and TopFlowDF (Scheidl & Rickenmann, 2011).

4.3.4 Debris move

The third process, with which the material is transported over the glacier, is the transport of debris along with the movement of the ice mass. The direction of the glacier movement for the wet and dry season is derived applying the COSI-Corr method to the orthophotos of the glacier. In the model, the data from Kraaijenbrink et al. (2016) is used, thus the direction of movement is based on the data of May and October 2013 (wet season) and October 2013 and May 2014 (dry season).

The glacier velocity related to the thickness of the velocity, along with other factors (Gantayat et al., 2014). The glacier velocity (m/s) is calculated according to

$$U = \frac{2}{3} A * H^4 * f^3 * (\rho g * \sin\alpha)^3 \quad (14)$$

The variable factors in this equation are the glacier thickness H (m) and the slope α (degrees) of the glacier along its flow path. Additional parameters complete the equation, which are a creep parameter A with a value of $3.24*10^{-24}$ ($Pa^{-3}s^{-1}$) for temperate glaciers (Cuffey and Paterson, 2010) and f, ρ and g as earlier described. Combining the direction and velocity of the glacier results in the final velocity maps, with which the debris and the glacier surface variability moves along with the glacier.

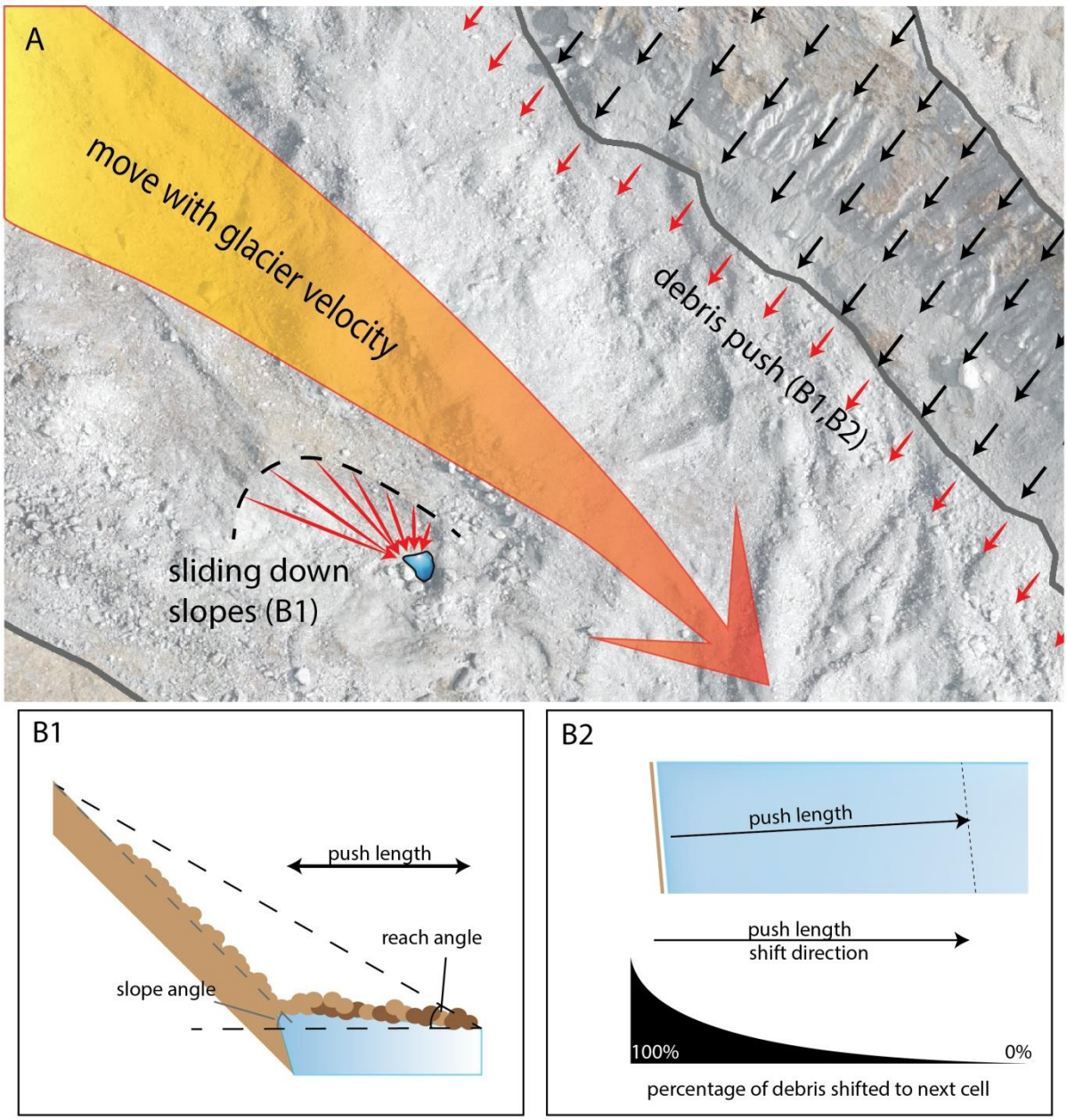

Figure 23; Ideal visualization of processes distributing debris over the glacier. (A) Debris push from the moraine side, sliding down slopes on the glacier surface, and the movement with glacier velocity are the transport processes modelled. From these, the push length (B1) is important, with the amount of material pushed decreasing away from the glacier edge (B2). Note the increase in dark (old) debris in comparison to light (new moraine derived) debris in B1.

4.4 Model runs

All the processes above play a role in supplying or distributing debris, and are used in two different model applications, which are linked to two possible hypotheses concerning the distribution of the glacial moraine derived debris. The first possibility (1) is that the moraine is the source of all debris on the glacier. The second option (2) is that the moraine is not the source of all debris, and that the debris originating on the moraines is mixed with supraglacial debris from other sources. If the first option is true, the model can make a simulation without additional information. However, if the second possibility is true, the other debris might influence the distribution of the moraine derived debris, for example in the sliding, as the debris threshold is exceeded earlier. To model this assumptions are made concerning the debris supply further up the glacier.

If we assume that the distribution of moraine debris is not affected by debris from another origin (1), the change in supraglacial debris is modelled, starting with a clean glacier, and without further debris input. When modelling the other option (2), the input of supraglacial debris of other sources is simulated by starting with a debris cover of 0.5 on the glacier. During simulation, a constant debris thickness of 0.5 m is created at the top of the glacier. To find the final distribution of the moraine sediment, a simulation with only debris from other sources is subtracted from a simulation with both the other source and moraine derived debris.

4.5 Sensitivity analysis

Finally, two types of sensitivity analysis were carried out. First, a one-at-a-time (OAT) sensitivity analysis was carried out, to find the sensitivity of the model to a change in a certain parameter (McCuen, 1973). This part indicates the relative effect of the input parameters on the model outcome, and indicates of which parameters validation is most important. Afterwards, a global sensitivity analysis (Monte Carlo simulation) was carried out with those parameters that had a large influence on the debris distribution pattern. This analysis indicates the total range of outcomes that is possible, given the uncertainties in all input parameters combined.

For the OAT analysis, the parameters are changed either with a percentage (+/- 20%), or within a range of values that is found suitable from literature or field experience (Table 3). The range of values indicates an uncertainty, which arose from assumptions regarding erosion and distribution processes, partly caused by a shortage of field observations of these processes. The Monte Carlo (MC) simulation was carried out using the parameters reach angle, surface variability change rate, debris threshold and erosion trend. The glacier velocity was not variable in the MC simulation, as the OAT analysis indicated that of these parameters it had the smallest influence on the final result (Figure 27). A uniform probability is assumed around the values, thus making them all equally likely to occur. Between minimum and maximum values of the parameters in Table 3, one value is taken at the center. This resulted in a total of 81 model runs.

Parameter	
Reach angle (^{o})	28; 30; 32; 34
Surface variability change rate (yr)	20; 30; 40
Debris threshold (m)	0.2; 0.4; 0.6; 0.8; 1.0
velocity (m yr^{-1})	*0.8; *1; *1.2
Erosion trend	-stdev; 0; +stdev

Table 3; Parameters and the corresponding values used for the sensitivity analysis.

5 Model results

This section will describe the results of the different parts of the model, as well as the results from the sensitivity analysis.

5.1 Moraine erosion model

The moraine erosion model calculates the amount of erosion on the moraine, which is equal to the debris input to the debris distribution part of the model. Note that this model does not simulate actual erosion processes, but only calculates the amount of erosion. Erosion only occurs in the wet season, and is calculated based on the section of the moraine that lies above the glacier surface, the mean measured erosion and the erosion probability given the slope and surface type.

Besides the melt of the glacier, the retreat of the glacier is also modelled. Therefore, the total debris supply to the glacier surface is not only dependent on the part of the moraine that is susceptible to erosion, but also on the length of the glacier. Therefore, the values in this section are based on the amount of erosion along the length of the current glacier. On this section of the moraine, the volume of eroded debris increases from 52 m^3 yr^{-1} to approximately 43.000 m^3 yr^{-1} (Figure 24, A). The increase is not linear, as erosion rates start to increase quickly after approximately 70 year. Two processes are responsible for this. First, the melt is fairly low during the first years of simulation, but also start to increase after approximately 70 years. From here on, the moraine is increasingly fast exposed and susceptible to erosion. Secondly, by that time the glacier has melted approximately 15 meters, and the loose part of the moraine starts to be exposed. As the erosion values on the loose part are much higher than on the firm part of the moraine during the wet season (0.5 and 0.1 m yr^{-1} respectively), the total erosion volume increases quickly. This development is even more distinct in the elevation loss (Figure 24, B), where the change in slope is more abrupt. The elevation loss is also more variable, as it decreases at the start of the simulation, starting from 0.03 m yr^{-1}. After the lowest value of approximately 0.02 m yr^{-1} is reached after 15 years, the elevation loss increases to almost 0.13 m yr^{-1}.

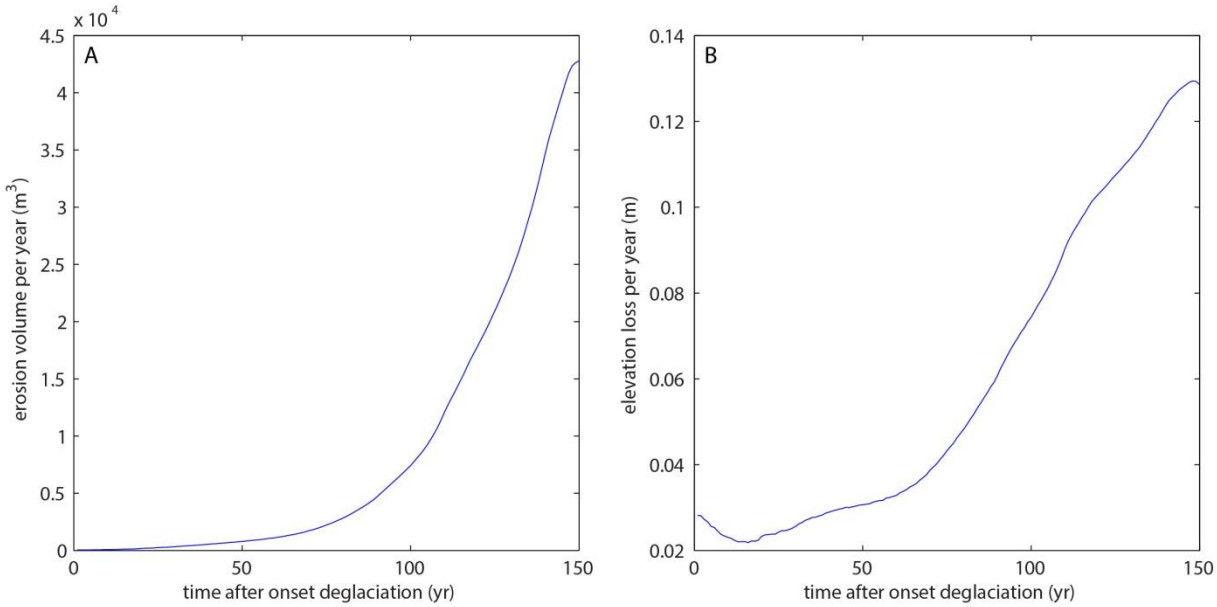

Figure 24; Results of the moraine erosion model. (A) shows the smooth increase of total erosion volume. The pattern is less smooth this value is converted to the elevation loss per year (B). Note that the values are the values along the current length of the glacier.

5.2 Supraglacial debris distribution

Based on two assumptions regarding the origin on the supraglacial debris, the simulation is done with different input parameters. In both simulation, an adapted version of the data discussed above is used. The debris distribution pattern will be discussed at four different time steps; after 50, 100, 125 and 150 years.

A first simulation is made, starting with an empty glacier surface, to which debris is supplied from the lateral moraine At all time steps, the maximum debris thickness is not found directly on the margin of the ice, but slightly inward (Figure 25), as new material coming from the moraine pushed the old material further onto the glacier. The debris derived from the moraine also does not reach the center of the moraine, as the maximum distance from the glacier edge towards the end of the moraine derived debris ranges between 54.4 and 68.1 m. Though the maximum debris distance from the edge decreases towards the end of the simulation, the mean distance increases throughout the period due to an increase in total debris volume. This also causes the mean debris thickness to increase to 2.18 m, at cells with a debris cover. As a final result, the percentage of the ice mass that is covered by moraine derived debris increases towards 22.4%. This is partly caused by the increase in distance to the moraine, but even more by a decrease in glacier surface area, due to both downwasting and terminus retreat. These values are in the same order as found by McCarthy et al. (2017) and Ragettli et al. (2015), who found debris thicknesses between 0.11 - 2.30 m and 0.2 - 2.5 m respectively on the current Lirung glacier If it is assumed that all the supraglacial debris is derived from the lateral moraines, only small bands along the moraine would be covered with debris. As the entire glacier is currently covered, other sources must also supply debris to the glacier. The debris derived from other sources, such as rockfall in the moraine cirque, also interferes with the moraine derived debris and changes its depositional pattern. The second model simulation thus calculates the moraine derived debris distribution incorporating the debris input to the glacier outside the study area.

On the current glacier, debris is still modelled to be mostly found in a band near the moraine-glacier boundary, but especially in the lower part a band of debris (> 2 m) can be found at the center of the moraine. After 50 years, the covered fraction of the glacier is 48.4% and afterwards decreased even further to 29.4% (Figure 26). The loss of debris cover is mostly along the moraines. The width of the band of debris along the moraine decreases from approximately 150 m to less than 30 meters over the simulation period. Also note the sudden loss of substantial debris cover near the glacier terminus from 25 years ago until now (Figure 26, C-D). Only at the upper margin the debris cover increases, due to constant debris feed at the upper boundary of the simulated area. Due a combination of the loss of debris cover and an ongoing debris supply to the glacier, the mean debris thickness increases from 0.64 m after 50 years to 9.2 m currently. Despite the larger spread of moraine derived debris across the glacier, the band along the moraine has nonetheless a smaller area as in the simulation without additional debris (Figure 26, E). No mean and maximum debris distance from the moraine is calculated, as the pattern is much more diverse and the debris is not only found along the moraine boundary.

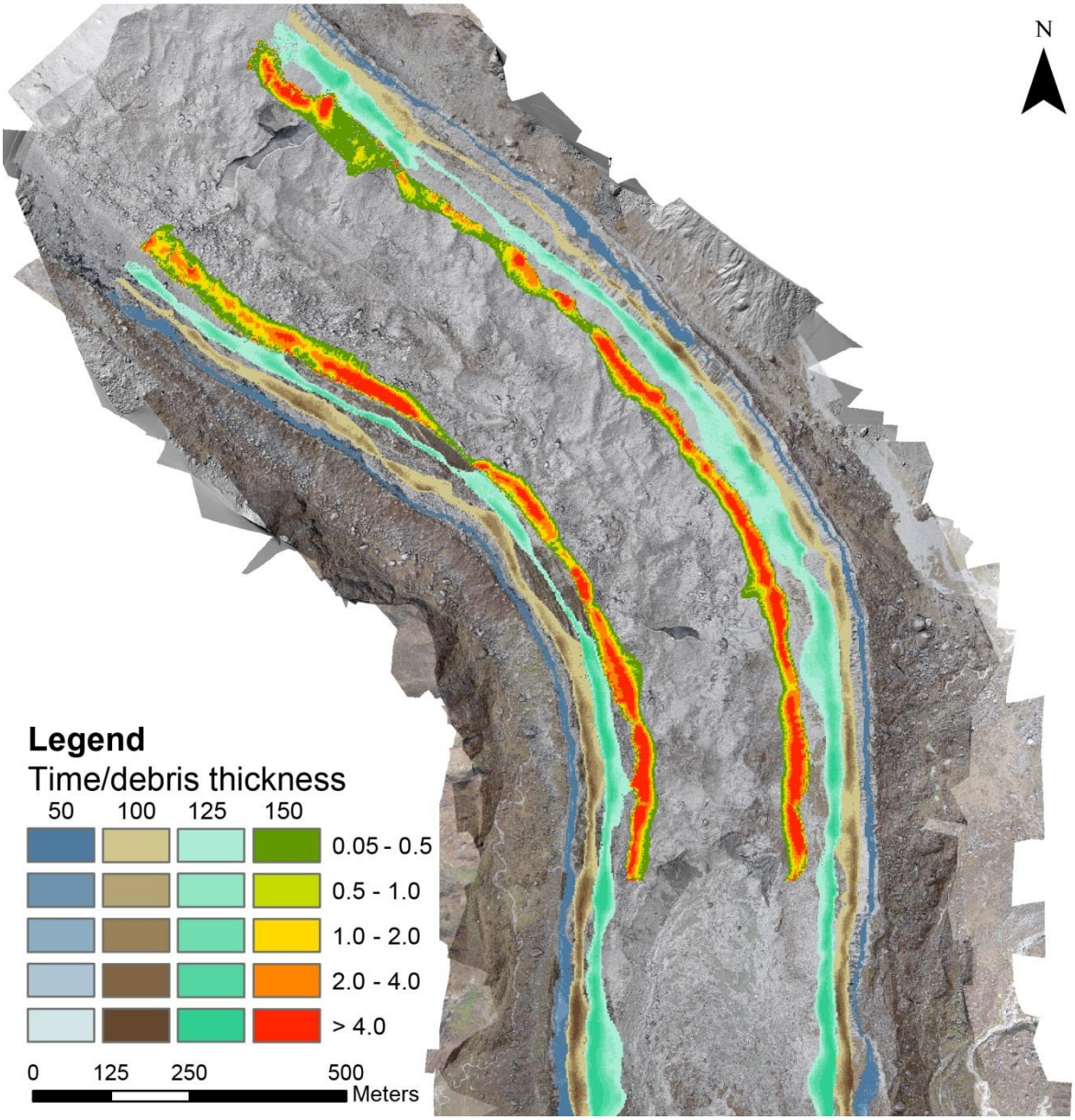

Figure 25; Model output at different timesteps visualized by different color scales. Current glacier thickness at timestep 150, has moved inward in comparison to the start of the simulation, as the glacier width decreased.

Timestep	Mean debris thickness (m)	Mean distance from moraine (m)	Maximum distance from moraine (m)	Percentage of glacier surface covered (%)
50	0.42	21.3	65.1	7.3
100	0.71	21.6	68.1	13.4
125	1.50	25.3	62.0	15.5
150	2.18	29.5	54.4	22.4

Table 4; Results of the model simulation, assuming all supraglacial debris is derived from the lateral moraines.

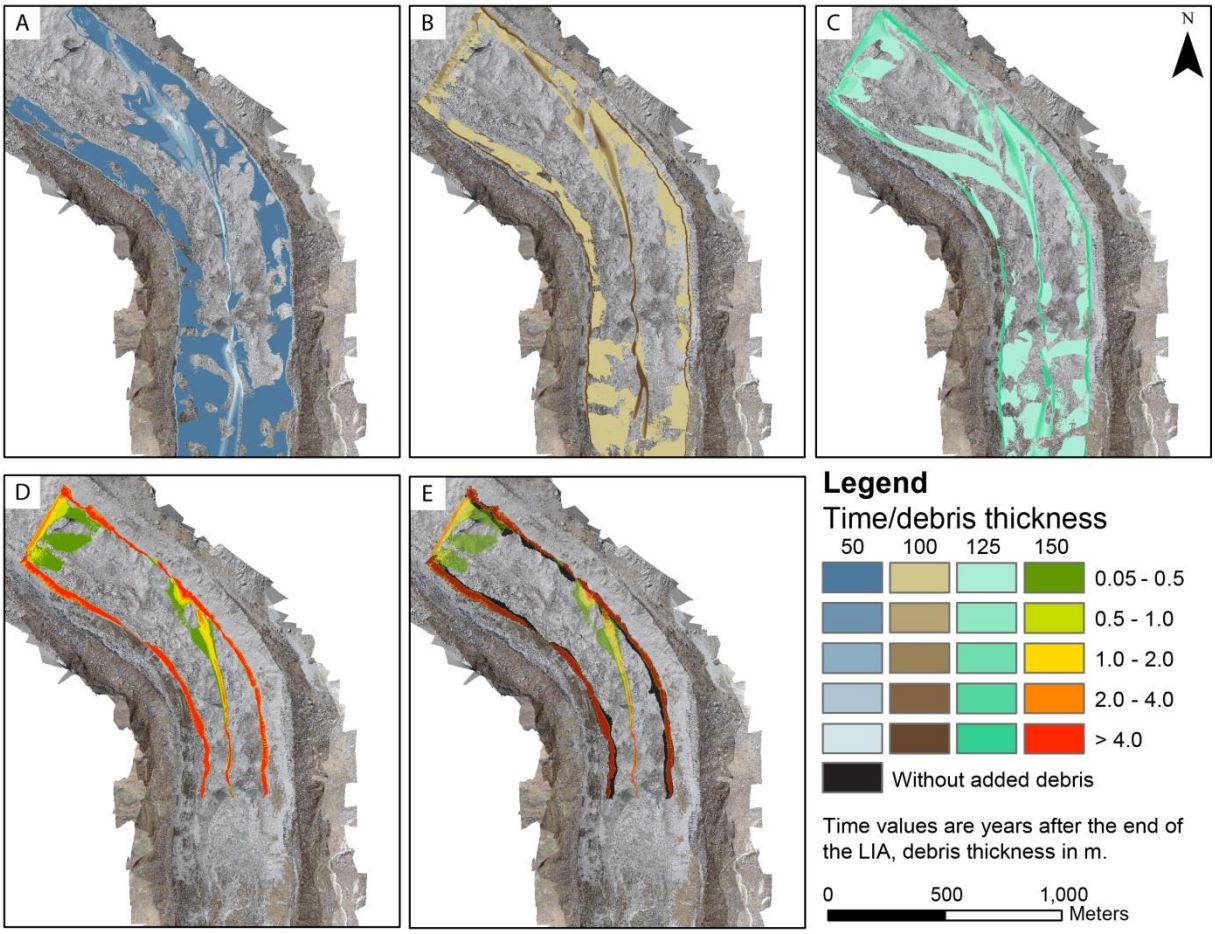

Figure 26; Debris distribution pattern from the model, assuming not all debris on the glacier is derived from the lateral moraine. The plots show the distribution pattern from time steps 50-100-125-150 (A-D), and a comparison with the result without additional debris supply (E).

Timestep	**Mean debris thickness (m)**	**Percentage of glacier surface covered (%)**
50	0.64	48.4
100	1.74	37.9
125	3.92	30.3
150	9.19	29.4

Table 5; Results of the model simulation, assuming not all supraglacial debris is derived from the lateral moraine. This other debris influences the moraine derived debris transport over the glacier.

5.3 Sensitivity Analysis

To quantify the robustness of these results, two types of sensitivity analysis were performed. One in which one parameter at a time was changes (OAT) and one Monte Carlo simulation where multiple parameters were altered (MC)

The first analysis (OAT) was carried out to determine the sensitivity of the model to individual parameters. Two simulation outcomes were examined to determine the effect of changing the input parameters to the model output: The area with a debris cover > 0.01 m, and the median debris thickness of these cells. A threshold of 0.01 is chosen as many cells have smaller debris thicknesses, which do not have a large effect on the glacier and weakens the sensitivity pattern.

The debris covered area and the median debris thickness are not equally affected by a change in input parameters. The median debris thickness is more affected than the area that is covered by moraine derived debris. Furthermore, they are not equally sensible to the same parameters. The most important parameter influencing the debris thickness is the debris threshold, before debris starts to slide. As this value increases from 0.2 to 1 m, the median debris thickness increases by 68% (Figure 27, A-B). Furthermore, the median debris thickness increases (10%) as the amount of moraine erosion increases by 10%. The debris thickness decreases by approximately 17% if the reach angle is increased from 28^{o} to 34^{o}, decreasing the push length by 25%. The other two input parameters, the velocity and surface variability rate change, have a smaller effect on the debris thickness. These also have a minor influence on the debris covered area. In addition to these, a change in erosion input also hardly influences the outcome. An increase in debris threshold causes a small decrease (4%) in debris distribution, but debris covered area is by far most influenced by the reach angle. An increase in reach angle of 6^{o}, results in a decrease of cells with a debris cover by 40%. The two parameters that mostly influence the model outcome are the debris threshold and the reach angle, of which validation thus is most important.

In the Monte Carlo simulation, the glacier velocity is not incorporated, as it had the least influence on the model outcome. The other input parameters together cause the debris thickness to vary between 1.75 and 2.86 m, while the debris covered area can vary between $9.88*10^{4}$ and $1.55*10^{5}$ m^{2} (Figure 27, C-D). The covered area represents 21% and 33% of the total glacier area. The input parameters used in the model thus result in a debris thickness which is around the center of the possible values (2.18), while the covered area is near the lower edge of possible values (22.4%). From the MC simulation, it is concluded that the debris thickness is most influenced by the debris threshold and the reach angle, and the debris spread is mostly determined by the reach angle. This can be seen in two ways: First, the steeper the slope, the larger the influence. Second, the smaller the standard deviation band, the smaller is the influence of the other parameters included.

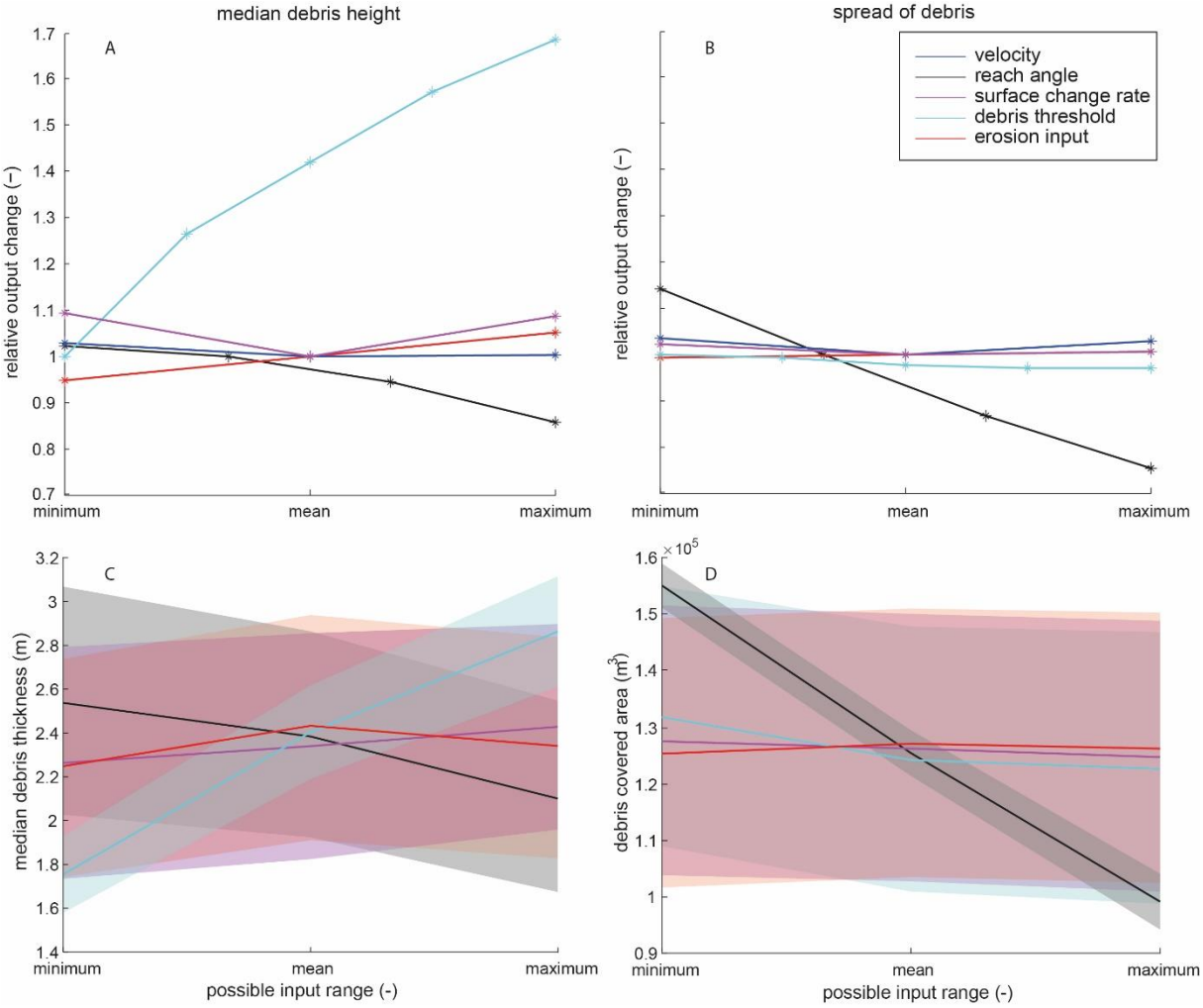

Figure 27; Sensitivity analysis for the debris distribution model. The minimum and maximum values on the x-axis are different per parameter, but can be seen in Table 3. The upper row (A-B) shows the results of the OAT simulations, the lower row (C-D) of the Monte Carlo simulation. If the value relative output change is 1 in A-B, it means that this value is used in the final model. It is thus possible that the relative output change is 1 at the minimum value, indicating that the minimum value within the possible range is chosen as most suitable for the model. In C-D the lines indicate the mean result, and the colored bands indicate the standard deviation of the results around the mean. Note that the OAT output is relative, while the Monte Carlo simulation is plotted using the actual values.

6. Discussion

6.1 Moraine characteristics

The general characteristics of the moraine seem to be typical for a paraglacial lateral moraine, as the slope is at many locations steeper than the angle of repose, and multiple moraine ridges below each other indicate different stages of glacial retreat and growth (Lukas et al., 2012). The general form of the moraine, with decreasing slopes towards the bottom and a difference between an intense gullied firm part of the moraine, and a loose rocky part at the bottom is also described by Curry et al. (2005), but can furthermore also be found at many glaciers in the Langtang area and worldwide (Figure 28). The moraines bordering the Lirung glacier are different from many other lateral moraines in the area, because large parts of the moraine are vegetated (Figure 28, A). It is known that there are many feedbacks between vegetation and geomorphic activity on a moraine, which influence the processes and decrease erosion (Eichel et al., 2016). However, by masking out these areas, but mostly by focusing on areas that along an across-moraine transect are free of vegetation, the interference with debris is kept to a minimum. The processes observed on the non-vegetated parts of the moraine are thus very unlikely to be influenced by the vegetation, and can also be applied to lateral moraines without vegetation on it.

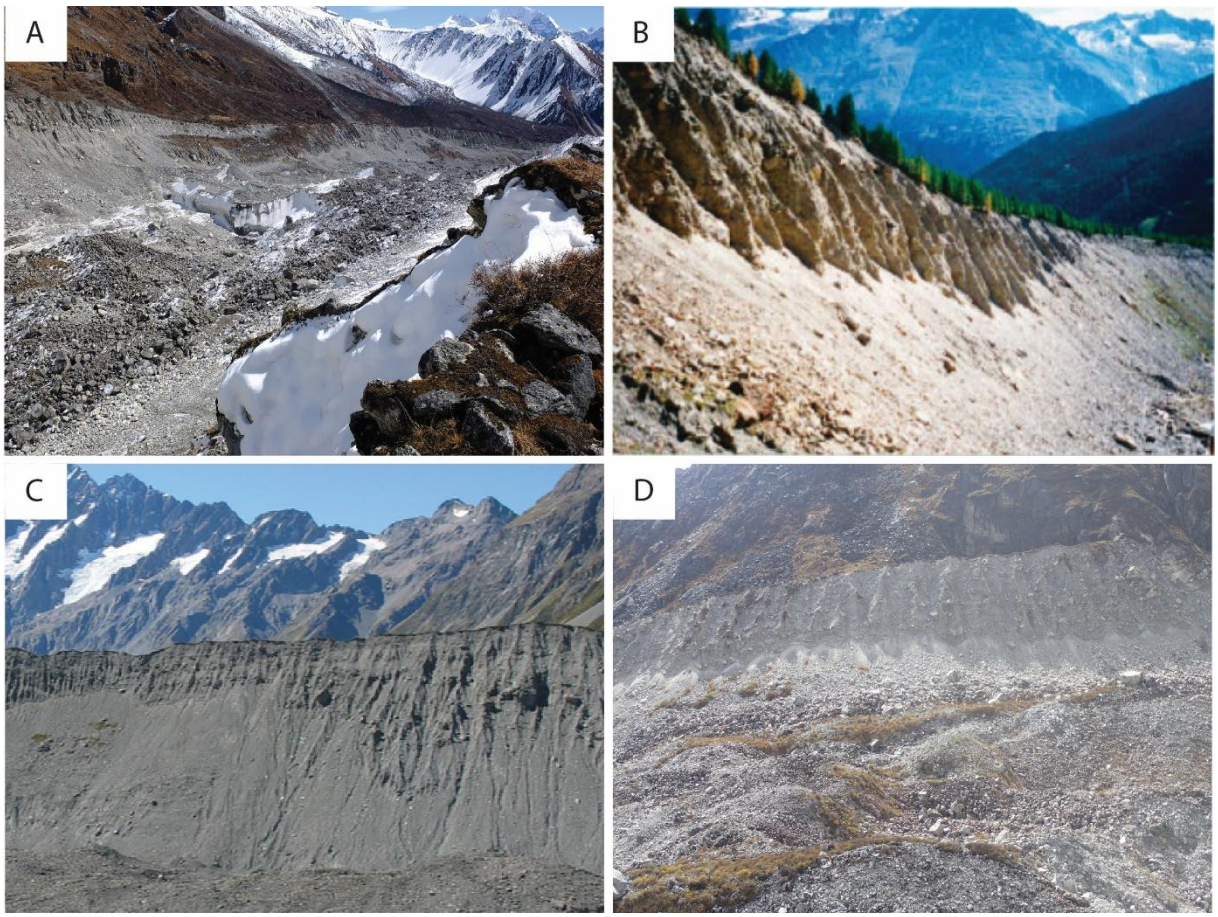

Figure 28; Lateral moraine comparison. Many glaciated or recently deglaciated areas across the world show the same characteristics as in the study area (A). Examples shown here are the Findelenglacier, Switserland (Curry et al., 2005), Cook glacier, New Zealand (©Burkhard Eherlinger, 2006) and Shalbacum glacier, Nepal (©Jakob Steiner, 2016).

6.2 Moraine elevation change

The elevation change on the firm part of the moraine equals +0.016 m yr^{-1} and +0.034 m yr^{-1} in the wet and dry season respectively. On the loose part of the moraine the elevation changes by -0.5 and -0.02 m yr^{-1} respectively. However, if the elevation change over the entire timespan is taken, the firm part has an elevation change of -0.10 m yr^{-1} and the loose part has an elevation change of -0.31 m yr^{-1} over a period of 4 years. These values do not match. This is caused by the fact that the period between October 2013 and May 2015 is not taken into account in calculating seasonal change, as no seasonal data was available for this period. However, as we assume that no erosion takes place in the dry season, the entire elevation change from this period happens in the two wet seasons within the timespan. Incorporating this data would result in a seasonal elevation change of -0.62 m yr^{-1} on the loose, and -0.08 m yr^{-1} on the firm part, which add up to -1.23 and -0.14 m over a period of 4 years, values near the actual erosion values. Though these assumptions seem reasonable, the actually measured seasonal elevation changes are used for comparison. Only in the model, the erosion value on the firm part is adapted, as using not adapted values would result in a large final error in the amount of erosion.

Though the average elevation change is below zero if it is taken over the entire timestep, it is still unlikely that on average sedimentation occurs on the firm part of the moraine, as there is nothing above to erode. However, the sedimentation values are very small (0.1 m yr^{-1}, and thus 0.05 m per season). As the data has an accuracy of approximately 20 cm, the sedimentation values are well within the uncertainty margin, and thus the area might actually be eroding.

As data with a seasonal resolution is scarce, comparison of erosion values are made using the yearly erosion rate of 0.25 m yr^{-1}. Average denudation rates over the last 550 years in the Langtang area (0.4 – 8 mm yr^{-1}) found by Wanatabe et al. (1998) are an order of magnitude smaller than the values found in this paper. They did also include the upper mountain slopes in their calculation, which substantially lowers the values found. Furthermore, it is known that erosion on paraglacial slopes diminishes after time, which can explain the difference between the current values and those found by Wanatabe et al. (1998). This seems plausible, as erosion values of more recent deglaciated moraines in Norway (-0.05 to -0.10 m yr^{-1}, Ballantyne & Benn (1994)) are already closer to the values observed on Lirung glacier. The same goes for the values observed by Curry et al. (2005), who found minimum erosion rates of 0.095 m yr^{-1} on recently glaciated terrain along the Findelenglacier in Switzerland. Besides being higher than paraglacial erosion near other glaciers, the values are even more extreme related to 'normal' erosion, indicating the extremely fast rate of slope alteration on debris-covered steep paraglacial slopes (Curry et al., 2005).

However, all of these only mention gully erosion, of which the values on the Lirung glacier indeed are in this range. The lower talus slope was left out of the investigation, as in this area sedimentation occurred. However, along Lirung glacier most erosion actually happens on these lower talus slopes, instead of on the gullied section. There are several possible causes that can explain this difference. As can be seen in (Figure 9) many of the debris/water flow marks run onto the glacier. These likely cause erosion on the moraine and deposit the material on the glacier, where thus the lower part also shows erosion. Secondly, a solifluction and or creep process can be responsible for this elevation change, which is not taken into account in these papers. At last, it is possible that the moraine is still ice cored, or that the loose part of the moraine is located on top of the glacier. In these cases, the elevation decrease might be caused by the downwasting of the glacier or the melt out of ice. The

presence of ice in the moraine, however, is unlikely, as this is mostly characterized by a hummocky topography of the moraine, which cannot be found (Lukas et al., 2012). The presence of ice underneath certain parts of the moraine cannot be excluded at this time, and further investigation with for example thermal of radio waves is needed to be able to find this out.

The downwasting rate of the glacier can be an explanation of this surprisingly high erosion value on the lower part of the glacier, but as there are also many erosive processes acting on this section, these alone are probably responsible for the entire elevation change.

6.2.1 Change correlation

When comparing possible causing factors to the elevation difference of the moraine, it was found that the slope steepness, moraine elevation and the slope aspect are hardly correlated to moraine erosion, which is in line with Curry et al. (2005). He did found a minimum slope angle of 30^{o} for gullies to form, which approximately matches the data from the Lirung glacier moraine.

The lack of a relation between erosion and aspect on the loose part of the moraine, indicates that the higher incoming radiation on South-West facing slopes is not high enough to substantially melt frozen soil (Nagai et al., 2013). This might indicate that solifluction processes do not play a role, but is more likely to be caused by the fact that the difference in incoming radiation is not large enough to substantially change the effect on solifluction.

However, the most striking and counterintuitive part is that the amount of erosion has a weak negative relationship with the slope. The absence of a strong relation is caused by the fact that erosion values in the loose zone are fairly constant in the across-moraine direction (Figure 8, 9), while the slope steepness is much more variable. The small variability in erosion values make sense, if it is assumed that the lower section of the glacier is gradually sliding down as a whole. The negative relation is probably caused by the fact that steeper slopes are already deprived of their debris cover, and less steep slopes have a substantial cover where more erosion possible is (Section 4.1.1).

Less counterintuitive is the relation between moraine displacement and moraine elevation change, as for the largest part of the cells (75%) there seems to be a clear relation between velocity and amount of erosion. With small displacements (< 2m yr^{-1}) higher velocities indicate higher erosion rates during the wet season. Furthermore, the highest amount of erosion is also found in this range of velocities. As these displacements are directly caused by a debris transport process, the moraine velocity is seen as an indicator for erosion, instead of the other way around. On the other hand, movement of the lower loose part of the moraine can be caused by lowering of the glacier, instead of erosional processes. However, as there is no relation found between the melt rate of the glacier and the velocity on the moraine, this is assumed not to be the case.

On glaciers, it is known that a slowing down generally coincides with a thickening of the glacier, where a speedup of glacier velocity stretches out the ice mass and causes a thinning of the glacier thickness (Joughin et al., 2004). This process also occurs on slow moving mass movements on slopes, such as occurring here. The difference in velocity on the loose part of the moraine between the dry and wet season, which on average changes from 0.80 to 1.24 m yr^{-1}, might cause differences in elevation across the moraine. This is supported by comparing the average wet season elevation difference with the difference in velocity between the wet and dry season. An increase in velocity

towards the wet season is clearly correlated to erosion, while a decrease of velocity towards the wet season is causing sedimentation in that area (Figure 29).

The roughness length (z0) on the moraine ranges between 0 and 3.5 m, but the 75-quantile of the data is located at 0.29. This is in line with values found on the glacier by Miles et al. (2017), who found values between 0.05 and approximately 0.5 m, which they linked to smooth surfaces and large boulders respectively. The maximum grain diameter of 0.27 m calculated from the roughness is thus likely underestimated in this calculation. From this it is assumed that the manually selected boulders do not represent the median grain size in its vicinity, or that the relation between slope diameter and roughness is not a power function. On the other hand, this problem might be solved for using a different window size for detrending the original elevation model, as this size greatly influences the result (Miles et al., 2017). Though the actual grain size values might be higher than those calculated, the pattern does not change, making the relation between erosivity and elevation change still reliable.

This relation indicates that larger grains are generally combined with less erosion, which makes perfectly sense regarding soil erosion and sediment entrainment laws (Renard, 1997; Garcia & Parker, 1991). Furthermore the smallest grain sizes are generally located just below the firm zone of the moraine, deposited there by small gravity flows or during smaller rain events. At these locations erosion is often relatively high, which seems to be caused by a combination of a fast flowing water input and a relatively high erodibility of the bed. Erodibility thus also decreases if grain size increases, and flows are hampered by the larger roughness, causing deposition (or less erosion) there.

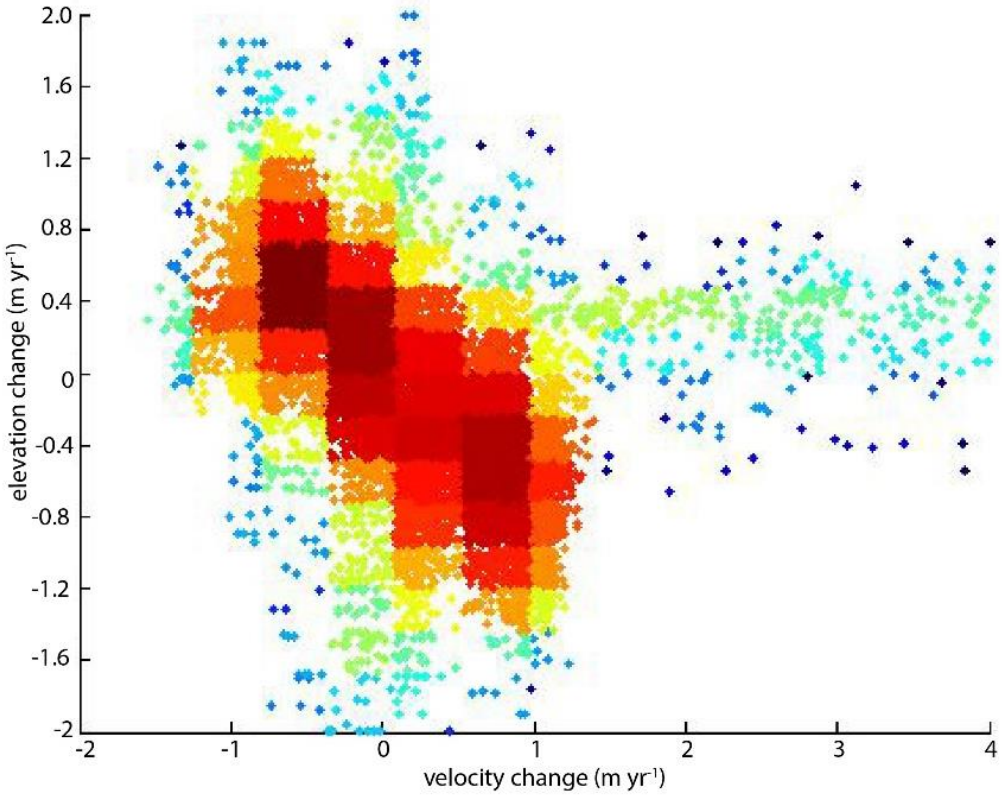

Figure 29; Change in moraine surface velocity and elevation change. The displacement change is calculated as wet season – dry season, thus negative displacement change values indicate a speeding up of the glacier in the wet season. From blue to red the colors indicate the point density.

6.3 Erosion process

Three different types of erosion are distinguished on the moraine, being (1) erosion due to water flow, (2) due to periglacial processes and (3) due to saturated slope failure. This section will try to quantify the relative importance of the different processes, and thus make a suggestion towards a general concept of moraine erosion.

Gullying and erosion by debris flows is assumed to play the most important role in moraine erosion (Curry et al., 2005; Ballantyne, 2002). Debris flows typically contain 20% to 60% water by volume, where normal flows have much smaller debris content (Costa, 1988). The runout length of debris flows is highly variable and is among other things dependent on composition (de Haas et al., 2015). Due to a constant high pore pressure, the distance over which sediment is transported is generally larger with debris flows than with general sediment entrainment in water flows. Furthermore, due to the same effect, debris flows are able to transport much larger grain sizes (Iverson, 1997). A maximum grain diameter of approximately 40 cm in the runout zone of flows supports the idea of erosion mainly generated by debris flows. Furthermore, visual interpretation shows distinct levees, along a central flow path, followed by depositional lobes at the bottom of such a distinct flow channel. However, many other small channels exist, which do not match the dimensions of debris flow features (Figure 30). They are thus caused by water flow and sediment entrainment. The lack of distinct depositional debris flow features along the entire moraine also indicates that not all of the sediment is transported by debris flows, or that the features are reworked quickly. A small water pond at the bottom of the moraine furthermore shows that running water reaches the glacier surface. Most likely debris flows are the main transporting mechanism on the upper part of the slopes, as their transport capacity is much higher than that of surface water flow (Iverson, 1997). A reworking of the sediment by flow entrainment, both in and besides the channels carved by the debris flows, transports sediment further down the moraine. The influence of both of these flows is diminished if the median grain size increases substantially further down the slope. On many parts of the glacier this is observed, especially where the moraine topography shows a small step in slope, or if the moraine is vegetated below. These flow processes are, together with the displacement of the entire moraine, most important.

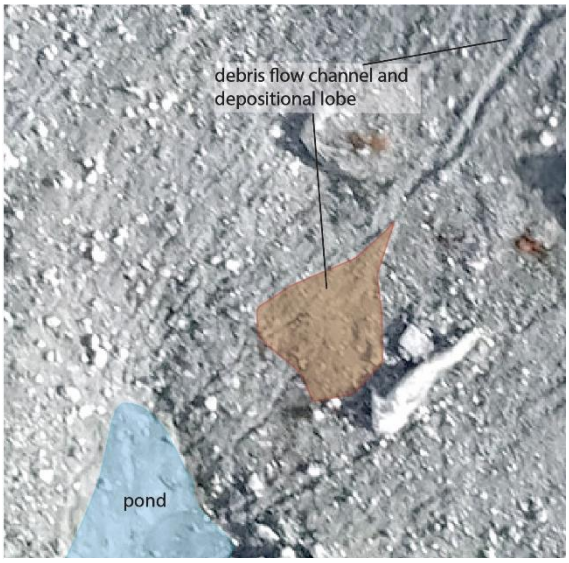

Figure 30; Comparison of debris flow patterns and patterns caused by normal water flow on the moraine.

On the loose part of the moraine, mean displacements were 1.1 m yr^{-1}. Maximum values were found up to 4 m yr^{-1}, but most were below 2 m yr^{-1}. Soil creep rates are much smaller (Kirkby, 1967), maximal up to several cm yr^{-1}, thus creep can only play a minor role in distributing sediment downslope. Nonetheless, it is likely that freeze/thaw processes play a role in this process. The permafrost elevation in the region had an average lower limit of 5400 m in 2004, and has probably risen ever since (Fukui et al., 2007). At some locations permafrost is found at elevations as low as 3500 m (Gruber et al., 2017), thus it can be argued that at least during the winter season the moraine

will be temporarily frozen, possibly triggering mass movement processes. Solifluction rates can reach up to 1 m yr^{-1}, but are generally much slower, and furthermore mostly happen on less steep slopes (Matsuoka, 2001). Also, the distinct lobes that generally form as a result of solifluction cannot be seen on the lateral moraine, though it is possible that the surges reach all the way to the glacier, where the pattern is disturbed by the existing debris. If the moraine is assumed to act like a miniature version of a rock glacier, movement rates also vary from centimeters to approximately 1 m yr^{-1} (Frauenfelder et al., 2005).

The higher velocities during the summer season can indicate that temporary freezing of the soil continues all year round. The higher availability of water in the summer (wet) season might favor the formation of ice lenses in this period, speeding up the solifluction rate of the moraine (Ballantyne & Matthews, 1982). Solifluction in mountainous areas results in smooth and stable slopes with an angle between 25-30^{o}. The average slope of the loose part of the moraine is 32^{o}, which is still slightly higher than those mostly observed, indicating that the mass wasting process has not yet formed these lower angle slopes. As deglaciation happened recently, this might make the moraine more susceptible to these processes, resulting in high displacement rates. Furthermore, the wet climate in the summer season when compared to most parts of the world, also is likely to increase the rate of movement. As velocities are high over the entire loose moraine, processes induced by freeze-thaw action such as solifluction, are of high importance in transporting sediment downslope on lower parts of the moraine. Though debris flows and sediment entrainment also play a role, they act on a much smaller area (Figure 30), contributing less to the total erosion than the solifluction process.

Saturated slope failure or small rockfalls due to undercutting of a boulder by other processes also plays a role on the moraine. However, though slumps locally cause a lot of erosion (elevation change < -3.2 m yr^{-1}), the material is mostly also deposited on the moraine, thus not contributing to the average elevation loss of the lateral moraine. These features are also not as abundant as gullied slopes caused by debris flows. Most slope failures are likely shallow translational sliding, flow and individual clast slide and/ or fall, rather than deep-seated rotational slip, because of the very small percentage of clay-sized particles, necessary to form slip surfaces (Selby, 1993). Though relatively sparse, slumps and slides might favor erosion, as the loose material can easily be reworked by other processes, as is also seen in the data.

6.4 Model results

First some modelled general characteristics of the glacier will be discussed, followed by a more in depth comparison of both model runs and the sensitivity analysis.

6.4.1 Glacier thickness

The glacier thickness is calculated using a method developed from Haeberli & Hoelze (1995), and decreases from 70 m at the upper study area margin to approximately 35 m at the current glacier terminus. The calculated thickness of the glacier, both currently and based on the melt rate, matches current and past observations (Figure 21).

In April 2017, the glacier height at the terminus ranges between 20 and 40 m. Radio echo-sounding measurements at Lirung glacier in 1999 (Gades et al., 2000) have determined a glacier thickness of approximately of 20 ± 5 m at the terminus back then (location A). They furthermore found an ice thickness of 50 m at approximately 250 m from the current terminus (location B), and an ice

thickness of 90 m approximately 700 m from the current terminus (location C) (Figure 21) , just outside of the study area used for this research. The modelled current ice thickness only partly matches these values, with 50-55 m at 250 m from the terminus, but 40-45 m at 700 m. However, if the absolute locations are used and the downwasting rate is taken into account, both values do match fairly well. Location C is currently only 200 m away from the terminus, and has a modelled ice thickness of approximately 50-55 m. This is only slightly less than the 65 m expected from the downwasting rate of approximately 1.99 m yr^{-1} over the past 18 years (Nuimura et al, 2017) and indicates that the downwasting rate in the lower reach of the glacier is higher than the average values (Brun et al., 2017). Comparing the calculated glacier thickness through time with the thickness based on absolute melt rates shows that the modelled glacier thickness matches the data, with a maximum offset of 6.9%.

The calculated shape of the glacier is relatively flat along its central flowline, and the glacier thickness decreases fast near the edges of the glacier (Figure 20). Echo images (Gades et al., 2000) indicate a flat bedrock surface underneath the glacier for most of its width, supporting the modelled shape of the glacier.

6.4.2 Modelled debris supply

The debris supply to the glacier is highly dependent on the melt rate of the glacier, which matches measured and calculated values. The supply rate to the glacier is thus also assumed to match measured and calculated values. First the moraine erosion at the last timestep is compared with the found erosion values on the moraine.

The calculated erosion volume is 43.000 m^3, which is about twice as small as the measured erosion if the entire moraine along Lirung glacier would be unvegetated. That would result in 83.000 m^3. This is also observed in the elevation loss (Figure 24), which also is about twice as small as the measured value of -0.25 m yr^{-1}. However, if it is assumed that the vegetated areas of the moraine are not eroding, the total yearly erosion volume is approximately 60.000 m^3, which is already a lot nearer to the modelled amount. The modelled debris supply to the glacier is thus close to the actual debris supply, which is also indicated by the debris thickness values as these are comparable with measured values (McCarthy et al., 2017; Ragettli et al., 2015). The erosion rates at the start of the simulation were probably higher than modelled, as the recently glaciated terrain was more susceptible to erosion and the upper part of the glacier is currently almost deprived from loose sediment (Curry et al., 2005; Ballantyne et al., 2002).

6.4.3 Supraglacial debris pattern

As two different model simulations were carried out, they will be discussed here separately. First the simulation without additional debris input is discussed, afterwards the simulation with additional debris input from other sources

6.4.3.1 Only lateral moraine derived debris

The deposition over time thus increases probably at higher rates than modelled, and accordingly the amount of material on the glacier tongue of the glacier increases fast, but not enough to cover the entire glacier surface. The moraine derived debris stays on the side of the glacier tongue, with a maximum on-glacier distance of approximately 70 m. With an actual erosion rate that is 1.4 times higher, the median debris thickness is also expected to increase by a factor of 1.4. The debris covered area is much less dependent on the debris input (Figure 27), and thus it is not expected that the

underestimation of debris supply to the glacier is large enough to cause the debris to be covering the entire glacier surface (as observed on the glacier).

Moraine derived debris is increasingly more important on smaller glaciers, as the fraction of the glacier that is covered increases. However, on debris covered glaciers, which generally have a larger width than Lirung glacier, moraine derived debris will only play a minor role in establishing a complete supraglacial debris cover.

A combination of two processes is probably responsible for the observed pattern. First of all, debris supply rates increase exponentially, as the downwasting rate of the glacier also does so, exposing more moraine area. This results in a rapid shrinking of the glacier width (Figure 25), forcing material on the newly deglaciated terrain back to the edge of the glacier. Though 2/3 of the material is assumed to stay on the moraine, still much debris is again deposited on the glacier edge. Furthermore, glacier velocities decrease with a decreasing glacier thickness (Equation 11). Most material is deposited on the glacier in the last 50 years, and over the same period the glacier velocity drops. Therefore relatively little debris can be transported away from the moraines by the glacier movement. As a result of both of these, debris remains mostly on the sides. The surface velocities calculated in the model, are towards the end of the simulation smaller than the current COSI-Corr derived velocities on the glacier (Kraaijenbrink et al., 2016). Calculated surface displacements range between 0.1 and 0.6 m yr^{-1} (Figure , while the actual surface velocities are up to several m yr^{-1}. However, the direction of the velocity is mostly along-glacier, with only minor surface velocities towards the center. The effect of too low final velocities is thus for the largest part not that important for sediment transport towards the center of the moraine.

Besides this pattern which can be observed along the entire glacier, small local variations in the spread and thickness of the supra glacial debris also exist. These are mostly caused by a combination of two processes. First, the local moraine slope steepness is an important factor. Though the amount of erosion was not related to the slope, there was a clear trend between the slope and the erosion probability (Figure 22). Therefore, sections of the glacier which generally have a less steep slope (Figure 7) deposit less debris on the lower boundary of the moraine. Also, a less steep slope results in a smaller push length. The debris cover in that section will thus be smaller. The second important factor is the flow direction of the glacier. The importance of this is obvious in the North-Eastern part of the moraine. As the glacier flow direction in this section is towards the moraine, the debris is not passively transported onto the glacier (Gibson et al., 2017), but is moved back to the glacier boundary. Several other processes are of minor importance, such as the local glacier variance. However, as these are more variable over time, they play a smaller role in creating the depositional pattern.

When comparing the modelled pattern to features currently observed on Lirung glacier, the pattern matches fairly well. First of all, ice cliffs and ponds are common features on debris covered glaciers, but their formation is inhibited by a thick debris cover (Gibson et al., 2017). On Lirung glacier, most of the ice cliffs and surface variation (Figure 31) are not located near the glacier boundary. An example is shows at Figure 31, (C), where the ice cliff is located near the moraine, but does not continue until the moraine, probably due to the very thick debris cover there that inhibits rapid melt rates. Second, if only the surface variability is considered (Figure 31, B), it is noticeable that near the moraine, there generally is a positive anomaly regarding the glacier surface elevation. The width of the higher

section along the moraine is approximately 20-70 meters, but is not present everywhere. Nonetheless, the modelled moraine extend seems to match with the higher elevations on the side. Finally, the model calculates the highest debris thicknesses not exactly at the moraine boundary, but just inside. Though this is cannot be seen in the surface variability, many photographs taken along the glacier seem to confirm this result (Figure 31, D).

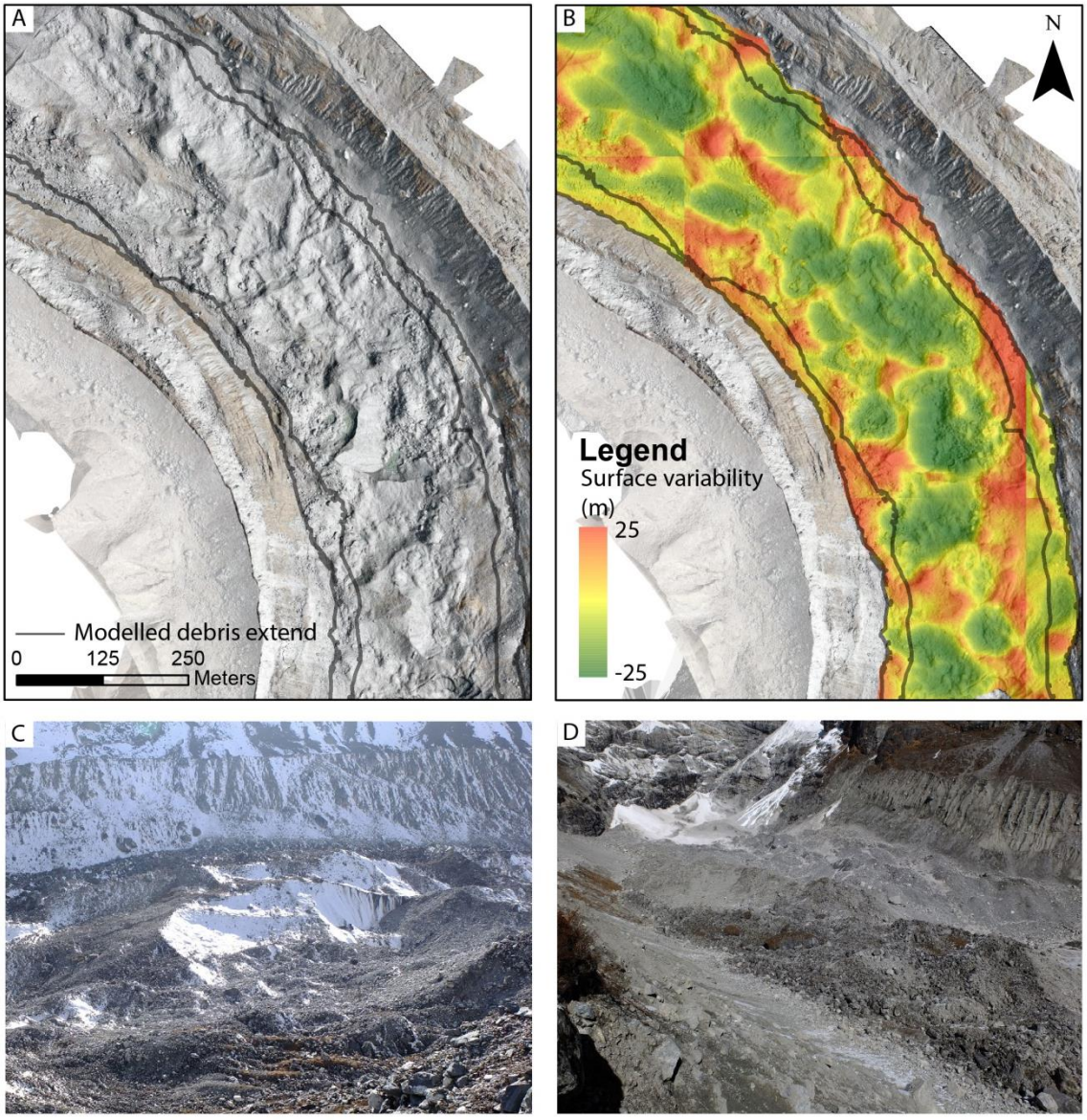

Figure 31; Comparison of modelled and observed supraglacial debris pattern. Many aspects of the pattern can also be seen on the actual Lirung glacier, such as a lack of ice cliffs near the moraine (A, C), higher elevations near the moraine (B) and the presence of a debris ridge just inside the glacier area (D).

6.4.3.2 Moraine derived debris and additional debris input

The model simulation which used an additional debris input on top of the lateral moraine derived debris resulted in a less distinct debris distribution pattern. The most striking results are the abundance of a supraglacial debris band along the glacier-moraine boundary, a decreasing debris cover (48%-29%) in combination with a high median debris thickness (9.2 m) and finally the presence of a medial band of debris cover on the lower reach of the glacier (Figure 26).

The band of debris along the moraine edge is present as in the previous simulation, though the width of this band decreases instead of increases. Towards the end of the simulation, the spread of debris along the glacier-moraine boundary is smaller than in the simulation without additional debris (Figure 26, E). The narrowing of these lateral bands of debris is, as we as the decrease in debris cover % and the presence of a medial band of debris are both likely caused by the transport of debris by the glacier velocity. As the spatial variability of the glacier causes material to concentrate at certain positions, the debris thickness increases substantially at converging locations, while it slowly disperses at diverging locations. These are clearly indicated on the glacier velocity plots (Figure 32). The decrease in debris cover, in combination with the increase in mean debris thickness, indicates that the debris cover pattern is changing from a widespread cover with a relatively small debris thickness to more concentrated patches of high debris thickness. Previously it is stated that the velocity has a smaller influence on transporting material onglacier, as glacier velocities rapidly decrease if erosion values increase. As the medial band of debris forms relatively quick, it is assumed that the higher velocities (>20 m yr^{-1}) near the start of the simulation are capable of transporting the already present debris cover. Nonetheless this pattern indicates that it is possible for moraine derived debris to reach further out from the moraine, though the actual values of debris covered area and debris thickness are less reliable.

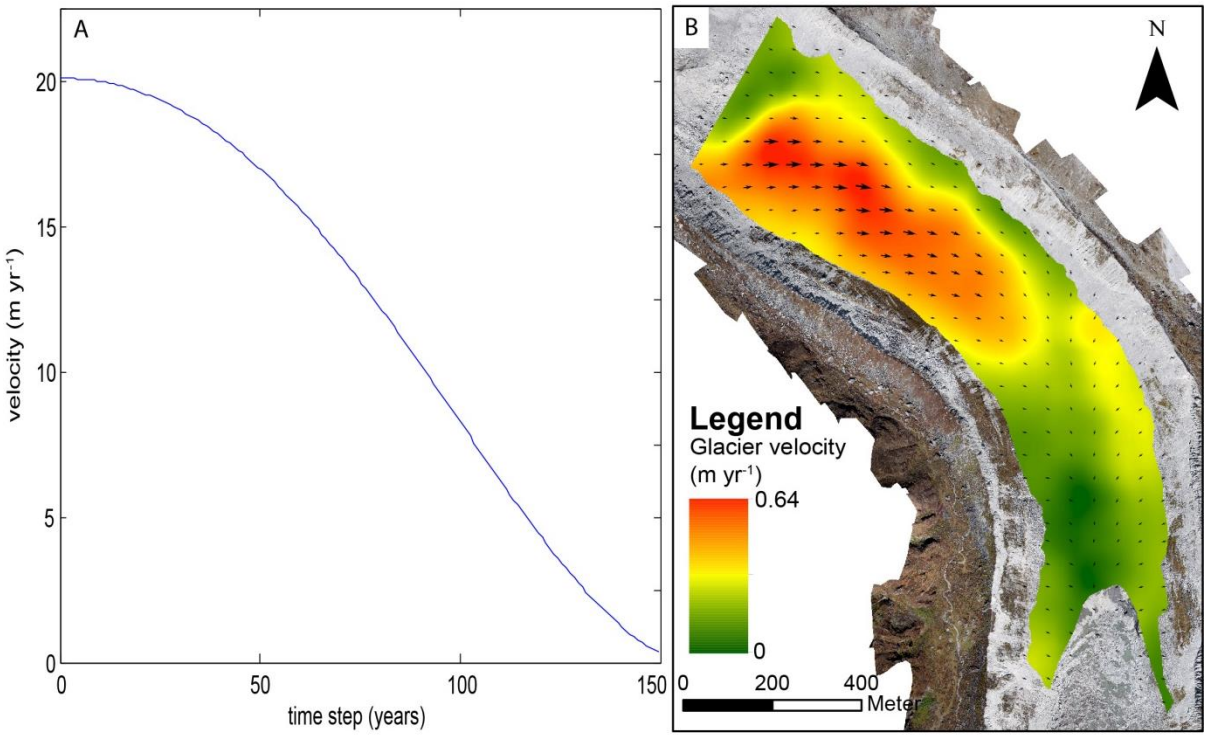

Figure 32; Glacier velocity through time (A), and spatially across the glacier (B, modified from Kraaijenbrink et al., 2016).

6.4.4 Debris thickness

Assuming a the debris on the glacier is moraine derived, the debris thickness increases up to 2.18 m along the margins of the glacier. This value is in line with the debris thickness on the lower part of the Baltoro glacier in the Karakoram, which had a debris thickness between 1-3 m on its lower section (Gibson et al., 2017) in 2012. If the increasing trend at this glacier continued, the current debris thickness is even higher. These values, however, are for the entire glacier, not only for the moraine derived sediment.

Many other studies indicate values of up to 0.5 m debris cover on similar glaciers (Huang et al., 2017). However, debris thickness estimations based on thermal remote sensing are often have a detection limit of approximately 0.5-1 m, which might be a reason that they do not observe the much thicker debris cover near the glacier edge. McCarthy et al. (2017) made debris thickness measurements in the same study area and mostly found values below 0.5 m, though the debris cover was spatially variable between 0.11 - 2.30 m. He did not make measurements inside the area modelled to have a moraine derived debris cover (Figure 33, A). Ragettli et al. (2015) calculated a debris cover thickness of 0.2 - 2.5 m. McCarthy et al. (2017) nonetheless observed a thickening of debris cover closer to the moraine. Due to the high variability on the glacier, probably caused by local slope processes (McCarthy et al., 2017), the data is still highly variable and does not show a linear decreasing trend away from the moraine (Figure 33, A).

The debris thickness that was calculated using additional supraglacial debris from other sources, had debris thickness values far outside the range currently found on Lirung glacier. However, the observation that debris is likely to travel further onto the glacier than assumed based on only moraine derived debris, also gives new insight in the debris thickness value based on only moraine derived debris supply. Though mean thickness is within the range of values found (McCarthy et al., 2017; Ragettli et al., 2015) it is on the upper end of the spectrum, while individual values are much higher. Two different causes are possibly responsible for this difference. First, no data was gathered or calculated for the zone close to the moraine. If the model predicts the debris thickness along the glacier edge correctly, it can nonetheless not be directly compared to the data. Second, the model run including other debris indicated that it is possible for moraine derived debris to move further to the center of the glacier. In the first model run, a debris cover of 22% coincides with a mean debris thickness of 2.2 meter. Assuming further transport is possible and all current debris has its origin on the moraine, the mean debris thickness across the glacier is 0.49 m. This value would fit perfectly with the mean debris thickness found by Huang et al. (2017) and McCarthy et al., (2017), but is lower than estimates by Gibson et al. (2017) and Ragettli et al. (2015).

Field validation and further model calibration is needed to find the definite importance of the glacier velocity and its importance for the moraine derived debris distribution on debris covered glaciers.

6.5 Sensitivity analysis

The sensitivity analysis showed that the model was mostly influenced by the debris threshold for sliding and the push length. These had a major influence on different processes, the push length was most important for the distribution of the material, while the debris threshold mainly influenced the debris thickness.

A reach angle of 34^{o} was used in the model, which is on the upper end of the most occurring values. However, rockfall angles in Andorra are often as large as 41^{o} or even steeper (Copons et al, 2009). Debris flows, which are among the most important processes on the firm part of the moraine, also can have reach angles up to 45^{o} (de Haas et al., 2015). Reach angles on the moraine are generally larger than 34^{o}, up to more than 40^{o}. Furthermore, the push length is based on the reach angle only, but is also influenced by the mass movement volume, as larger volumes can exert a larger force on the near-boundary supraglacial debris. As smaller flows generally have a larger reach angle, the reach angle is likely to decrease with increasing moraine height, as this gives the possibility for larger mass movements. The observed reach angle is at a large moraine height, thus with a smaller moraine elevation the push length has been even smaller. Finally, as noted before, flows seem to be hampered by rough terrain, not being able to reach the runout length expected from the flow characteristics (de Haas et al., 2015). Though this information is included in the distribution of reach angles for debris flows, it is assumed that the rough terrain nonetheless also decreases the runout length and thus increases the reach angle of flows on the lateral moraine. These three factors combined indicate that the push length can be seen as a maximum push length, and will be smaller on most locations across the glacier. As a higher reach angle both has a negative effect on the debris distribution and the debris thickness, the modelled debris cover is slightly overestimated.

The debris thickness threshold for sliding is set to 0.2 m in the model. It is assumed that the lowest layer of debris, which is in touch with the glacier ice, is partially frozen into the ice, and is therefore not susceptible to slope sliding mechanisms. Therefore a higher debris threshold increases the mean debris thickness substantially (Table 4). The glacier roughness had approximately the same range as the moraine roughness (Miles et al., 2016), and was related to a maximum grain size of approximately 0.3 m. Though known that these are slightly underestimated, an average height of 0.2 m to a single layer of debris seems suitable for the current glacier. However, as the grain size distribution across the glacier and between glaciers may vary substantially (Miles et al., 2016), field data or a more advanced method to calculate the grain size properties from remote sensed data might improve the model performance considerably.

Though a change of erosion probability by the standard deviation of the data only results in a 5% change, this might be larger if the sediment availability of the moraine is taken into account. Curry et al. (2005) found that metastable sediment sources on recently glaciated terrain are usually exhausted between 50 – 200 years after deglaciation. Especially for the upper part of the Lirung glacier moraine, this might indicate a deprivation of sediment for the last 100 years. Thus, erosion rates on this upper section might have been higher earlier on, depositing more material on the glacier in the early stage after deglaciation. This material then had a larger timespan to distribute across the glacier, as also velocities were higher. This might result in a slightly larger distribution of material than currently modelled.

6.6 Relative importance of redistribution processes

The relative importance of debris distribution processes is examined using only lateral moraine derived debris. This is done by simulating the debris distribution by only one of the processes in the model. The results indicate that the push factor is most importance, which results in a debris covered area of 13% and an outward boundary of moraine derived debris of on average 20.7 m (Table 6). Afterwards sliding down local slopes, which resulted in debris cover of 2.2%. The very low mean debris thickness is caused by the fact that the glacier is narrowing more quickly than the material is transported inward. Therefore, most of the debris is redeposited on the moraine, as is not found on the glacier after 150 years (Section 6.4.3.1). The glacier velocity is least capable of transporting debris in this simulation, though the second model run indicated that its importance might be underestimated in the first model (Figure 34). The most important result however, is that an addition of these processes (resulting in a covered fraction of 17%) is not enough to reach the debris spread calculated by combining the different processes (22.4%).

Besides that the push function accounts for the largest distribution of debris, it is also the parameter to which the model is most sensitive (Figure 27). The effect of the push function is determined by the reach angle, which is based on the main transporting mechanisms on the lateral moraine (Lied, 1997; Evans and Hungr, 1993; de Haas et al., 2015). Therefore, knowledge of transporting mechanisms is important for defining the influence of these processes on the glacier distribution. Further research on the transporting processes to quantify the reach angle or influence length is thus of great importance.

These results partly contradict the findings by Gibson et al. (2017), who assumed that glacier velocity is most important in distributing sediment on Baltoro glacier. However, Baltoro glacier has much higher glacier velocities (up to 150 m yr^{-1}, 30 m yr^{-1} at the terminus), making glacier velocity more important. Furthermore, the influence of erosional mechanisms on the debris distribution is also mentioned, but not quantified.

Process	**Mean debris thickness (m)**	**Mean distance from moraine (m)**	**Maximum distance from moraine (m)**	**Percentage of glacier surface covered (%)**
Push	8.9	20.7	39.3	13.3
Slide	0.63	24.6	68.1	2.2
Move	7.4	3.0	7.2	1.8
Combine	2.18	29.5	54.4	22.4

Table 6; Results indicating relative importance of processes for moraine derived supraglacial debris.

6.7 Incorporation in glacier flow and energy balance models

The debris thickness is important for energy balance and glacier flow models, and though the debris cover is often included, it is as many times assumed to be stable. However, this research indicated the debris near the glacier margins is dynamic due to an ongoing sediment influx, and others (Gibson et al., 2017) also found that the debris cover is also dynamic over the entire glacier. This matches the result from the model developed in this study, which clearly shows that also without sediment input, the debris cover changes over time. A more dynamic debris distribution model could enhance glacier flow models, such as those of Anderson & Anderson (2016), Rowan et al. (2015) and Banerjee (2017). The same is true for models which simulate glacial change using the energy balance, which is also altered by the thickness of the debris cover (Reid & Brock, 2010; Carenzo et al., 2016). Furthermore, a dynamic debris input rate based on adjacent slopes is also likely to improve the applicability of these models, which now often choose a static debris input to the glacier. As discussed before, these rates are also dependent on the sediment availability on the slopes, which generally decrease relatively fast after deglaciation in the case of lateral moraines (Curry, 2005). Together with others who studied the spatial pattern of supraglacial debris variation (Gibson et al., 2017), and debris input from rock avalanches (Dunning et al., 2015), this research opens up new opportunities to model the formation of a supraglacial debris layer. About the transport of englacial debris is still little known, but McCarthy et al. (2017) gives new insight on this process, which however still needs a larger spatial and temporal data coverage to understand the feedback links. After that, the translation of these new insights to a glacial change model is one step closer.

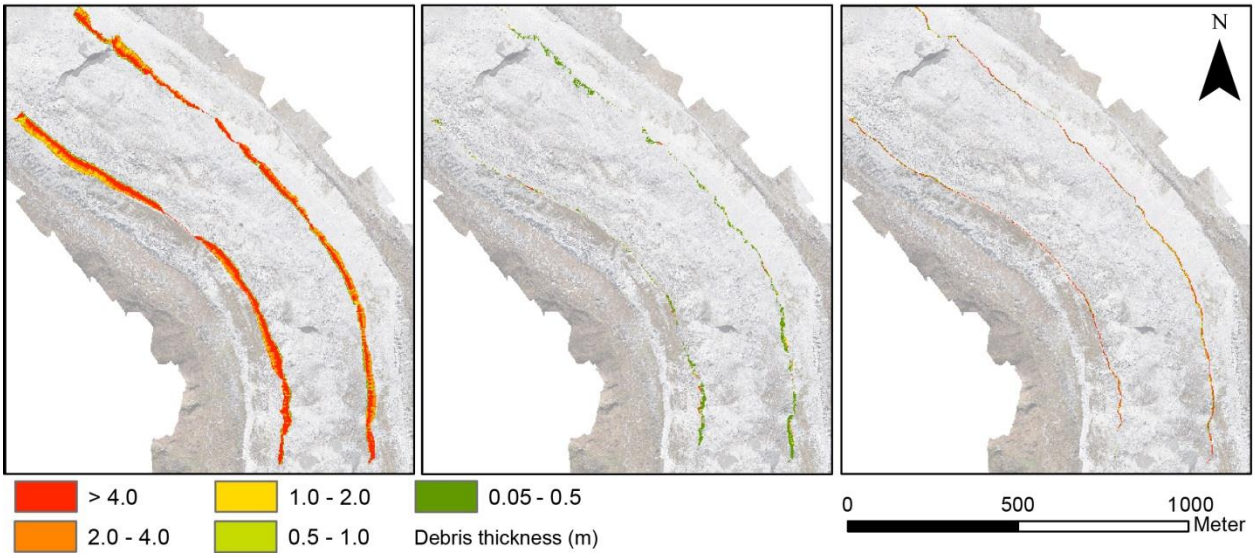

Figure 33; Relative importance of debris distribution processes.

7. Conclusion

Using high resolution images from a UAV, moraine erosion and debris distribution is studied at Lirung glacier in the Langtang region, Nepal. The lateral moraine bordering the glacier can be divided in an upper firm part (glacial till) and a lower part consisting of loose material. The firm part is intensely gullied, and below the gullies a zone with fine material (washout zone) is distinguished.

By calculating the elevation difference between different timesteps, it was found that the lateral moraine bordering the glacier erodes at a rate of 0.25 m yr^{-1}. This value is not uniform, but shows a high variability through space and time. All erosion occurs during the wet season, and also mostly on the loose part of the moraine (0.5 m yr^{-1}) during the wet season. The gullied firm part of the moraine seems to have a small negative erosion rate (-0.02 m yr^{-1}), indicating sedimentation, but is actually also eroding at a rate of 0.1 m yr^{-1} during the wet season.

The amount of erosion is unrelated to the moraine elevation, aspect and slope, except for the loose part in the wet season. This section has a negative relation with slope, as a result of a fast deprivation of sediment from steep slopes after deglaciation. Furthermore, the loose section slides down the moraine with a rate of 0.89 m yr^{-1}. Also, the amount of erosion increases with smaller roughness of the moraine, indicating that smaller grains are more easily eroded. These results point towards a concept of moraine erosion and debris transport. On the firm part, debris and water flows are most important, together with occasional rock fallout and small slumps. This material is mostly deposited on the loose moraine (washout zone). From the loose part of the moraine, solifluction processes and further water flows transport material all the way down to the glacier.

At the moraine-glacier boundary debris is deposited, from where debris is distributed over the glacier by three processes: debris push from new eroding material, debris slide from local glacier variation and movement along with the glacier velocity. Of these, the pushing of debris away from the edge is most important. The distance the material is pushed away is dependent on the transport processes on the moraine, via the reach angle. Therefore, more mobile processes (such as debris flows) have influence on the glacier. Slow moving processes as solifluction can exert a large constant force on the supraglacial debris, pushing it further on the glacier, but their reach is generally very small.

As the sliding and movement factors are of less importance for the debris distribution, sediment generally remains close to the moraine (70 m), resulting in a moraine derived debris cover of 22%. Close to the moraine, a debris thickness of on average 2.2 m is calculated. The outline of the debris seems to match with observed features on Lirung glacier. However, if other sources of debris are also taken into account, the moraine derived debris does reach the center by passive glacier transport. The importance of the other factors is thus possibly underestimated in the model.

Nonetheless, it is clear that the processes that displace sediment on the moraine (debris flows, slumps and solifluction) do have a large influence on the distribution of moraine derived debris, as the pushing of debris further on the glacier is found to be most important. However, the model is very sensitive to changes in this value, and though the other processes seem of minor importance, there are indications that their importance is underestimated. In order to include the variability of debris supply and distribution in glacier flow and energy balance models, field validation and further calibration of the processes and their influence on the debris distribution on a debris covered glacier needs to be further determined.

Acknowledgements

Hereby I greatly thank Jakob Steiner for his help and active attitude in helping me write this MSc Thesis. Furthermore, Walter Immerzeel and Philip Kraaijenbrink were very helpful in thinking along and sharing data to further improve the reading. Also, Tjalling de Haas must get credits for his idea to include the reach angle, which turned out to be of great importance. Last but not least, I thank Benthe Göbel for her caring attitude and patience, as my entire was often swallowed by this thesis. At last, I thank Jakob, Walter and Philip for introducing me to this very interesting topic, which I'd find very interesting to investigate further in the future.

References

Agisoft (2013). PhotoScan professional 0.9.1 user manual. St. Petersburg, 1-62.

Anderson, L. S., & Anderson, R. S. (2016). Modeling debris-covered glaciers: response to steady debris deposition. The Cryosphere, 10(3), 1105.

Andre, M. F. (1997). Holocene rockwall retreat in Svalbard: a triple-rate evolution. Earth Surface Processes and Landforms, 22(5), 423-440.

Augustinus, P. C. (1995). Glacial valley cross-profile development: the influence of in situ rock stress and rock mass strength, with examples from the Southern Alps, New Zealand. Geomorphology, 14(2), 87-97.

Ayoub, F., Leprince, S., Avouac, J.-P. (2017). User's Guide to COSI-CORR; Co-registration of Optically Sensed Images and Correlation. California Institute of Technology.

Ballantyne, C. K. (2002). Paraglacial geomorphology. Quaternary Science Reviews, 21(18), 1935-2017.

Ballantyne, C. K., & Benn, D. I. (1994). Paraglacial slope adjustment and resedimentation following recent glacier retreat, Fåbergstølsdalen, Norway. Arctic and Alpine Research, 255-269.

Ballantyne, C. K., & Matthews, J. A. (1982). The development of sorted circles on recently deglaciated terrain, Jotunheimen, Norway. Arctic and Alpine Research, 341-354.

Banerjee, A. (2017). Brief communication: Thinning of debris-covered and debris-free glaciers in a warming climate. The Cryosphere, 11(1), 133-138.

Bell, I., Gardner, J., & De Scally, F. (1990). An estimate of snow avalanche debris transport, Kaghan Valley, Himalaya, Pakistan. Arctic and Alpine Research, 317-321.

Benn, D. I., & Owen, L. A. (2002). Himalayan glacial sedimentary environments: a framework for reconstructing and dating the former extent of glaciers in high mountains. Quaternary International, 97, 3-25.

Bhardwaj, A., Joshi, P. K., Singh, M. K., Sam, L., & Gupta, R. D. (2014). Mapping debris-covered glaciers and identifying factors affecting the accuracy. Cold Regions Science and Technology, 106, 161-174

Bolch, T., Kulkarni, A., Kääb, A., Huggel, C., Paul, F., Cogley, J. G., Frey, H., Kargel, J. S., Fujita, K., Scheel, M., Bajracharya, S. & Stoffel, M. (2012). The state and fate of Himalayan glaciers. Science, 336(6079), 310-314.

Brun, F., Berthier, E., Wagnon, P., Kääb, A., & Treichler, D. (2017). A spatially resolved estimate of High Mountain Asia glacier mass balances, 2000-2016. Nature geoscience, 10(9), 668.

Buri, P., Miles, E. S., Steiner, J. F., Immerzeel, W. W., Wagnon, P., & Pellicciotti, F. (2016). A physically based 3-D model of ice cliff evolution over debris-covered glaciers. Journal of Geophysical Research: Earth Surface.

Carenzo, M., Pellicciotti, F., Mabillard, J., Reid, T., & Brock, B. W. (2016). An enhanced temperature index model for debris-covered glaciers accounting for thickness effect. Advances in Water Resources, 94, 457-469.

Cerdà, A. (1998). The influence of aspect and vegetation on seasonal changes in erosion under rainfall simulation on a clay soil in Spain. Canadian Journal of Soil Science, 78(2), 321-330.

Christen, M., Kowalski, J., & Bartelt, P. (2010). RAMMS: Numerical simulation of dense snow avalanches in three-dimensional terrain. Cold Regions Science and Technology, 63(1), 1-14.

Costa, J. E. (1988). Rheologic, geomorphic, and sedimentologic differentiation of water floods, hyperconcentrated flows, and debris flows. Flood Geomorphology. John Wiley & Sons New York. p 113-122. 5.

Copons, R., Vilaplana, J. M., & Linares, R. (2009). Rockfall travel distance analysis by using empirical models (Solà d'Andorra la Vella, Central Pyrenees). Natural Hazards and Earth System Sciences, 9(6), 2107.

Cuffey, K. & Paterson, W. (2010). The physics of glaciers, 4th edn. Butterworth-Heinemann, Oxford.

Curry, A. M. (2000). Observations on the distribution of paraglacial reworking of glacigenic drift in western Norway. Norsk Geografisk Tidsskrift, 54(4), 139-147.

Curry, A. M., Cleasby, V., & Zukowskyj, P. (2005). Paraglacial response of steep, sediment-mantled slopes to post-'Little Ice Age'glacier recession in the central Swiss Alps. Journal of Quaternary Science, 21(3), 211-225.

Dunning, S. A., Rosser, N. J., McColl, S. T., & Reznichenko, N. V. (2015). Rapid sequestration of rock avalanche deposits within glaciers. Nature communications, 6.

Eichel, J., Corenblit, D., & Dikau, R. (2016). Conditions for feedbacks between geomorphic and vegetation dynamics on lateral moraine slopes: a biogeomorphic feedback window. Earth Surface Processes and Landforms, 41(3), 406-419.

Evans, S. G., & Hungr, O. (1993). The assessment of rockfall hazard at the base of talus slopes. Canadian geotechnical journal, 30(4), 620-636.

Fischer, L., Kääb, A., Huggel, C., & Noetzli, J. (2006). Geology, glacier retreat and permafrost degradation as controlling factors of slope instabilities in a high-mountain rock wall: the Monte Rosa east face. Natural Hazards and Earth System Science, 6(5), 761-772.

Foster, L. A., Brock, B. W., Cutler, M. E. J., & Diotri, F. (2012). A physically based method for estimating supraglacial debris thickness from thermal band remote-sensing data. Journal of Glaciology, 58(210), 677-691.

Frauenfelder, R., Laustela, M., & Kääb, A. (2005). Relative age dating of Alpine rockglacier surfaces. Zeitschrift für Geomorphologie, NF, 145-166.

Fukui, K., Fujii, Y., Ageta, Y., & Asahi, K. (2007). Changes in the lower limit of mountain permafrost between 1973 and 2004 in the Khumbu Himal, the Nepal Himalayas. Global and Planetary Change, 55(4), 251-256.

Furukawa, Y., & Ponce, J. (2009). Accurate camera calibration from multi-view stereo and bundle adjustment. International Journal of Computer Vision, 84(3), 257-268.

Gades, A., Conway, H., Nereson, N., Naito, N., & Kadota, T. (2000). Radio echo-sounding through supraglacial debris on Lirung and Khumbu Glaciers, Nepal Himalayas. IAHS PUBLICATION, 13-24.

Gantayat, P., Kulkarni, A. V., & Srinivasan, J. (2014). Estimation of ice thickness using surface velocities and slope: case study at Gangotri Glacier, India. Journal of Glaciology, 60(220), 277-282.

Garcia, M., & Parker, G. (1991). Entrainment of bed sediment into suspension. Journal of Hydraulic Engineering, 117(4), 414-435.

Gibson, M. J., Glasser, N. F., Quincey, D. J., Mayer, C., Rowan, A. V., & Irvine-Fynn, T. D. (2017). Temporal variations in supraglacial debris distribution on Baltoro Glacier, Karakoram between 2001 and 2012. Geomorphology.

Goudie, A. S. (2004). Encyclopedia of geomorphology, Routledge, 2, 1156 pp.

Gruber, S., Fleiner, R., Guegan, E., Panday, P., Schmid, M. O., Stumm, D., Wester, P., Zhang, Y. & Zhao, L. (2017). Inferring permafrost and permafrost thaw in the mountains of the Hindu Kush Himalaya region. The Cryosphere, 11(1), 81-99.

de Haas, T. , & van Woerkom, T. (2016). Bed scour by debris flows: experimental investigation of effects of debris-flow composition. Earth Surface Processes and Landforms, 41(13), 1951-1966.

de Haas, T., Braat, L., Leuven, J. R., Lokhorst, I. R., & Kleinhans, M. G. (2015). Effects of debris flow composition on runout, depositional mechanisms, and deposit morphology in laboratory experiments. Journal of Geophysical Research: Earth Surface, 120(9), 1949-1972.

Haeberli, W., & Hölzle, M. (1995). Application of inventory data for estimating characteristics of and regional climate-change effects on mountain glaciers: a pilot study with the European Alps. Annals of glaciology, 21(1), 206-212.

Hewitt, K. (2009). Rock avalanches that travel onto glaciers and related developments, Karakoram Himalaya, Inner Asia. Geomorphology, 103(1), 66-79.

Huang, L., Li, Z., Tian, B. S., Han, H. D., Liu, Y. Q., Zhou, J. M., & Chen, Q. (2017). Estimation of supraglacial debris thickness using a novel target decomposition on L-band polarimetric SAR images in the Tianshan Mountains. Journal of Geophysical Research: Earth Surface, 122(4), 925-940.

Immerzeel, W. W., Droogers, P., De Jong, S. M., & Bierkens, M. F. P. (2009). Large-scale monitoring of snow cover and runoff simulation in Himalayan river basins using remote sensing. Remote sensing of Environment, 113(1), 40-49.

Immerzeel, W. W., Kraaijenbrink, P. D. A., Shea, J. M., Shrestha, A. B., Pellicciotti, F., Bierkens, M. F. P., & De Jong, S. M. (2014b). High-resolution monitoring of Himalayan glacier dynamics using unmanned aerial vehicles. Remote Sensing of Environment, 150, 93-103.

Immerzeel, W. W., Petersen, L., Ragettli, S., & Pellicciotti, F. (2014a). The importance of observed gradients of air temperature and precipitation for modeling runoff from a glacierized watershed in the Nepalese Himalayas. Water Resources Research, 50(3), 2212-2226.

Iverson, R. M. (1997). The physics of debris flows. Reviews of geophysics, 35(3), 245-296.

Joughin, I., Abdalati, W., & Fahnestock, M. (2004). Large fluctuations in speed on Greenland's Jakobshavn Isbrae glacier. Nature, 432(7017), 608.

Kääb, A., & Vollmer, M. (2000). Surface geometry, thickness changes and flow fields on creeping mountain permafrost: automatic extraction by digital image analysis. Permafrost and Periglacial Processes, 11(4), 315-326.

Kellerer-Pirklbauer, A. (2008). The supraglacial debris system at the Pasterze Glacier, Austria: spatial distribution, characteristics and transport of debris. Zeitschrift für Geomorphologie, Supplementary Issues, 52(1), 3-25.

Kirkby, M. J. (1967). Measurement and theory of soil creep. The Journal of Geology, 75(4), 359-378.

Kraaijenbrink, P., Meijer, S. W., Shea, J. M., Pellicciotti, F., De Jong, S. M., & Immerzeel, W. W. (2016). Seasonal surface velocities of a Himalayan glacier derived by automated correlation of unmanned aerial vehicle imagery. Annals of Glaciology, 57(71), 103-113.

Kraaijenbrink, P. D. A., Bierkens, M. F. P., Lutz, A. F., & Immerzeel, W. W. (2017). Impact of a global temperature rise of 1.5 degrees Celsius on Asia's glaciers. Nature, 549(7671), 257.

Leprince, S., Berthier, E., Ayoub, F., Delacourt, C., & Avouac, J. P. (2008). Monitoring earth surface dynamics with optical imagery. Eos, Transactions American Geophysical Union, 89(1), 1-2.

Lied, K., 1977. Rockfall problems in Norway. Rockfall Dynamics and Protective Work Effectiveness, ISMES publ., 90, 51–53.

Lucieer, A., Jong, S. M. D., & Turner, D. (2014). Mapping landslide displacements using Structure from Motion (SfM) and image correlation of multi-temporal UAV photography. Progress in Physical Geography, 38(1), 97-116.

Lukas, S., Graf, A., Coray, S., & Schlüchter, C. (2012). Genesis, stability and preservation potential of large lateral moraines of Alpine valley glaciers–towards a unifying theory based on Findelengletscher, Switzerland. Quaternary Science Reviews, 38, 27-48.

Marion, J., Filion, L., & Hétu, B. (1995). The Holocene development of a debris slope in subarctic Québec, Canada. The Holocene, 5(4), 409-419.

Matsuoka, N. (2001). Solifluction rates, processes and landforms: a global review. Earth-Science Reviews, 55(1), 107-134.

Mattson, L. E., & Gardner, J. S. (1991). Mass wasting on valley-side ice-cored moraines, Boundary Glacier, Alberta, Canada. Geografiska Annaler. Series A. Physical Geography, 123-128.

McCarthy, M., Pritchard, H., Willis, I., & King, E. (2017). Ground-penetrating radar measurements of debris thickness on Lirung Glacier, Nepal. Journal of Glaciology, 63(239), 543-555.

McColl, S. T., Davies, T. R. H., & McSaveney, M. J. (2010). Glacier retreat and rock-slope stability: debunking debuttressing. In Geologically active: delegate papers 11th Congress of the International Association for Engineering Geology and the Environment, Auckland, Aotearoa (5-10).

McCuen, R. H. (1973). The role of sensitivity analysis in hydrologic modeling. Journal of Hydrology, 18(1), 37-53.

McSaveney, M. J. (2002). Recent rockfalls and rock avalanches in Mount Cook national park, New Zealand. Reviews in Engineering Geology, 15, 35-70.

Miles, E., Willis, I., Arnold, N., Steiner, J. & Pellicotti, F. (2016). Spatial, seasonal and interannual variability of supraglacial ponds in the Langtang Valley of Nepal, 1999–2013.

Miles, E. S., Steiner, J. F., & Brun, F. (2017). Highly variable aerodynamic roughness length (z0) for a hummocky debris-covered glacier. Journal of Geophysical Research: Atmospheres, 122(16), 8447-8466.

Moore, J. R., Egloff, J., Nagelisen, J., Hunziker, M., Aerne, U., & Christen, M. (2013). Sediment transport and bedrock erosion by wet snow avalanches in the Guggigraben, Matter Valley, Switzerland. Arctic, Antarctic, and Alpine Research, 45(3), 350-362.

Moore, P. (in press). Stability of supraglacial debris. Earth Surface Processes and Landforms.

Munro, D. S. (1989). Surface roughness and bulk heat transfer on a glacier: comparison with eddy correlation. Journal of Glaciology, 35(121), 343-348.

Nagai, H., Fujita, K., Nuimura, T., & Sakai, A. (2013). Southwest-facing slopes control the formation of debris-covered glaciers in the Bhutan Himalaya. The Cryosphere, 7(4), 1303-1314.

Nield, J. M., J. King, G. F. S. Wiggs, J. Leyland, R. G. Bryant, R. C. Chiverrell, S. E. Darby, F. D. Eckardt, D. S. G. Thomas, L. H. Vircavs, and R. Washington (2013), Estimating aerodynamic roughness over complex surface terrain, Journal of Geophysical Research: Atmospheres, 118(23), 12,948–12,961, doi:10.1002/2013JD020632

Nuimura, T., Fujita, K., & Sakai, A. (2017). Downwasting of the debris-covered area of Lirung Glacier in Langtang Valley, Nepal Himalaya, from 1974 to 2010. Quaternary International.

Östrem, G. (1959). Ice melting under a thin layer of moraine, and the existence of ice cores in moraine ridges. Geografiska Annaler, 41(4), 228-230.

Palacios, D. (1998). Natural hazards in relation to present stratovolcano deglaciation: Popocatepetl and Citlaltepetl, Mexico. In Geomorphological Hazards in High Mountain Areas (pp. 177-209).

Pfeffer, W. T., Arendt, A. A., Bliss, A., Bolch, T., Cogley, J. G., Gardner, A. S., ... & Miles, E. S. (2014). The Randolph Glacier Inventory: a globally complete inventory of glaciers. Journal of Glaciology, 60(221), 537-552.

Ragettli, S., Pellicciotti, F., Immerzeel, W. W., Miles, E. S., Petersen, L., Heynen, M., Shea, J. M., Stumm, D., Joshi, S. & Shrestha, A. (2015). Unraveling the hydrology of a Himalayan catchment through integration of high resolution in situ data and remote sensing with an advanced simulation model. Advances in Water Resources, 78, 94-111.

Ragettli, S., Bolch, T., & Pellicciotti, F. (2016). Heterogeneous glacier thinning patterns over the last 40 years in Langtang Himal. The Cryosphere, 10, 2075-2097.

Reid, T. D., & Brock, B. W. (2010). An energy-balance model for debris-covered glaciers including heat conduction through the debris layer. Journal of Glaciology, 56(199), 903-916.

Renard, K. G. (1997). Predicting soil erosion by water: a guide to conservation planning with the revised universal soil loss equation (RUSLE).

Reznichenko, N. V., Davies, T. R., & Alexander, D. J. (2011). Effects of rock avalanches on glacier behaviour and moraine formation. Geomorphology, 132(3), 327-338.

Römkens, M. J., Helming, K., & Prasad, S. N. (2002). Soil erosion under different rainfall intensities, surface roughness, and soil water regimes. Catena, 46(2), 103-123.

Rowan, A. V. (2017). The 'Little Ice Age' in the Himalaya: A review of glacier advance driven by Northern Hemisphere temperature change. The Holocene, 27(2), 292-308.

Rowan, A. V., Egholm, D. L., Quincey, D. J., & Glasser, N. F. (2015). Modelling the feedbacks between mass balance, ice flow and debris transport to predict the response to climate change of debris-covered glaciers in the Himalaya. Earth and Planetary Science Letters, 430, 427-438.

Schauwecker, S., Rohrer, M., Huggel, C., Kulkarni, A., Ramanathan, A. L., Salzmann, N., Stoffel, M. & Brock, B. (2015). Remotely sensed debris thickness mapping of Bara Shigri glacier, Indian Himalaya. Journal of Glaciology, 61(228), 675-688.

Scheidl, C., & Rickenmann, D. (2011). TopFlowDF - a simple GIS based model to simulate debris-flow runout on the fan. In 5th international conference on debris-flow hazards mitigation: mechanics, prediction and assessment, Padua, Italy (pp. 14-17).

Scherler, D., Bookhagen, B., & Strecker, M. R. (2011a). Spatially variable response of Himalayan glaciers to climate change affected by debris cover. Nature geoscience, 4(3), 156-159.

Scherler, D., Bookhagen, B., & Strecker, M. R. (2011b). Hillslope-glacier coupling: The interplay of topography and glacial dynamics in High Asia. Journal of Geophysical Research: Earth Surface, 116(F2).

Schomacker, A. (2008). What controls dead-ice melting under different climate conditions? A discussion. Earth-Science Reviews, 90(3), 103-113.

Selby M. J. (1993). Hillslope Materials and Processes (Oxford University Press, Oxford), 2nd edn.

Smith, M. W. (2014), Roughness in the Earth Sciences, Earth-Science Reviews, 136, 202–842225, doi:10.1016/j.earscirev.2014.05.016

Soldati, M., Corsini, A., & Pasuto, A. (2004). Landslides and climate change in the Italian Dolomites since the Late glacial. Catena, 55(2), 141-161.

Van Rijn, L. C. (1984). Sediment transport, part I: bed load transport. Journal of hydraulic engineering, 110(10), 1431-1456.

Watanabe, T., Dali, L., & Shiraiwa, T. (1998). Slope denudation and the supply of debris to cones in Langtang Himal, Central Nepal Himalaya. Geomorphology, 26(1), 185-197.